

X-RAY BAND DEPENDENCE OF X-RAY TEMPERATURES IN GALAXY CLUSTERS

KENNETH W. CAVAGNOLO^{1,2}, MEGAN DONAHUE¹, G. MARK VOIT¹, AND MING SUN¹

Draft version September 14, 2007

ABSTRACT

We explore the band-dependence of the inferred X-ray temperature of the intracluster medium (ICM) for 179 well-observed ($N_{photons} > 1500$) clusters of galaxies selected from the Chandra data archive. If the hot gas in a cluster is nearly isothermal in the projected region of interest, the X-ray temperature inferred from a broad-band (0.7-7.0 keV) spectrum should be identical to the X-ray temperature inferred from a hard-band (2.0-7.0 keV) spectrum. However, if there are excess soft X-ray photons contributed by cooler lumps of gas or by non thermal processes, the temperature of a best-fit single-temperature thermal model will be cooler for a broad-band spectrum than for a hard-band spectrum. Such a diagnostic may indicate such contamination even when the X-ray spectrum itself may not have sufficient signal-to-noise to resolve multiple temperature components. To test this possible diagnostic, we extract X-ray spectra from annular regions between $R = 70$ kpc and $R = R_{2500}$, R_{5000} for each cluster in our archival sample. We compare the X-ray temperatures inferred for single-temperature fits of global spectra when the energy range of the fit is 0.7-7.0 keV (full) and when the energy range is 2.0/(1+z)-7.0 keV (hard). We find, on average, the hard-band temperature is significantly higher than the full-band temperature. Upon further exploration, we find the ratio $T_{HFR} = T_{2.0-7.0}/T_{0.7-7.0}$ is enhanced preferentially for clusters which are known merger systems and for clusters which are isothermal. Clusters with temperature decrements in their cores (known as cool-core clusters) tend to have best-fit hard-band temperatures that are statistically consistent with their best fit full-band temperatures. We show, using simulated spectra, that this test is sensitive to cool components with emission measures $> 4\%$ of the hot component for $2.0 \leq T_X \leq 15.0$ keV and for $z < 0.6$.

We show this test is relatively insensitive to second components in an individual cluster when the total counts in the spectrum are < 2500 , but that investigation of a sample of low-count clusters may still reveal interesting trends. A comparison to the predicted distribution of temperature ratios and their relationship to putative cool lumps and/or non-thermal soft X-ray emission in cluster simulations would be a very useful next step.

Subject headings: catalogs – galaxies: clusters: general – X-rays: galaxies: clusters – cosmology: observations – methods: data analysis

1. INTRODUCTION

Cluster mass functions and the evolution of the cluster mass function are useful for measuring cosmological parameters (Evrard 1989; Wang & Steinhardt 1998; Haiman et al. 2001; Hu 2003; Wang et al. 2004). Cluster evolution tests the effect of dark matter and dark energy on the evolution of dark matter halos, and therefore provide a complementary and distinct constraint on cosmological parameters to those tests which constrain them geometrically (e.g. supernovae (Riess et al. 1998, 2007) and baryon acoustic oscillations (Eisenstein et al. 2005)).

However, clusters are a useful cosmological tool only if we can infer cluster masses – the fundamental cluster property inferred from cosmological simulations (Evrard 1990) – from observable properties such as X-ray luminosity, X-ray temperature, lensing shear, optical luminosity, and galaxy velocity dispersion. Empirically, the relationship of mass and these observable properties is well-established (Voit 2005). However, if we could identify a “3rd parameter” – possibly reflecting the degree of relaxation in the cluster – we could improve the utility of clusters as cosmological probes.

Toward this end, we desire to understand the dynamical state of a cluster beyond identifying which clusters appear to be relaxed and those which appear to be unrelaxed. More

likely, clusters have a dynamical state which is somewhere in between (O’Hara et al. 2006; Kravtsov et al. 2006). The degree to which a cluster is virialized must be quantified within simulations and then observationally calibrated with an unbiased statistical sample of clusters.

One such study to quantify the dynamical state of clusters was performed by Mathiesen & Evrard (2001) (hereafter ME01) using the ensemble of simulations by Mohr & Evrard (1997). ME01 found clusters which had experienced a recent merger were much cooler than the cluster mass-observable scaling relations predict. They attribute this to the presence of cool, spectroscopically unresolved accreting subclusters which introduce energy into the ICM which requires a long timescale to dissipate. The consequence being an under-prediction of cluster binding masses of 15–30% (Mathiesen & Evrard 2001).

One method of quantifying the underestimate of the cluster temperature (and therefore cluster mass) employs the ratios of X-ray surface brightness moments to quantify the degree of relaxation (Buote & Tsai 1995, 1996; Jeltema et al. 2005). Although an excellent tool, power ratios suffer from being aspect dependent. ME01 found an auxiliary measure of substructure which does not depend on perspective and could be combined with power ratio to yield a more robust metric for quantifying a cluster’s degree of relaxation. They found hard-band (2.0_{rest}-9.0 keV) temperatures were $\sim 20\%$ hotter than broad-band (0.5-9.0 keV) temperatures. The cooler broad-band temperature being caused by unresolved accreting cool

¹ Department of Physics and Astronomy, Michigan State University, BPS Building, East Lansing, MI 48824

² cavagnolo@pa.msu.edu

subclusters contributing significant amounts of line emission to the soft-band ($E < 2$ keV). Work by Mazzotta et al. (2004) and Vikhlinin (2006) have confirmed this effect in simulated *Chandra* and *XMM-Newton* spectra.

ME01 proposed this temperature skewing, and consequently the fingerprint of accretion, could be detected utilizing the energy resolution and soft-band sensitivity of *Chandra*. They proposed comparing single-phase temperature fits to a hard band and full band for a sufficiently large sample of clusters covering a broad dynamical range then checking for a net skew in the ratio of hard and full temperatures above unity.

In this paper we present our findings of just such a temperature ratio test using *Chandra* archival data. We find on average, the hard-band temperature exceeds the broad-band temperature by $\sim 15\%$ in multiple flux-limited samples of X-ray clusters from the Chandra archive. This mean excess is weaker than the 20% predicted by ME01, but is significant at the 11σ level nonetheless. Hereafter, we refer to the hard-band to broad-band temperature ratio as T_{HFR} .

This paper proceeds in the following manner. In §2 we outline sample selection criteria and *Chandra* observations selected under these criteria. Data reduction and handling of the X-ray background is discussed in §3. Spectral extraction is discussed in §4 while fitting and simulated spectra are discussed in §5. Results and discussion of our analysis are presented in §6. A final summary of our work is presented in §7. For this work we have assumed a flat Λ CDM Universe with cosmology $\Omega_M = 0.3$, $\Omega_\Lambda = 0.7$, and $H_0 = 70 \text{ km s}^{-1} \text{ Mpc}^{-1}$. All quoted uncertainties are at the 1.6σ level (90% confidence).

2. SAMPLE SELECTION

Our sample is selected from observations publicly available in the *Chandra* X-ray Telescope's Data Archive (CDA). Our initial selection pass came from the *ROSAT* Brightest Cluster Sample (Ebeling et al. 1998), RBC Extended Sample (Ebeling et al. 2000), and *ROSAT* Brightest 55 Sample (Edge et al. 1990; Peres et al. 1998). The portion of our sample at $z \gtrsim 0.4$ can also be found in a combination of the *Einstein* Extended Medium Sensitivity Survey (Gioia et al. 1990), North Ecliptic Pole Survey (Henry et al. 2006), *ROSAT* Deep Cluster Survey (Rosati et al. 1995), *ROSAT* Serendipitous Survey (Vikhlinin et al. 1998), and Massive Cluster Survey (Ebeling et al. 2001). We later extended our sample to include clusters found in the REFLEX Survey (Böhringer et al. 2004). Once we had a master list of possible targets, we cross-referenced this list with the CDA and gathered observations where a minimum of R_{5000} (defined below) is fully within the aimpoint CCD's field of view.

R_{Δ_c} is defined as the radius at which the average cluster density is Δ_c times the critical density of the Universe, $\rho_c = 3H_0^2/8\pi G$. For our calculations of R_{Δ_c} we adopt the relation from Arnaud et al. (2002):

$$R_{\Delta_c} = 2.71 \text{ Mpc } \beta_T \Delta_z^{-1/2} (1+z)^{3/2} \left(\frac{kT_X}{10 \text{ keV}} \right)^{1/2} \quad (1)$$

$$\Delta_z = \frac{\Delta_c \Omega_M}{18\pi^2 \Omega_z}$$

$$\Omega_z = \frac{\Omega_M (1+z)^3}{[\Omega_M (1+z)^3] + [(1-\Omega_M - \Omega_\Lambda)(1+z)^2] + \Omega_\Lambda}$$

where R_{Δ_c} is in units of h_70^{-1} , Δ_c is the assumed density contrast of the cluster at R_{Δ_c} , and β_T is a numerically deter-

mined, cosmology-independent ($\lesssim \pm 20\%$) normalization for the virial relation $GM/2R = \beta_T kT$. We use $\beta_T = 1.05$ taken from Evrard et al. (1996).

The result of our CDA search is a total of 374 observations of which 224 are used from 179 clusters. The bolometric ($E \sim 0.1 - 100$ keV) luminosities, L_{bol} , for our sample clusters plotted as a function of redshift are shown in Figure 1. These L_{bol} values are limited to the region of the spectral extraction (from $R = 70$ kpc to $R = R_{2500}$).

Basic properties of our sample are listed in Table 1. For the sole purpose of computing extraction regions as is discussed in §4, fiducial temperatures and redshifts were taken from the Ph.D. thesis of Don Horner³ (all redshifts confirmed with NED⁴). For clusters not observed with *ASCA* and thus not listed in Horner's thesis, we used a literature search to locate temperature values. If no published value could be located, we approximated a temperature by recursively extracting a spectrum in the region $0.1 < r < 0.2 R_{500}$ fitting a temperature and recalculating R_{500} . This process was repeated until three consecutive iterations produced R_{500} values which differed by $\leq 1\sigma$. This method of temperature determination has been employed in other studies, see Sanderson et al. (2006) and Henry et al. (2006) as examples.

3. CHANDRA DATA

3.1. Reprocessing and Reduction

All datasets were reduced utilizing the Chandra Interactive Analysis of Observations package (CIAO) and accompanying Calibration Database (CALDB). Using CIAO v3.3.0.1 and CALDB v3.2.2, standard data analysis was followed for each observation to apply the most up-to-date time-dependent gain correction and charge transfer inefficiency (CTI) correction (when appropriate) (Townsley et al. 2000). ~~Observations taken in FAINT mode had possible background events flagged using the check_vf_pha mode switch in acis_process_events.~~

The X-ray events were then filtered for bad grades. Only events recorded during the good time intervals (GTI) were used. For observations taken prior to standard data processing version (SDP) 7.4, we flagged, inspected, and then removed the afterglow correction applied as part of the older SDP pipeline. ~~For observations taken prior to SDP 7.4 and using FAINT mode, or SDP 7.6 and FAINT mode, a new bad pixel file was constructed.~~

To detect and remove point sources we used the adaptive wavelet tool wavdetect (Freeman et al. 2002) on events files filtered in the energy range $0.3 - 9.0$ keV. ~~This energy window extends below and above the energy range of interest for our spectral analysis as the photons below 0.7 keV and above 7.0 keV, while useless for diffuse emission studies, are a good diagnostic for detecting point sources.~~

~~Or visually inspecting an image of the observation overlaid with the source regions generated by wavdetect, we added regions for point sources which were missed by wavdetect and deleted regions for spuriously detected "sources" thus creating a point source mask. Spurious sources are typically CCD features~~ ~~fully removed by dividing out the exposure map.~~ Each remaining source was then masked out using 2σ ellipses as calculated from wavdetect. This process results in an events file (at "level 2") that has been cleaned of point

³ Available at <http://asd.gsfc.nasa.gov/Donald.Horner/thesis.html>

⁴ <http://nedwww.ipac.caltech.edu>

sources.

To check for contamination from background flares or periods of excessively high background, light curve analyses were performed using Maxim Markevitch's contributed CIAO script `lc_clean.s1`⁵. Periods with count rates $\geq 3\sigma$ and/or a factor ≥ 1.2 of the mean background level of the observation were removed from the GTI file. As prescribed by Markevitch's cookbook⁶, ACIS front-illuminated (FI) chips were analyzed in the 0.3 – 12.0 keV range with time bins of 259.28 sec in length, and for the ACIS back-illuminated (BI) chips, 2.5 – 7.0 keV energy range with time bins of 1037.12 sec.

If possible, we compared light curves from a FI and BI chip in an effort to detect long duration, soft-flares which can go undetected on the FI chips but show up on the BI chips. While rare, this class of flare needs to be filtered out of the data as it introduces a spectral component which artificially increases the best-fit temperature via a high energy tail. 

Determining a cluster “center” is essential for the later purpose of removing cool cores from our spectral analysis (see §4). To determine the cluster center, we calculated the centroid of the ~~resulting flare clean, point source free~~ level-2 events file filtered to include only photons in the 0.7 – 7.0 keV range. Before centroiding, the events file is exposure corrected and “holes” created by excluding point sources are filled using interpolated values taken from a narrow annular region just outside the hole.  ~~last step is implemented using the Poisson method of the CIAO tool dmfilth~~. Prior to centroiding we define the emission peak by heavily binning the image, finding the peak value within a circular region extending from the peak to the chip edge (defined by the radius, R_{max}), reducing R_{max} by 5% and the binning by a factor of two, and finding the peak again. This process is repeated until the image is unbinned (binning factor of one). We then return to an unbinned image with an aperture centered on the emission peak with a radius R_{max} and find the centroid using CIAO’s `dmstat`. The centroid, (x_c, y_c) , for a distribution of N good pixels with coordinates (x_i, y_i) and values $f(x_i, y_i)$ is defined as:

$$Q = \sum_{i,j=1}^N f(x_i, y_i) \quad (2)$$

$$x_c = \frac{\sum_{i,j=1}^N x_i \cdot f(x_i, y_i)}{Q}$$

$$y_c = \frac{\sum_{i,j=1}^N y_i \cdot f(x_i, y_i)}{Q} \quad (3)$$

If the centroid was within 70 kpc of the emission peak the emission peak is selected as the center, otherwise the centroid is used as the center. This selection was made to ensure all “peaky” cool cores are at the cluster center thus maximizing their exclusion later in our analysis. All cluster centers are verified by-eye.

3.2. X-ray Background

Because we are attempting to measure a global cluster temperature, specifically looking for a temperature ratio shift in

energy bands which can be contaminated by the high-energy particle background or the soft local background, it is important to carefully analyze the background and subtract it from our resulting spectra.

We use blank-sky observations of the X-ray background from Markevitch et al. (2001) supplied within the CXC CALDB. First, we compare the flux from the diffuse soft X-ray background of the *ROSAT* All-Sky Survey (*RASS*) combined bands⁷ R12, R45, and R67 to the 0.7–7.0 keV flux in each extraction aperture for each observation. For the purpose of simplifying the subsequent analysis, we discarded observations with an R45 flux $\geq 10\%$ of the total cluster X-ray flux.

The appropriate blank-sky dataset for each observation was selected from the CALDB, reprocessed exactly as the observation, and then reprojected using the aspect solutions provided with each observation. For observations on the ACIS-I array, we constructed blank-sky backgrounds for chips I0-I3 plus chips S2 and/or S3. For ACIS-S observations, we created blank-sky backgrounds only for the S3 chip plus chips I2 and/or I3. The additional off-aimpoint chips were included only if they were active during the observation and had available blank-sky data sets for the observation time period. For observations which did not have a matching off-aimpoint blank-sky background in the CALDB a source-free region of the active chips is located and used for background normalization. Off-aimpoint chips were cleaned for point sources and diffuse sources using the method outlined in §3.1.

The additional off-aimpoint chips were included in data reduction since they contain data which is farther from the cluster center and are therefore more useful in analyzing the observation background. To normalize the hard particle component we measured fluxes for identical chips in the blank-sky field and target field in the 9.5–12.0 keV range. The effective area of the ACIS arrays above 9.5 keV is zero and thus the collected photons there are exclusively from the particle background.

A histogram of the ratios of the 9.5–12.0 keV count rate from an observation’s off-aimpoint chip to that of the observation specific blank-sky background are presented in Figure 2. The majority of the observations are in agreement to $\lesssim 20\%$ of the blank-sky background rate, which is small enough to not affect our analysis; regardless, we re-normalize all blank-sky backgrounds.

Normalization brings the observation background and blank-sky background into agreement for energies > 2 keV, but even after normalization, typically, there still exists a soft excess/deficit associated with the spatially varying soft Galactic background. Following the technique detailed in Vikhlinin et al. (2005) we construct and fit soft residuals for this component. For each observation we first compare the 0.3–2.0 keV flux of the blank-sky field and off-aimpoint field. We then subtract a spectrum of the blank-sky field from a spectrum of the off-aimpoint field to create a residual. The residual is fit with a solar abundance, zero redshift MeKaL model (Mewe et al. 1985, 1986; Kaastra 1992; Liedahl et al. 1995) where the normalization is allowed to be negative. The resulting best-fit temperatures for all of the soft residuals identified here were between 0.2–1.0 keV, which is in agreement with results of Vikhlinin et al. (2005). The normalization of this background component was then scaled to the cluster sky area. The re-

⁷ RASS combined bands give fluxes for energy ranges of 0.12–0.28 keV, 0.47–1.21 keV, and 0.76–2.04 keV respectively corresponding to R12, R45, and R67.

⁵ Available at <http://cxc.harvard.edu/contrib/maxim/acisbg/>

⁶ <http://cxc.harvard.edu/contrib/maxim/acisbg/COOKBOOK>

scaled component is included as a fixed background component during fitting of a cluster's spectra.

3.3. Notes for Individual Clusters

We find evidence for long duration soft flares in the observations of Abell 1758 (David & Kempner 2004), CL J2302.8+0844, and IRAS 09104+4109. These flares were handled by adding the XSPEC CUTOFFPL/b model during spectral analysis, freezing the spectral index at $\Gamma = -0.15$, freezing the high energy exponential cut-off at 5.6 keV, and allowing the normalization to be the only free parameter. This procedure follows directly from the recommendations of Markevitch et al. (2003). IRAS 09104+4109 presented a special, troubling circumstance which resulted in its removal from the sample.

4. SPECTRAL EXTRACTION

The simulated spectra calculated by ME01 were analyzed in the energy ranges 0.5–9.0 keV and 2.0_{rest} –9.0 keV, but to make a reliable comparison with *Chandra* data we restrict our focus to a full energy band, 0.7–7.0 keV, and a hard energy band, 2.0_{rest} –7.0 keV. We exclude data below 0.7 keV to avoid the effective area and quantum efficiency variations of the ACIS detectors, and exclude energies above 7.0 keV in which diffuse emission is dominated by the background and *Chandra*'s effective area is small. We also account for cosmic redshift by shifting our hard energy band from 2.0 keV to $2.0/(1+z)$ keV (henceforth, assume the 2.0 keV cut is in the rest frame unless otherwise stated).

ME01 calculated the relation between $T_{0.5-9.0}$ and $T_{2.0-9.0}$ using apertures of R_{200} and R_{500} in size. While it is trivial to calculate a temperature out to R_{200} or R_{500} from a simulation, such a measurement at these scales is extremely difficult with *Chandra* observations (see Vikhlinin et al. (2005) for a detailed explanation). However, in typical Chandra fields of view, apertures with $R = R_{200}$ or even R_{500} are not fully included. Thus we chose to extract spectra from regions with radius R_{2500} when possible and R_{5000} otherwise. Clusters analyzed only within R_{5000} are denoted in Table 1 by a dagger.

The cores of some clusters are dominated by cool cores which affect the global temperature, therefore we excise the central 70 kpc of each aperture. These excised apertures are denoted by “CORE” in the text. Recent work by Maughan (2007) has shown excising 0.15 R_{500} rather than 70 kpc reduces scatter in mass-observable scaling relations. But such a reduction does not effect this work as the conclusions drawn from our spectral analysis are strongly related to the uncertainties of $T_{2.0-7.0}$ and not on the best-fit value of $T_{0.7-7.0}$ where the effect of a cool core is the strongest.

Although some clusters are not circular in projection, but rather are elliptical or asymmetric, we find that extracting from a circular annulus does not significantly change the best-fit values. For another such example see Bauer et al. (2005).

After defining annular apertures, we extracted source spectra from the target cluster and background spectra from the corresponding normalized blank-sky dataset. By standard CIAO means we created effective area functions (ARF files) and redistribution matrices (RMF files) for each cluster using a flux-weighted map (WMAP) across the entire extraction region. The WMAP was calculated over the energy range 0.3–2.0 keV to weight calibrations that vary as a function of position on the chip. Each spectrum was then binned to contain a minimum of 25 counts per channel.

5. SPECTRAL ANALYSIS

5.1. Fitting

Spectra were fit with XSPEC 11.3.2ag (Arnaud 1996) using a single-temperature MeKaL model in combination with the photoelectric absorption model WABS (Morrison & McCammon 1983) for Galactic absorption. Galactic absorption values, N_{HI} , are taken from Dickey & Lockman (1990). The parameters which can be fit in the WABS (MeKaL) model are N_{HI} , X-ray temperature (T_X), metal abundance (Z/Z_\odot), and a normalization proportional to the integrated emission measure of the cluster. The spectra from clusters with multiple observations were fit simultaneously. Results from the fitting are presented in Table 4 and Table 5. No systematic error is added during fitting and thus all quoted errors are statistical only.

Additional statistical error is introduced into our fitting through inclusion of the soft local background component discussed in §3.2. To account for this error we use the differences between T_X of the model using the scaled normalization and T_X of the model using $\pm 1\sigma$ of the scaled normalization as the errors associated with this additional component. The statistical error and the error inferred from the range of normalization to the soft X-ray background component are then added in quadrature to produce a final error. In all cases this additional background error on the temperature is $\sim 10\%$ of the total statistical error and represents a minor inflation of the error budget.

In all fits the metal abundance is allowed to be free. When comparing fits using N_{HI} free and N_{HI} fixed we find the best-fit N_{HI} values did not significantly alter T_X or improve the goodness of fit, thus N_{HI} is fixed at the Galactic value with the exception of three cases: Abell 399 (Sakelliou & Ponman 2004), Abell 520, and Hercules A.

After fitting we reject several datasets as their best-fit $T_{2.0-7.0}$ had no upper bound in the 90% confidence interval and thus we gain nothing from their inclusion in the final analysis. All R_{5000} and R_{5000} -CORE fits of the clusters Abell 781, Abell 1682, CL J1213+0253, CL J1641+4001, MS 0302.7+1658, RX J1053+5735, and RX J1525+0958 are rejected; we also reject all fits for R_{2500} and R_{2500} -CORE apertures of Lynx E and MACS J1824.3+4309.

5.2. Simulated Spectra

To quantify the effect a second, cooler gas component has on a single-phase spectral model, we used the fakeit command within XSPEC to create an ensemble of simulated spectra for our entire sample. With these simulated spectra we are attempting to answer the question: How bright must a second temperature component be to see it in the 2.0–7.0 over the 0.7–7.0 keV bandpass? Put another way, we are asking at what flux ratio a second gas phase skews T_{HFR} to greater than unity at the 1σ level.

We began by convolving the observation-specific background, ARF, and RMF with a WABS (MeKaL₁+MeKaL₂) model for a time period equal to the observation exposure time and adding Poisson noise. We define the MeKaL₁ component to have the best-fit temperature and metallicity of the R_{2500} -CORE, 0.7–7.0 keV fit for that observation.

For each realization of an observation's simulated spectrum, we vary the MeKaL₂ component temperature over values 0.5, 0.75, and 1.0 keV. The MeKaL₂ metallicity is assumed to be equal to the value of MeKaL₁.

We adjust the normalization of the simulated two-

component spectra to achieve equivalent count rates to that in the real spectra. We increment the MeKaL₁ normalization, K_1 , away from the best-fit value by a prescribed factor, ξ , while leaving the MeKaL₂ normalization, K_2 , free. We explore a wide variety of K_2 by using ξ values of 0.8, 0.85, 0.9, 0.95, 0.96, 0.97, 0.98, and 0.99 K_1 .

We also simulate a control sample of single-temperature models. The control sample is essentially a simulated version of the best-fit model. This control provides us with a check of how often a hard component temperature might differ from a broad-band temperature statistically (i.e. calibration effects under control).

For each observation, we have 59 total simulated spectra—35 single-temperature control spectra and 24 two-component simulated spectra (three second temperatures, each with 8 different ξ). Our resulting simulated spectra ensemble contains 11269 spectra. After generating all the spectra we follow the same fitting routine detailed in §5.1.

There are two important results taken away from the analysis of these simulated spectra:

1. A single temperature component rarely (frequency $\sim 2\%$) gives a significantly different $T_{0.7-7.0}$ and $T_{2.0-7.0}$ temperature as demonstrated with the control sample shown in the first panel of Figure 3. The two real data distributions are qualitatively in agreement with the distribution of the multicomponent simulated distribution, while the control sample distribution is roughly Gaussian and peaked around $T_{HFR} = 1.0$. ~~This is a strong indication the calibration of *Chandra* is under control and will not be the driver for any measured temperature skew.~~

2. A significantly bright second temperature component, for example $\xi > 0.96$ where ~~the effect of a second spectral temperature diminishes to < 10%~~, must be present in order to get significant deviations of T_{HFR} from 1.0 as large as 1.1–1.2, as seen in the real data. Figure 4 highlights this fact further. Even in the extreme case of a second component only accounting for 1% of the observed flux, the weighted-average of T_{HFR} registers a skew of 1.06 ± 0.005 . The control sample however has a T_{HFR} weighted-average of 1.00 ± 0.001 .

6. RESULTS AND DISCUSSION

6.1. Temperature Ratios

We estimate a temperature ratio $T_{HFR} = T_{2.0-7.0} / T_{0.7-7.0}$ for each cluster. We find a clear departure of the mean T_{HFR} from unity for our entire sample at greater than 11σ . The weighted mean values for our sample are shown in Table 2. Presented in Figure 5 are the binned weighted-means and raw T_{HFR} values of R₂₅₀₀-CORE and R₅₀₀₀-CORE. Each bin contains 25 clusters with the exception of the highest temperature bins which have 6 and 20 for the R₂₅₀₀-CORE and R₅₀₀₀-CORE, respectively. The peculiar points with $T_{HFR} < 1$ are all statistically consistent with $T_{HFR} = 1$. In addition, ratios less than one in the real data occur at nearly the same frequency in the simulated data, $\sim 0.3\%$, suggesting that these ratios are consistent with statistical uncertainties in the data. The presence of clusters where $T_{HFR} = 1$ suggests that the calibration is not the sole reason for deviations of T_{HFR} from 1. We also do not find the temperature ratio depends on the best-fit full-band temperature.

The uncertainty associated with each value of T_{HFR} is dominated by the larger error in $T_{2.0-7.0}$, and on average, $\Delta T_{2.0-7.0} \approx 2.3\Delta T_{0.7-7.0}$. This error interval discrepancy naturally results from excluding the bulk of a cluster's emission occurring below 2 keV. While choosing a temperature-sensitive cut-off energy for the hard-band (other than 2.0_{rest} keV) might main-

tain a more consistent error budget across our sample (see Figure 6), we do not find any systematic TREND in the ratio with cluster temperature.

6.2. Systematics

Aside from instrumental and calibration effects there may be additional systematics in our analysis which do not present themselves on an individual basis but emerge as underlying trends in the sample as a whole. Three possible sources of these systematics are signal-to-noise (S/N), redshift selection, and Galactic absorption. Presented in Figure 7 are these three parameters versus T_{HFR} . The trend in T_{HFR} with redshift is expected as the $2.0/(1+z)$ keV hard-band lower boundary nears convergence with the 0.7 keV full-band lower boundary which occurs at $z \sim 1.85$. We find no systematic trends with S/N or Galactic absorption, which might occur if the ratio skew were a consequence of poor calibration. ~~Also shown in panel four of Fig. 7 is a comparison of the best-fit results for R₂₅₀₀-CORE and R₅₀₀₀-CORE. Our results are robust at the 1σ level against change in aperture size.~~

Shown in Figure 8 is the ratio of ASCA temperatures taken from Don Horner's thesis to *Chandra* temperatures derived in this work. Not all of our sample clusters have an ASCA temperature, but a sufficient number (57) are available to make this comparison reliable. Apertures used in the extraction of ASCA spectra had no core region removed and were substantially larger than R₂₅₀₀. Thus we compare the unexcised R₂₅₀₀ temperatures as it gets us the closest to replicating the ASCA apertures. We note a trend of comparatively hotter *Chandra* temperatures for clusters > 10 keV.

If we exclude the hottest clusters ($T_X > 10$ keV where ASCA and *Chandra* disagree) from our sample, the mean temperature ratio for the sample remains 1.16 and the error increases from ± 0.014 to ± 0.015 for R₂₅₀₀-CORE; T_{HFR} increases by 0.9% for R₅₀₀₀-CORE from 1.14 ± 0.013 to 1.15 ± 0.014 . Our results are not being influenced by the inclusion of hot clusters.

6.3. Using T_{HFR} to Select for Relaxation

6.3.1. Cool Core Versus Non-Cool Core

The process of virialization may robustly result in the formation of a cool core (Ota et al. 2006). Flux-limited surveys have found the prevalence of CCs to be 34–60% (White et al. 1997; Peres et al. 1998; Bauer et al. 2005; Chen et al. 2007) depending upon definition, completeness, and possible selection biases. As discussed in §1, ME01 give us reason to believe the observed skewing of T_{HFR} to greater than unity is related to the dynamic state of a cluster. We thus seek to identify which clusters in our sample have cool cores (CC), which have (NCC), and if the presence or absence of a cool core is correlated to T_{HFR} . We also ask about the number of cool core (CC) and non-cool core (NCC) clusters as a function of T_{HFR} . Recall that we exclude the cool core itself from the cluster spectrum.

To identify a CC cluster, we extract spectra for a 50 kpc region surrounding the cluster center, then we define a temperature decrement using the ratio of temperatures for the inner 50 kpc, T_{50} , and the R₂₅₀₀-CORE aperture, $T_{dec} = T_{50} / T_{R_{5000}-CORE}$ (clusters without R₂₅₀₀-CORE fits are excluded from this analysis). When finding T_{50} we alter the fitting method outlined in §5.1 to use XSPEC's modified Cash statistic (Cash 1979), $cstat$, on ungrouped spectra. This choice is made because the distribution of counts per bin in low count spectra is not

Gaussian but instead Poisson. As a result the best-fit temperature using χ^2 is typically cooler (Nousek & Shue 1989; Balestra et al. 2007). We have explored this systematic in *all* our fits and only found it to be significant in the lowest count spectra of the inner 50 kpc apertures discussed here. But for consistency, we fit all inner 50 kpc spectra using the modified Cash statistic.

If $T_{dec} < 1$ at the 2σ level then we define it as a CC cluster, otherwise it is a NCC cluster. We find CCs in 46% of our sample using 1σ and 35% using 2σ thus indicating we are consistent with more detailed studies of CC/NCC populations.

With each cluster classified we then take cuts in T_{HFR} at the 1σ level and ask how many CC and NCC clusters are above these cuts. Figure 9 shows the normalized number of CC and NCC clusters as a function of cuts in T_{HFR} . If T_{HFR} were insensitive to the dynamical state of a cluster we would expect, for normally distributed T_{HFR} values, to see the number of CC and NCC clusters monotonically decreasing. However, the number of CC clusters falls off more rapidly than the number of NCC clusters. This effect is dramatically reduced - as expected - if the core is included. All curves demonstrate linear behavior in the region $0.9 \leq T_{HFR,cut} \leq 1.2$. The slope of the linear curve segment for R_{2500} -CORE CC is -3.10 ± 0.26 and for NCC is -2.41 ± 0.07 . For R_{5000} -CORE the CC slope is -2.55 ± 0.21 and for NCC is -2.37 ± 0.13 . All fits have excellent goodness of fit. This steeper fall-off of CCs indicates the contribution of soft emission is indeed playing a role in affecting T_{HFR} . This result is insensitive to our choice of significance level in both the core classification and T_{HFR} cuts.

However, cluster redshift is playing a role in our ability to classify CCs and NCCs. As redshift increases cool gas is shifted out of the observable X-ray band and we lose spectral information about the core which would aid in its classification. An analog of this effect can be seen in our spectral simulations. Shown in Figure 10 is T_{HFR} plotted against redshift. The first three panels of Fig. 10 are the most interesting as they clearly show this effect in the extreme cases of a second, cooler temperature component which is 10–20% the brightness of the hot gas phase. At redshifts > 0.6 T_{HFR} begins to scatter about unity and a skew in T_{HFR} only shows up under weight averaging making a cluster by cluster detection of the coolest cluster gas difficult. Thus we are likely not detecting weak CCs in the highest redshift clusters of our sample.

Because of the CC/NCC definition we've selected, our identification of CCs and NCCs is only as robust as the errors on T_{50} allow. One can thus ask the question, does our loose definition bias us towards finding more NCCs than CCs? Aside from the redshift effect, how often would a CC be classified as a NCC because of low S/N? To explore these questions we simulated 20 spectra for each observation following the method outlined in §5.2 for the control sample but using the inner 50 kpc spectral best-fit values as input. For each simulated spectrum we then calculate the temperature decrement as described above and re-classify the cluster as a CC or NCC. These classifications based on simulated data are then compared to the classification made from the real data. Based on this comparison we can assign a reliability factor to each real classification. This reliability factor is simply the percent of simulated spectra which agree with the real classification. Values of 1.0 mean complete agreement and 0.0 mean no agreement.

If we remove clusters with reliability factors less than 0.9 and repeat the analysis above we find no significant change in the number of CC clusters as a function of T_{HFR} .

6.3.2. Mergers Versus Non-Mergers

We further define a subclass of NCC clusters as known mergers. Known mergers are NCC clusters which have been identified as mergers in the cluster literature. From Figure 11 we can see clusters exhibiting the highest significant values of T_{HFR} are all ongoing or recent mergers. At the 2σ level, we find increasing values of T_{HFR} favor merger systems with NCCs over relaxed, CC clusters. Mergers have left a spectroscopic imprint on the ICM which is predicted by ME01 and which we observe in our sample.

To further investigate T_{HFR} we list the identities of clusters with $T_{frac} > 1.1$ at the 1σ level. These are presented in Table 3. Of the 29 clusters, only six have CCs. Three of those, MKW3S, 3C 28.0, and RX J1720.1+2638 have their apertures centered on the bright, dense cores in confirmed mergers. Two more clusters, Abell 2384 and RX J1525+0958, while unconfirmed mergers have morphologies which are consistent with powerful ongoing mergers. Abell 2384 has a long gas tail extending out to a gaseous clump which has presumably passed through the cluster recently. RXJ1525 has a core which is shaped like an arrowhead and is reminiscent of the bow shock seen in 1E0657-56. Abell 907 is the remaining CC of the six listed. It has no signs of being a merger system but the highly compressed surface brightness contours to the west of the core are indicative of a prominent cold front which are tell-tale signs of a subcluster merger event (Markevitch & Vikhlinin 2007).

The unclassified systems, RX J0439.0+0715, MACS J2243.3-0935, MACS J0547.0-3904, ZWCL 1215, MACS J2311+0338, and Abell 267, have NCCs and X-ray morphologies consistent with an ongoing or post-merger scenario. Two clusters, Abell 1204 and MACS J1427.6-2521, show no signs of recent or ongoing merger activity, however, they reside at the bottom of the arbitrary T_{HFR} cut, and as evidenced by Abell 401 and Abell 1689, exceptional spherical symmetry is no guarantee of relaxation.

Returning to the discussion in §6.3.1, we find no cluster with $T_{HFR} > 1.1$ has a reliability factor < 0.9 . The correlation of T_{HFR} with a cluster's dynamical state is robust.

7. SUMMARY AND CONCLUSIONS

We have explored the band-dependence of the inferred X-ray temperature of the intracluster medium (ICM) for 179 well-observed ($N_{counts} > 1500$) clusters of galaxies selected from the Chandra data archive.

We extracted spectra from the annulus between $R = 70$ kpc and $R = R_{2500}$, R_{5000} for each cluster. We compare the X-ray temperatures inferred for single-temperature fits to global spectra when the energy range of the fit is 0.7–7.0 keV (full) and when the energy range is 2.0/(1+z)-7.0 keV (hard). We find that, on average, the hard-band temperature is significantly higher than the full-band temperature. Upon further exploration, we find that the ratio T_{HFR} is enhanced preferentially for clusters which are known merger systems and for clusters which are isothermal. Clusters with temperature decrements in their cores (known as cool-core clusters) tend to have best-fit hard-band temperatures that are statistically consistent with their best fit full-band temperatures.

As was the original motivation from ME01, we suggest T_{HFR} can be utilized as an indicator for the degree of relaxation/virialization. A test for this prediction can be made with simulations by tracking T_{HFR} during hierarchical assembly of clusters.

If T_{HFR} is correlated with a cluster's degree of relaxation

then along with other methods of substructure measure, such as power ratio, axial ratio, and centroid shift, we can assemble a powerful metric for measuring a cluster's expected deviation from mean scaling relations such as L_X - T_X and L_X - M . Because T_{HFR} is aspect independent this metric will have two components, spatial and spectroscopic, by adding spectroscopic information to our understanding of cluster virialization we may be able to reduce the scatter introduced into observational studies of scaling relations which will in turn yield smaller uncertainties in cosmological studies. However, to reach such a lofty goal we need to expand our observational sample and begin getting information about the underlying distribution of T_{HFR} and the intrinsic scatter in T_{HFR} which was not possible with this sample.

This work was supported through *Chandra* grant XXX-

REFERENCES

- Andersson, K. E., & Madejski, G. M. 2004, ApJ, 607, 190
 Arnaud, K. A. 1996, in ASP Conf. Ser. 101: Astronomical Data Analysis Software and Systems V, ed. G. H. Jacoby & J. Barnes, 17–+
 Arnaud, M., Aghanim, N., & Neumann, D. M. 2002, A&A, 389, 1
 Bagchi, J., Durret, F., Neto, G. B. L., & Paul, S. 2006, Science, 314, 791
 Balestra, I., Tozzi, P., Ettori, S., Rosati, P., Borgani, S., Mainieri, V., Norman, C., & Viola, M. 2007, A&A, 462, 429
 Bauer, F. E., Fabian, A. C., Sanders, J. S., Allen, S. W., & Johnstone, R. M. 2005, MNRAS, 359, 1481
 Bliton, M., Rizza, E., Burns, J. O., Owen, F. N., & Ledlow, M. J. 1998, MNRAS, 301, 609
 Böhringer, H., Schuecker, P., Guzzo, L., Collins, C. A., Voges, W., Crudace, R. G., Ortiz-Gil, A., Chincarini, G., De Grandi, S., Edge, A. C., MacGillivray, H. T., Neumann, D. M., Schindler, S., & Shaver, P. 2004, A&A, 425, 367
 Buote, D. A., & Tsai, J. C. 1995, ApJ, 452, 522
 —. 1996, ApJ, 458, 27
 Burns, J. O., Roettiger, K., Pinkney, J., Perley, R. A., Owen, F. N., & Voges, W. 1995, ApJ, 446, 583
 Cash, W. 1979, ApJ, 228, 939
 Chen, Y., Reiprich, T. H., Böhringer, H., Ikebe, Y., & Zhang, Y.-Y. 2007, A&A, 466, 805
 Dahle, H., Kaiser, N., Irgens, R. J., Lilje, P. B., & Maddox, S. J. 2002, ApJS, 139, 313
 David, L. P., & Kempner, J. 2004, ApJ, 613, 831
 Dickey, J. M., & Lockman, F. J. 1990, ARA&A, 28, 215
 Ebeling, H., Edge, A. C., Allen, S. W., Crawford, C. S., Fabian, A. C., & Huchra, J. P. 2000, MNRAS, 318, 333
 Ebeling, H., Edge, A. C., Böhringer, H., Allen, S. W., Crawford, C. S., Fabian, A. C., Voges, W., & Huchra, J. P. 1998, MNRAS, 301, 881
 Ebeling, H., Edge, A. C., & Henry, J. P. 2001, ApJ, 553, 668
 Edge, A. C., Stewart, G. C., Fabian, A. C., & Arnaud, K. A. 1990, MNRAS, 245, 559
 Eisenstein, D. J., Zehavi, I., Hogg, D. W., Scoccimarro, R., Blanton, M. R., Nichol, R. C., Scranton, R., Seo, H.-J., Tegmark, M., Zheng, Z., Anderson, S. F., Annis, J., Bahcall, N., Brinkmann, J., Burles, S., Castander, F. J., Connolly, A., Csabai, I., Doi, M., Fukugita, M., Frieman, J. A., Glazebrook, K., Gunn, J. E., Hendry, J. S., Hennessy, G., Ivezić, Z., Kent, S., Knapp, G. R., Lin, H., Loh, Y.-S., Lupton, R. H., Margon, B., McKay, T. A., Meiksin, A., Munn, J. A., Pope, A., Richmond, M. W., Schlegel, D., Schneider, D. P., Shimasaku, K., Stoughton, C., Strauss, M. A., SubbaRao, M., Szalay, A. S., Szapudi, I., Tucker, D. L., Yanny, B., & York, D. G. 2005, ApJ, 633, 560
 Ettori, S., & Lombardi, M. 2003, A&A, 398, L5
 Evrard, A. E. 1989, ApJ, 341, L71
 —. 1990, ApJ, 363, 349
 Evrard, A. E., Metzler, C. A., & Navarro, J. F. 1996, ApJ, 469, 494
 Feretti, L., Boehringer, H., Giovannini, G., & Neumann, D. 1997, A&A, 317, 432
 Freeman, P. E., Kashyap, V., Rosner, R., & Lamb, D. Q. 2002, ApJS, 138, 185
 Gioia, I. M., Maccacaro, T., Geller, M. J., Huchra, J. P., Stocke, J., & Steiner, J. E. 1982, ApJ, 255, L17
 Gioia, I. M., Maccacaro, T., Schild, R. E., Wolter, A., Stocke, J. T., Morris, S. L., & Henry, J. P. 1990, ApJS, 72, 567
 YY-123456. We thank the Chandra X-Ray Observatory Science Center, operated for the National Aeronautics and Space Administration (NASA) by the Smithsonian Astrophysical Observatory (SAO), for maintaining the Chandra Data Archive (CDA) and for supplying and supporting the Chandra Interactive Analysis of Observations (CIAO) software and Calibration Database (CALDB). This project also utilized the NASA/IPAC Extragalactic Database (NED), which is operated by the Jet Propulsion Laboratory, California Institute of Technology, under contract with NASA, and of NASA's Astrophysical Data System Bibliographic Services. We also extend a special thanks to Keith Arnaud for personally providing support for XSPEC, obtained from the High Energy Astrophysics Science Archive Research Center (HEASARC) and supported by NASA's Goddard Space Flight Center.

- Riess, A. G., Filippenko, A. V., Challis, P., Clocchiatti, A., Diercks, A., Garnavich, P. M., Gilliland, R. L., Hogan, C. J., Jha, S., Kirshner, R. P., Leibundgut, B., Phillips, M. M., Reiss, D., Schmidt, B. P., Schommer, R. A., Smith, R. C., Spyromilio, J., Stubbs, C., Suntzeff, N. B., & Tonry, J. 1998, AJ, 116, 1009
- Riess, A. G., Strolger, L.-G., Casertano, S., Ferguson, H. C., Mobasher, B., Gold, B., Challis, P. J., Filippenko, A. V., Jha, S., Li, W., Tonry, J., Foley, R., Kirshner, R. P., Dickinson, M., MacDonald, E., Eisenstein, D., Livio, M., Younger, J., Xu, C., Dahlén, T., & Stern, D. 2007, ApJ, 659, 98
- Rosati, P., della Ceca, R., Burg, R., Norman, C., & Giacconi, R. 1995, ApJ, 445, L11
- Sakelliou, I., & Ponman, T. J. 2004, MNRAS, 351, 1439
- Sanderson, A. J. R., Ponman, T. J., & O'Sullivan, E. 2006, MNRAS, 1068
- Smith, G. P., Kneib, J.-P., Smail, I., Mazzotta, P., Ebeling, H., & Czoske, O. 2005, MNRAS, 359, 417
- Teague, P. F., Carter, D., & Gray, P. M. 1990, ApJS, 72, 715
- Townsley, L. K., Broos, P. S., Garmire, G. P., & Nousek, J. A. 2000, ApJ, 534, L139
- Tucker, W., Blanco, P., Rappoport, S., David, L., Fabricant, D., Falco, E. E., Forman, W., Dressler, A., & Ramella, M. 1998, ApJ, 496, L5+
- Vikhlinin, A. 2006, ApJ, 640, 710
- Vikhlinin, A., Markevitch, M., Murray, S. S., Jones, C., Forman, W., & Van Speybroeck, L. 2005, ApJ, 628, 655
- Vikhlinin, A., McNamara, B. R., Forman, W., Jones, C., Quintana, H., & Hornstrup, A. 1998, ApJ, 502, 558
- Voit, G. M. 2005, Reviews of Modern Physics, 77, 207
- Wang, L., & Steinhardt, P. J. 1998, ApJ, 508, 483
- Wang, S., Khouri, J., Haiman, Z., & May, M. 2004, Phys. Rev. D, 70, 123008
- White, D. A., Jones, C., & Forman, W. 1997, MNRAS, 292, 419
- Yang, Y., Huo, Z., Zhou, X., Xue, S., Mao, S., Ma, J., & Chen, J. 2004, ApJ, 614, 692
- Yuan, Q.-R., Yan, P.-F., Yang, Y.-B., & Zhou, X. 2005, Chinese Journal of Astronomy and Astrophysics, 5, 126

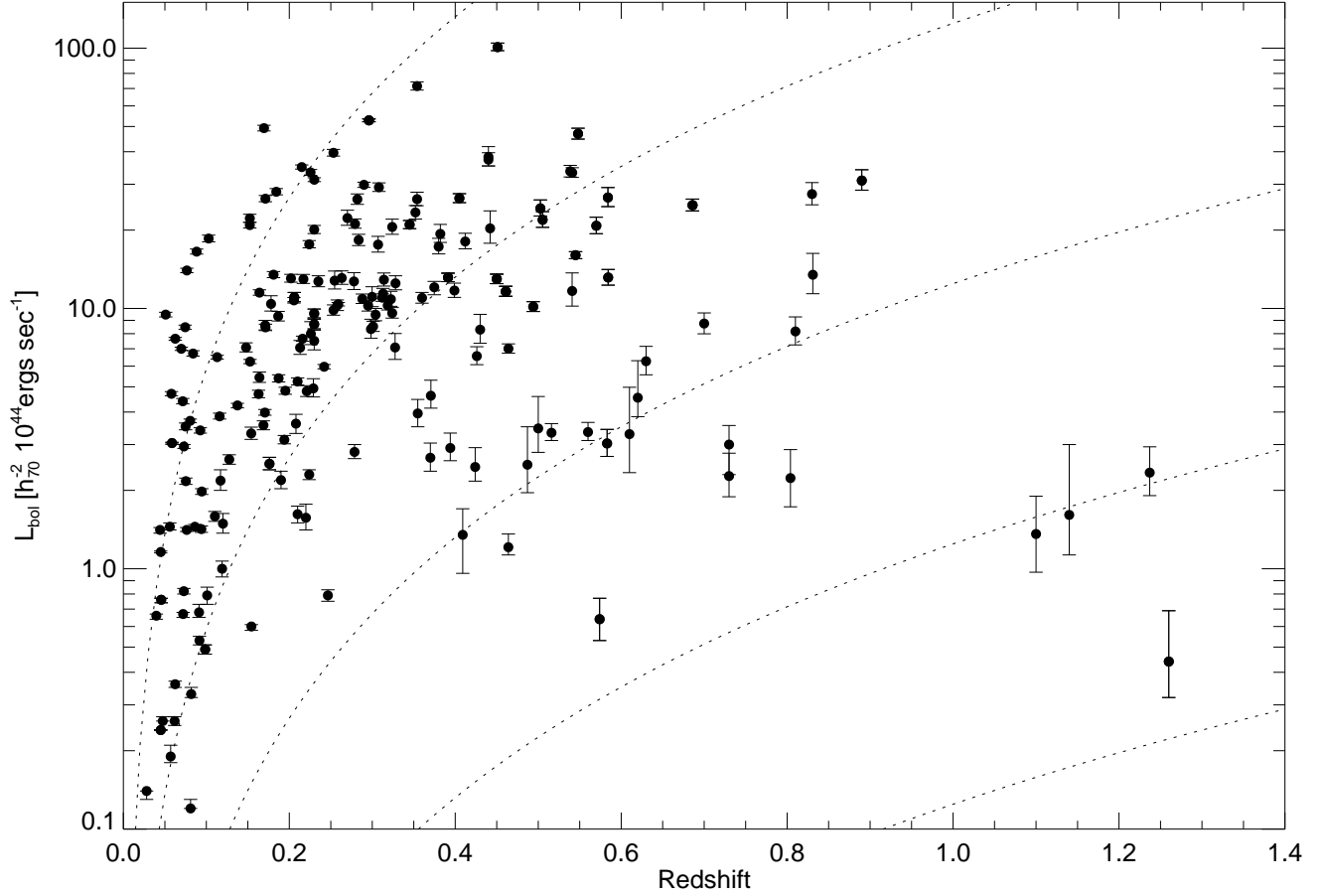


FIG. 1.— Bolometric luminosity ($E = 0.1 - 100$ keV) plotted as a function of redshift for the full sample. L_{bol} values are limited to the region of spectral extraction $R=R_{2500-\text{CORE}}$, or $R=R_{5000-\text{CORE}}$ for clusters without R_{2500} fits). Dotted lines represent constant fluxes of 3.0×10^{-15} , 10^{-14} , 10^{-13} , and 10^{-12} ergs sec $^{-1}$ cm $^{-2}$.

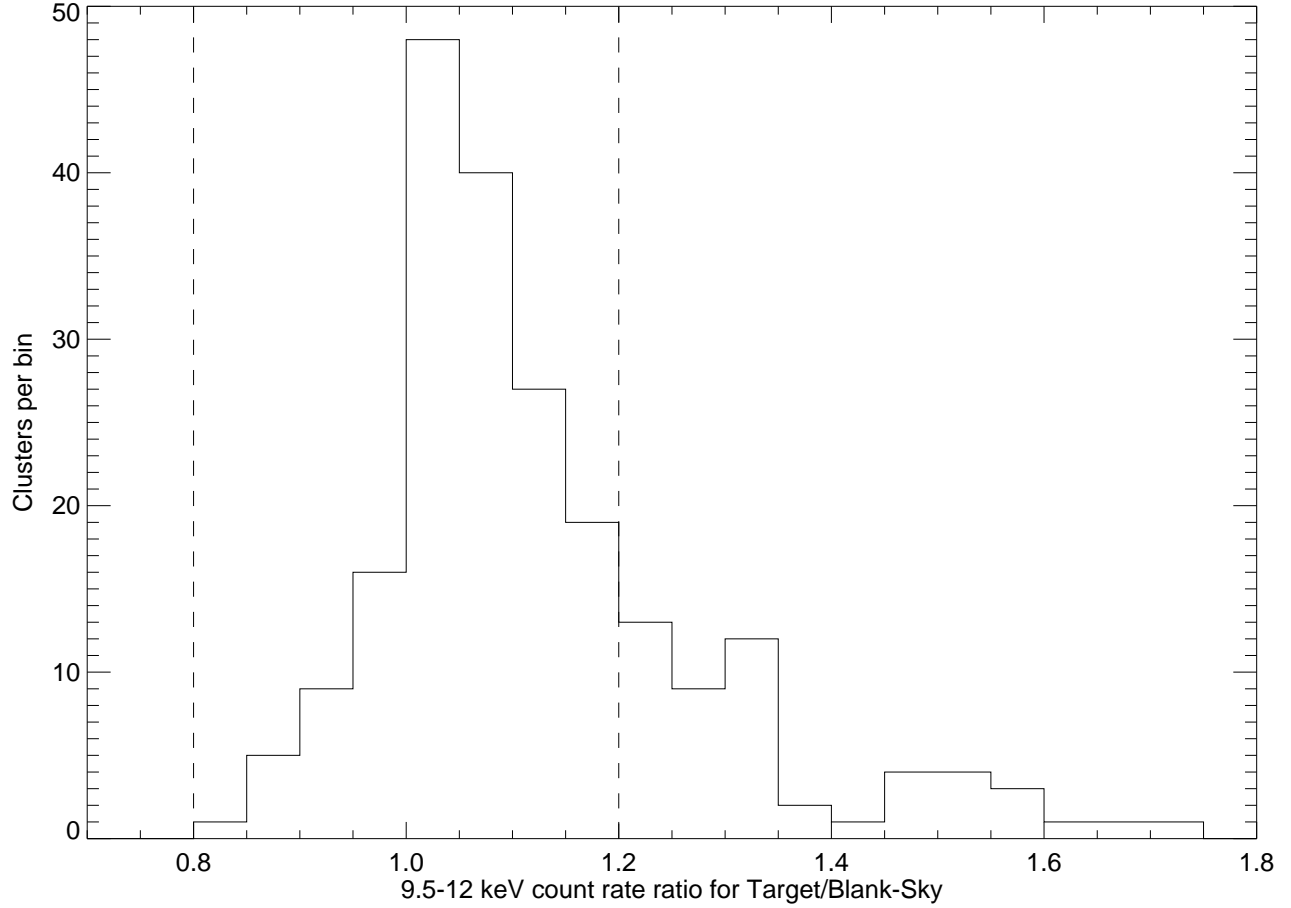


FIG. 2.— Ratio of target field and blank-sky field count rates in the 9.5-12.0 keV band for each observation. Vertical dashed lines represent $\pm 20\%$ of unity.

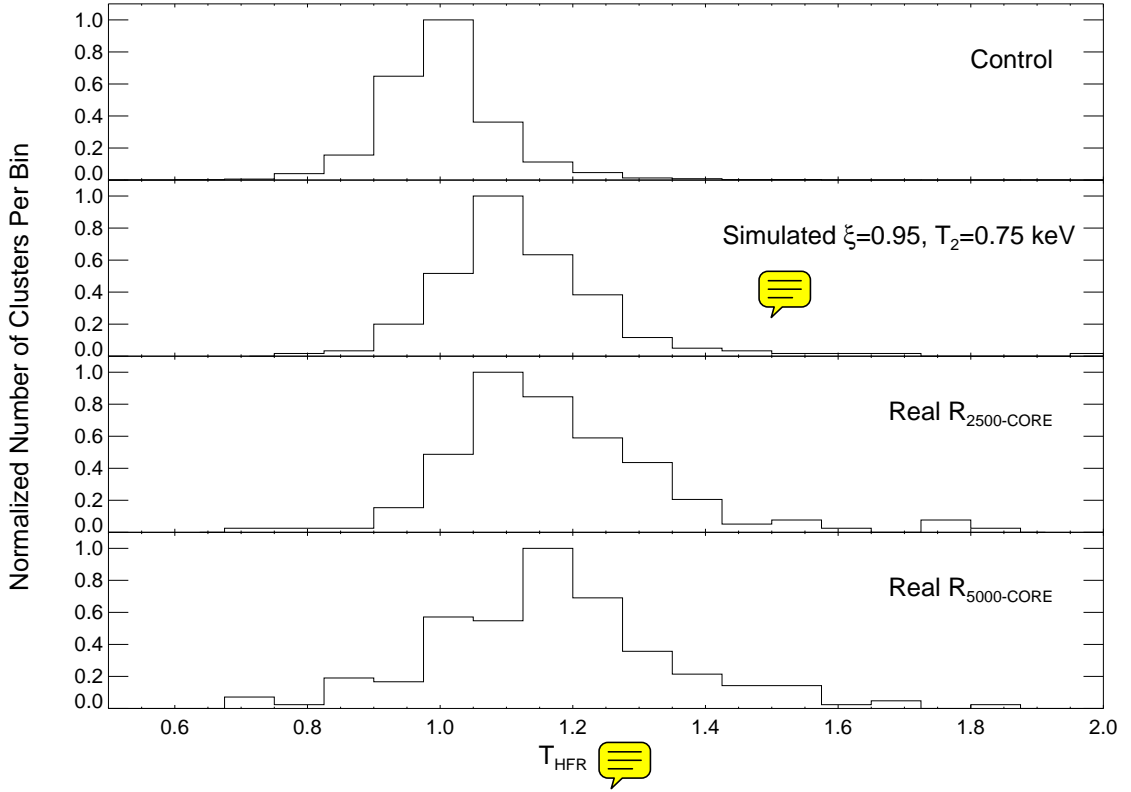


FIG. 3.— Normalized distributions for the control, simulated, $R_{2500\text{-CORE}}$, and $R_{5000\text{-CORE}}$ samples as a function of T_{HFR} . The Simulated distribution is culled to only include spectra for $\xi = 0.95$ and $T_2 = 0.75$ keV (see §5.2 for discussion). Bins are 0.075 in width.

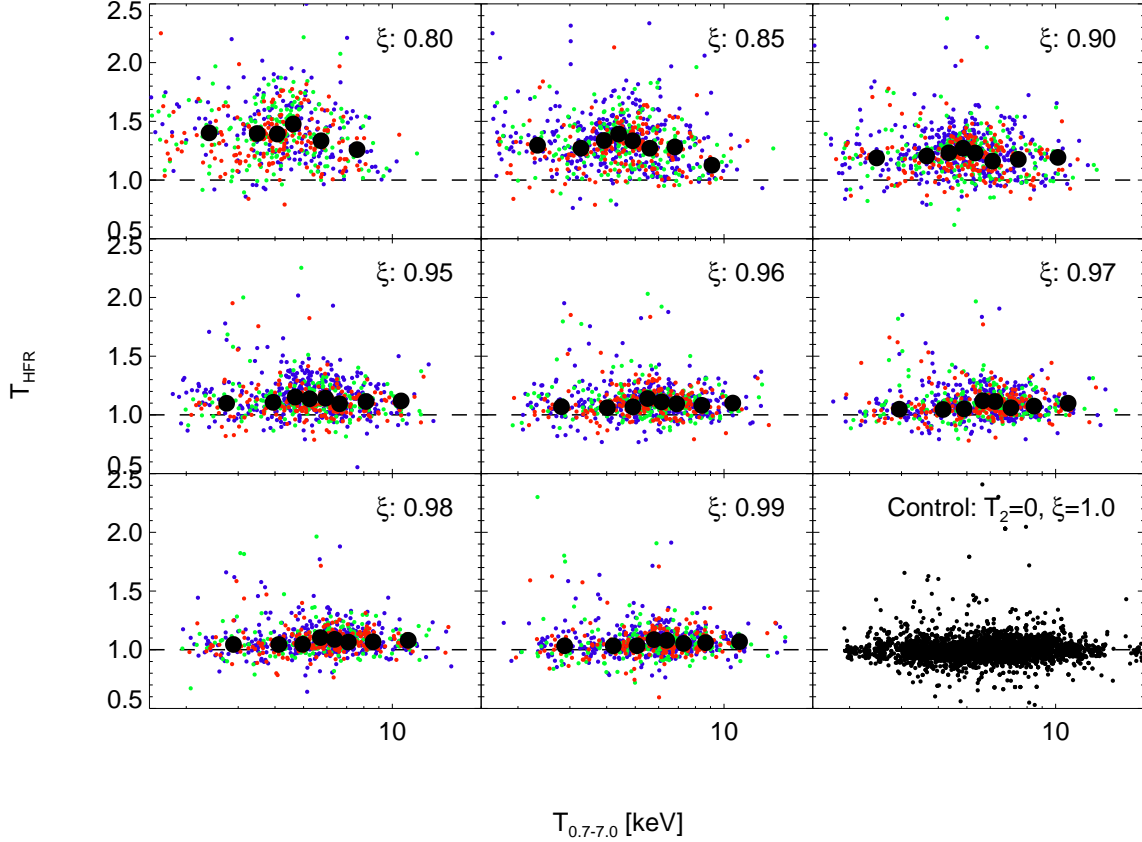


FIG. 4.— T_{HFR} plotted as a function of $T_{0.7-7.0}$ for our ensemble of simulated spectra. Each panel contains the fits for all three T_2 values (blue=0.5 keV, green=0.75 keV, and red=1.0 keV) of a specific ξ . Recall ξ is the factor by which the best-fit normalizations of the real spectra are adjusted. The last panel is for the control sample which has no T_2 and $\xi = 1.0$. Solid black circles are the weight-averaged values for bins containing 100 data points. The dashed line represents unity.

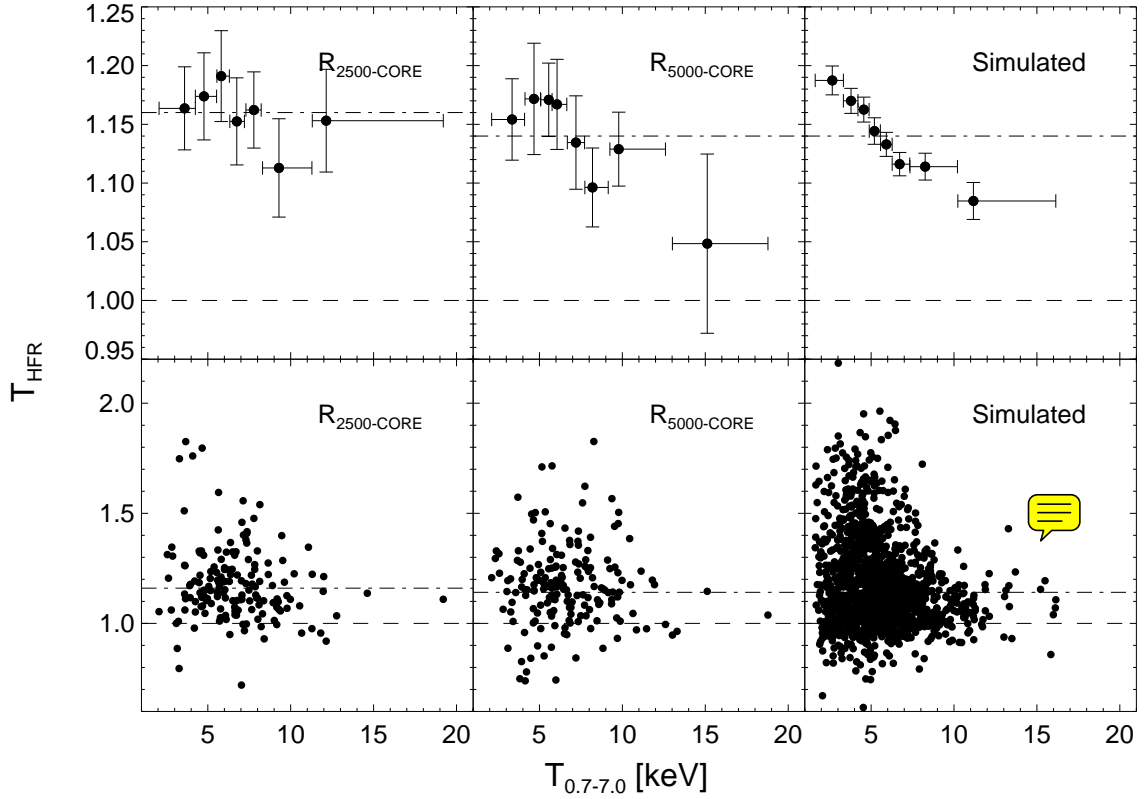


FIG. 5.— Best-fit temperatures for the hard bandpass, $T_{2.0-7.0}$, divided by the full bandpass, $T_{0.7-7.0}$ plotted against the full bandpass temperature. For binned data, each bin contains 25 clusters, with the exception of the highest temperature bins which contain 6 and 20 for $R_{2500-\text{CORE}}$ and $R_{5000-\text{CORE}}$, respectively. The simulated data bins contain 200 clusters with the last bin having 120 clusters. The line of equality is shown as a dashed line and the weighted mean for the full sample is shown as a dashed-dotted line. Error bars are omitted in the unbinned data for clarity.

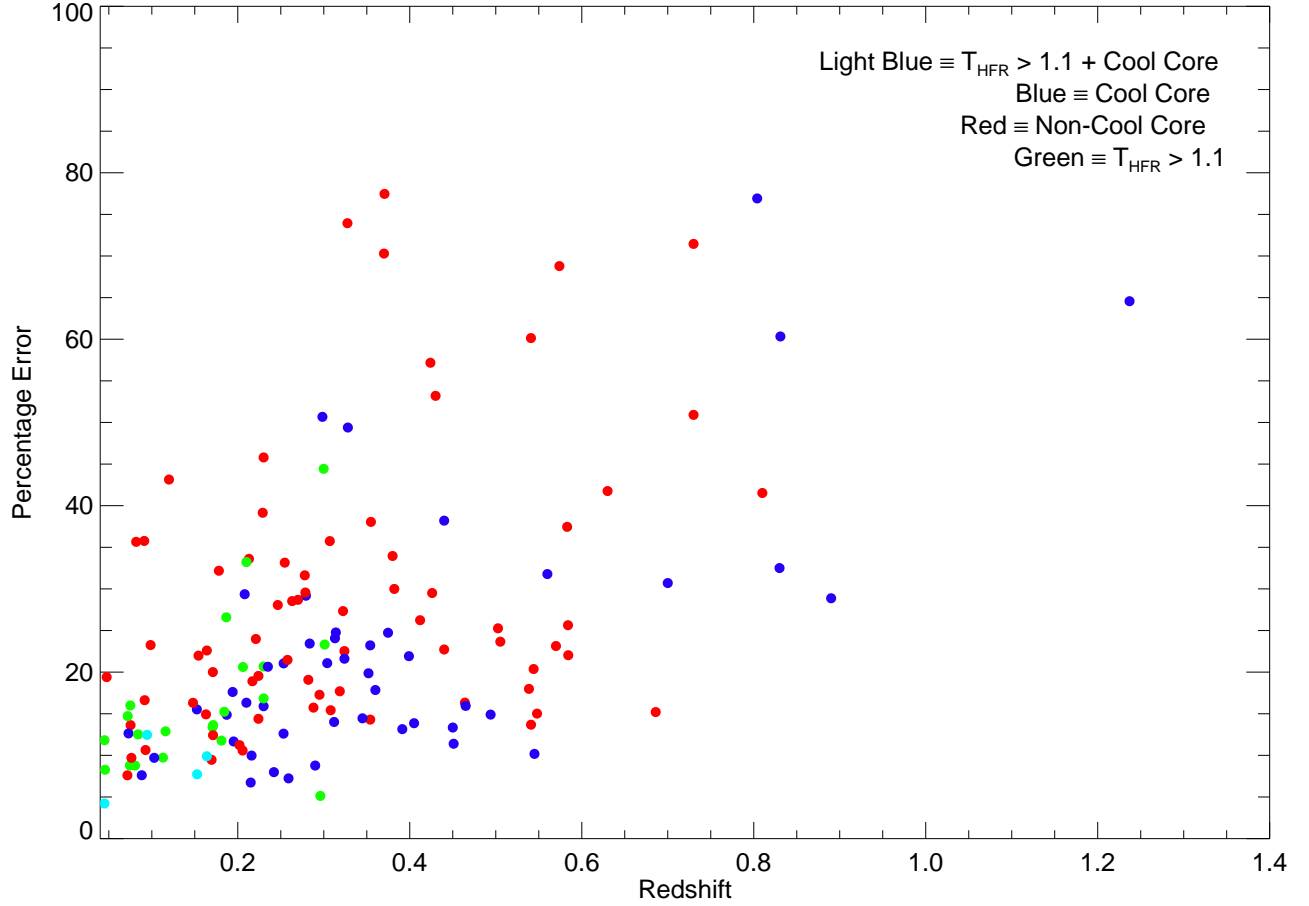


FIG. 6.— Percentage error of T_{HFR} plotted against redshift. The error budget across our sample is a function of redshift. As z increases, $2.0/(1+z)$ approaches 0.7 keV and the uncertainty in T_{HFR} accordingly increases. A temperature sensitive cut-off may create more consistent errors but more importantly we find no trends in T_{HFR} with cluster temperature. 

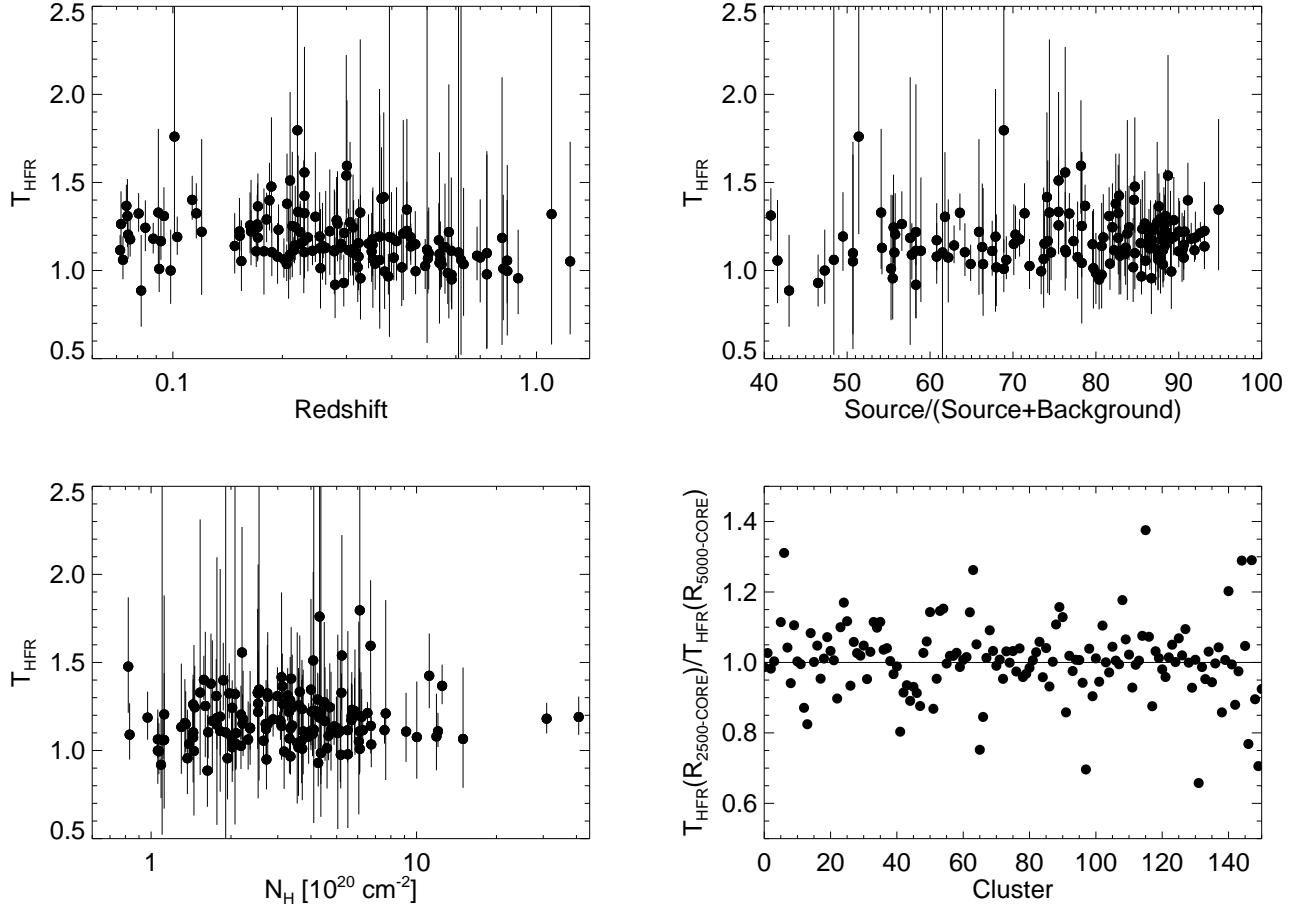


FIG. 7.— Three possible sources of systematics are plotted versus T_{HFR} plus a comparison of T_{HFR} for our two physically motivated apertures, R_{2500} and R_{5000} . Error bars have been omitted in the last plot for clarity as they all cross the line of equality. The trend in T_{HFR} with redshift is expected as the $2.0/(1+z)$ keV hard band lower boundary nears convergence with the 0.7 full band lower boundary which occurs at $z \sim 1.85$. We find no other trends in the plotted relations.

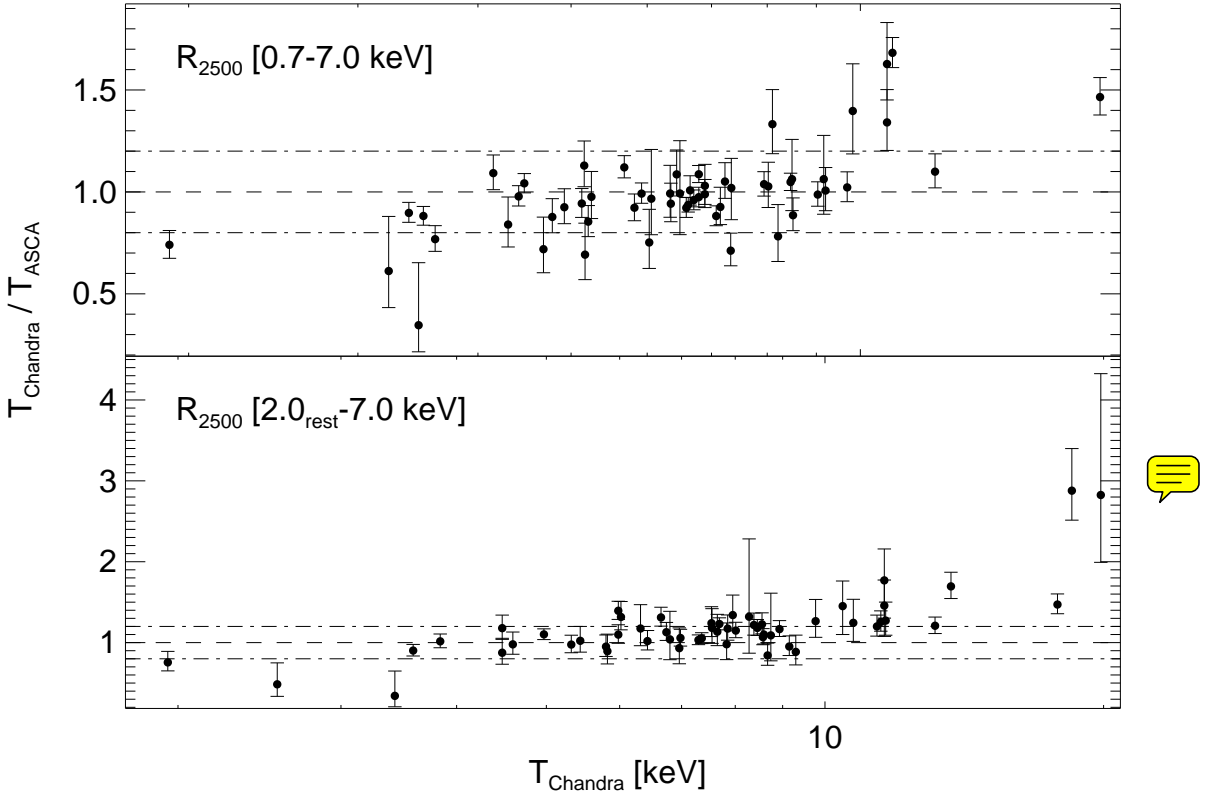


FIG. 8.— Ratio of *Chandra* temperatures derived in this work to *ASCA* temperatures taken from Don Horner’s thesis. We note a trend of hotter *Chandra* temperatures for clusters $> 10 \text{ keV}$. Excluding these hot clusters from our analysis does not effect the results. We are not being influenced by the presence of clusters with $T_X > 10 \text{ keV}$. The spurious point below 0.5 is MS 2053.7-0449 which has a poorly constrained *ASCA* temperature. Our derived temperature of $\sim 3.5 \text{ keV}$ is in agreement with recent work of Maughan et al. (2007).

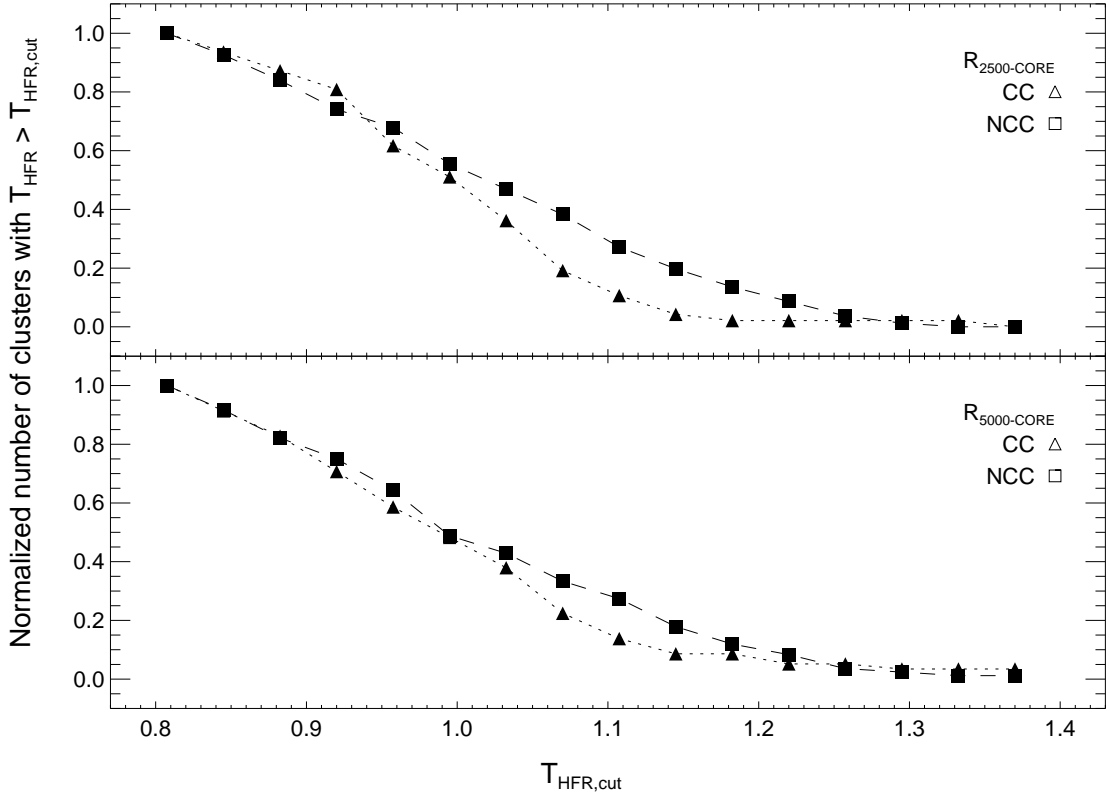


FIG. 9.— We have defined a cluster as having a cool core (CC) when the temperature for the 50 kpc around the cluster center divided by the temperature for $R_{2500-\text{CORE}}$ was less than 1 at the 2σ level. We then take cuts in T_{HFR} at the 1σ level and ask how many CC and NCC clusters are above these cuts. The number of CC clusters falls off more rapidly than NCC clusters in this classification suggesting higher values of T_{HFR} prefer less relaxed systems which do not have cool cores. This result is insensitive to our choice of significance level in both the CC classification and T_{HFR} cuts.

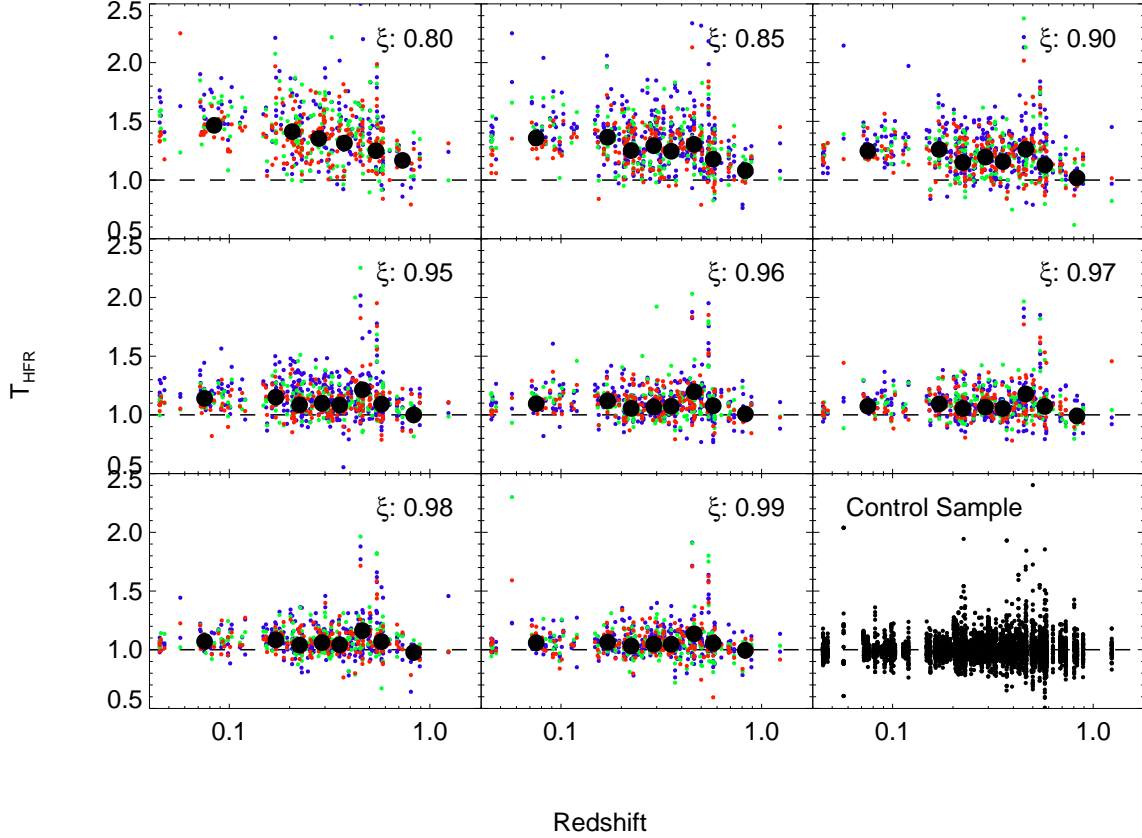


FIG. 10.— T_{HFR} plotted as a function of redshift for our ensemble of simulated spectra. Each panel contains the fits for all three T_2 values (blue=0.5 keV, green=0.75 keV, and red=1.0 keV) of a specific ξ . Recall ξ is the by which the best-fit normalizations of the real spectra are adjusted. The last panel is for the control sample which has no T_2 and $\xi = \sqrt{\sigma_0}$. Solid black circles are the weight-averaged values for bins containing 100 data points. The dashed line represents unity. Note as redshift increases T_{HFR} approaches unity. This is the effect of cool gas being redshifted out of the hard-band and thus losing information about the presence of cool gas. This inhibits our ability to classify high-redshift cool cores in a cluster.

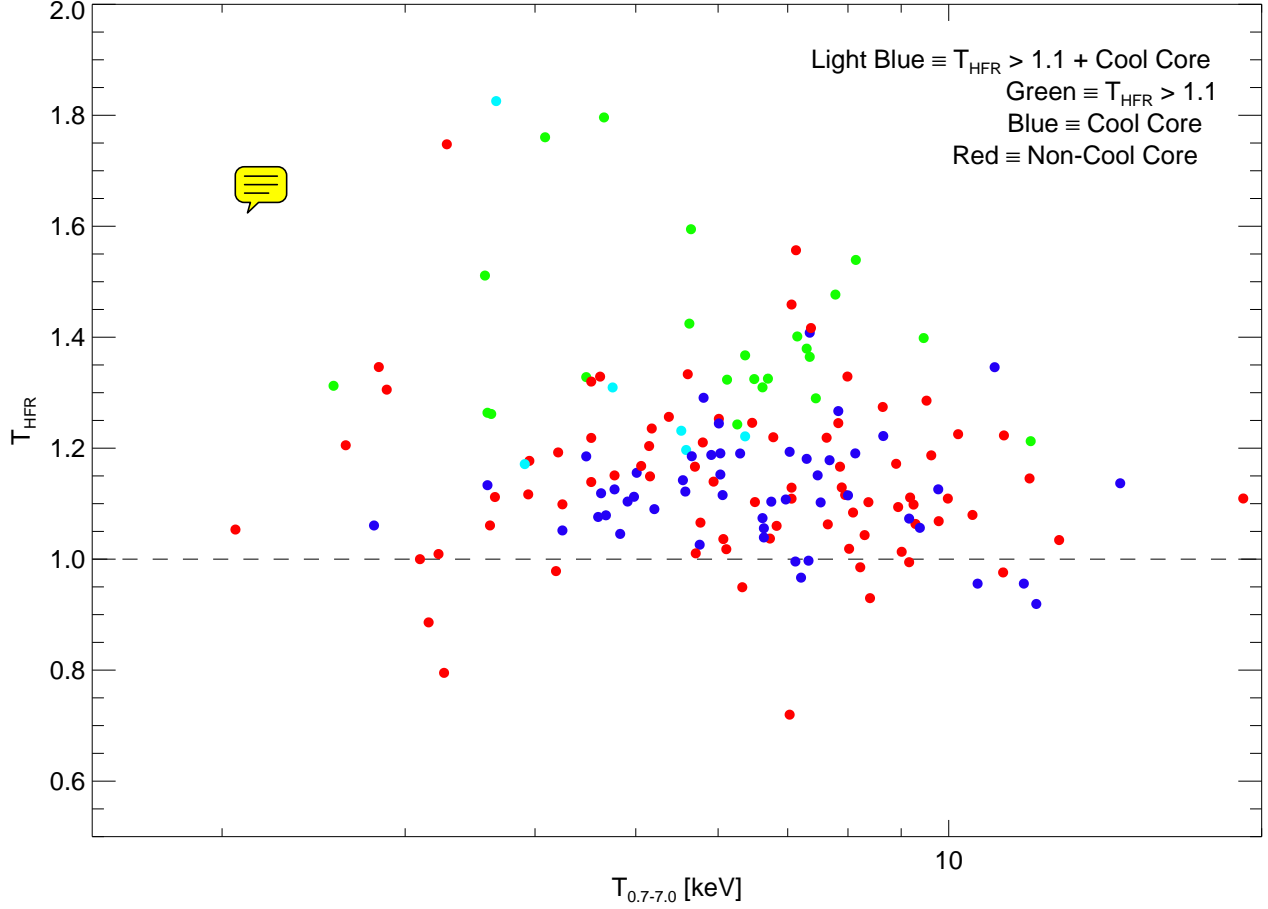


FIG. 11.— T_{HFR} plotted against $T_{0.7-7.0}$ for our sample. Points are color coded based on the presence of a cool core (CC) and/or they have a significant T_{HFR} value greater than 1.1. Light blue indicates a cluster with a CC and $T_{HFR} > 1.1$, green are NCC clusters with $T_{HFR} > 1.1$, blue are CC clusters, and red are NCC clusters. We have determined most, if not all, of the clusters with high T_{HFR} ($\gtrsim 1.1$) are on-going or recent mergers.

TABLE 1
SUMMARY OF SAMPLE

Cluster	Obs.ID	R.A. hr:min:sec (3)	Dec. ° : ' : '' (4)	ExpT ksec (5)	Mode	ACIS	z (8)	$L_{bol.}$ $10^{44} h_{70}^{-2}$ ergs s ⁻¹ (9)
(1)	(2)				(6)	(7)		
1E0657 56	3184	06:58:29.510	-55:56:39.79	87.5	VF	I3	0.296	52.79
1E0657 56	5356	06:58:29.619	-55:56:39.35	97.2	VF	I2	0.296	52.79
1E0657 56	5361	06:58:29.436	-55:56:40.30	82.6	VF	I3	0.296	52.79
1RXS J2129.4-0741	3199	21:29:26.274	-07:41:29.18	19.9	VF	I3	0.570	20.78
1RXS J2129.4-0741	3595	21:29:26.016	-07:41:29.36	19.9	VF	I3	0.570	20.78
2PIGG J0011.5-2850	5797	00:11:21.623	-28:51:14.44	19.9	VF	I3	0.075	2.17
2PIGG J0311.8-2655 †	5799	03:11:33.904	-26:54:16.48	39.6	VF	I3	0.062	0.26
2PIGG J2227.0-3041	5798	22:27:54.560	-30:34:34.84	22.3	VF	I2	0.073	0.82
3C 220.1	839	09:32:40.218	+79:06:29.46	18.9	F	S3	0.610	3.29
3C 28.0	3233	00:55:50.401	+26:24:36.47	49.7	VF	I3	0.195	4.83
3C 295	2254	14:11:20.280	+52:12:10.55	90.9	VF	I3	0.464	7.01
3C 388	5295	18:44:02.365	+45:33:29.31	30.7	VF	I3	0.092	0.53
4C 55.16	4940	08:34:54.923	+55:34:21.15	96.0	VF	S3	0.242	5.97
ABELL 0013 †	4945	00:13:37.883	-19:30:09.10	55.3	VF	S3	0.094	1.42
ABELL 0068	3250	00:37:06.309	+09:09:32.28	10.0	VF	I3	0.255	12.79
ABELL 0119 †	4180	00:56:15.150	-01:14:59.70	11.9	VF	I3	0.044	1.41
ABELL 0168	3203	01:14:57.909	+00:24:43.04	40.6	VF	I3	0.045	0.24
ABELL 0168	3204	01:14:58.377	+00:24:42.70	37.6	VF	I3	0.045	0.24
ABELL 0209	3579	01:31:52.565	-13:36:38.79	10.0	VF	I3	0.206	11.04
ABELL 0209	522	01:31:52.730	-13:36:37.28	10.0	VF	I3	0.206	11.04
ABELL 0267	1448	01:52:42.302	+01:00:44.34	7.9	F	I3	0.230	8.70
ABELL 0267	3580	01:52:42.170	+01:00:45.63	19.9	VF	I3	0.230	8.70
ABELL 0370	515	02:39:53.169	-01:34:36.96	88.0	F	S3	0.375	12.06
ABELL 0383	2321	02:48:03.364	-03:31:44.69	19.5	F	S3	0.187	5.39
ABELL 0399	3230	02:57:54.931	+13:01:58.41	48.6	VF	I0	0.072	4.40
ABELL 0401	518	02:58:56.896	+13:34:14.97	18.0	F	I3	0.074	8.47
ABELL 0478	6102	04:13:25.214	+10:27:55.13	10.0	VF	I3	0.088	16.53
ABELL 0514	3578	04:48:19.229	-20:30:28.79	44.5	VF	I3	0.072	0.67
ABELL 0520	4215	04:54:09.711	+02:55:23.69	66.3	VF	I3	0.202	13.05
ABELL 0521	430	04:54:07.004	-10:13:26.72	39.1	VF	S3	0.253	9.85
ABELL 0586	530	07:32:20.339	+31:37:58.59	10.0	VF	I3	0.171	8.61
ABELL 0611	3194	08:00:56.832	+36:03:24.09	36.1	VF	S3	0.288	10.88
ABELL 0644 †	2211	08:17:25.225	-07:30:40.03	29.7	VF	I3	0.070	7.00
ABELL 0665	3586	08:30:59.231	+65:50:37.78	29.7	VF	I3	0.181	13.48
ABELL 0697	4217	08:42:57.549	+36:21:57.65	19.5	VF	I3	0.282	26.28
ABELL 0773	5006	09:17:52.566	+51:43:38.18	19.8	VF	I3	0.217	12.96
ABELL 0781	534	09:20:25.431	+30:30:07.56	9.9	VF	I3	0.298	8.33
ABELL 0907	3185	09:58:21.880	-11:03:52.20	48.0	VF	I3	0.153	6.25
ABELL 0963	903	10:17:03.744	+39:02:49.17	36.3	F	S3	0.206	10.74
ABELL 1063S	4966	22:48:44.294	-44:31:48.37	26.7	VF	I3	0.354	71.49
ABELL 1068 †	1652	10:40:44.520	+39:57:10.28	26.8	F	S3	0.138	4.24
ABELL 1201 †	4216	11:12:54.489	+13:26:08.76	39.7	VF	S3	0.169	3.56
ABELL 1204	2205	11:13:20.419	+17:35:38.45	23.6	VF	I3	0.171	3.98
ABELL 1361 †	2200	11:43:39.827	+46:21:21.40	16.7	F	S3	0.117	2.18
ABELL 1423	538	11:57:17.026	+33:36:37.44	9.8	VF	I3	0.213	7.07
ABELL 1651	4185	12:59:22.830	-04:11:45.86	9.6	VF	I3	0.084	6.71
ABELL 1664 †	1648	13:03:42.478	-24:14:44.55	9.8	VF	S3	0.128	2.63
ABELL 1682	3244	13:06:50.764	+46:33:19.86	9.8	VF	I3	0.226	7.99
ABELL 1689	5004	13:11:29.474	-01:20:25.17	19.9	VF	I3	0.184	28.07
ABELL 1758	2213	13:32:42.978	+50:32:44.83	58.3	VF	S3	0.279	21.12
ABELL 1763	3591	13:35:17.957	+40:59:55.80	19.6	VF	I3	0.187	9.33
ABELL 1795 †	5289	13:48:52.645	+26:35:25.00	15.0	VF	I3	0.062	7.65
ABELL 1835	495	14:01:01.951	+02:52:43.18	19.5	F	S3	0.253	39.62
ABELL 1914	3593	14:26:01.399	+37:49:27.83	18.9	VF	I3	0.171	26.40
ABELL 1942	3290	14:38:21.878	+03:40:12.97	57.6	VF	I2	0.224	2.30
ABELL 1995	906	14:52:57.758	+58:02:51.34	0.0	F	S3	0.319	10.27
ABELL 2029 †	6101	15:10:56.064	+05:44:40.40	9.9	VF	I3	0.076	13.99
ABELL 2034	2204	15:10:11.003	+33:30:46.46	53.9	VF	I3	0.113	6.50
ABELL 2065 †	31821	15:22:29.220	+27:42:46.54	0.0	VF	I3	0.073	2.95
ABELL 2069	4965	15:24:09.181	+29:53:18.05	55.4	VF	I2	0.116	3.85
ABELL 2111	544	15:39:41.432	+34:25:12.26	10.3	F	I3	0.230	7.51
ABELL 2125	2207	15:41:14.154	+66:15:57.20	81.5	VF	I3	0.246	0.79
ABELL 2163	1653	16:15:45.705	-06:09:00.62	71.1	VF	I1	0.170	49.28
ABELL 2204 †	499	16:32:46.986	+05:34:30.89	10.1	F	S3	0.152	20.90
ABELL 2204	6104	16:32:46.944	+05:34:31.22	9.6	VF	I3	0.152	22.19
ABELL 2218	1666	16:35:50.831	+66:12:42.31	48.6	VF	I0	0.171	8.46
ABELL 2219 †	896	16:40:21.069	+46:42:29.07	42.3	F	S3	0.226	33.32
ABELL 2255	894	17:12:40.385	+64:03:50.63	39.4	F	I3	0.081	3.70
ABELL 2256 †	1386	17:03:44.567	+78:38:12.01	12.4	F	I3	0.058	4.70
ABELL 2259	3245	17:20:08.299	+27:40:11.53	10.0	VF	I3	0.164	5.43
ABELL 2261	5007	17:22:27.254	+32:07:58.60	24.3	VF	I3	0.224	17.63
ABELL 2294	3246	17:24:10.149	+85:53:09.77	10.0	VF	I3	0.178	10.41
ABELL 2384	4202	21:52:21.178	-19:32:51.90	31.5	VF	I3	0.095	1.98

TABLE 1 — *Continued*

Cluster (1)	Obs.ID (2)	R.A. hr:min:sec (3)	Dec. ° : ' : " (4)	ExpT ksec (5)	Mode (6)	ACIS (7)	z (8)	$L_{bol.}$ $10^{44} h_{70}^{-2}$ ergs s ⁻¹ (9)
ABELL 2390 †	4193	21:53:36.825	+17:41:44.38	95.1	VF	S3	0.230	31.22
ABELL 2409	3247	22:00:52.567	+20:58:34.11	10.2	VF	I3	0.148	7.08
ABELL 2537	4962	23:08:22.313	-02:11:29.88	36.2	VF	S3	0.295	10.24
ABELL 2550	2225	23:11:35.806	-21:44:46.70	59.0	VF	S3	0.154	0.60
ABELL 2554 †	1696	23:12:19.939	-21:30:09.84	19.9	VF	S3	0.110	1.59
ABELL 2556 †	2226	23:13:01.413	-21:38:04.47	19.9	VF	S3	0.086	1.45
ABELL 2631	3248	23:37:38.560	+00:16:28.64	9.2	VF	I3	0.278	12.70
ABELL 2667	2214	23:51:39.395	-26:05:02.75	9.6	VF	S3	0.230	20.09
ABELL 2670	4959	23:54:13.687	-10:25:08.85	39.6	VF	I3	0.076	1.41
ABELL 2717	6974	00:03:11.996	-35:56:08.01	19.8	VF	I3	0.048	0.26
ABELL 2744	2212	00:14:14.396	-30:22:40.04	24.8	VF	S3	0.308	29.21
ABELL 3128 †	893	03:29:50.918	-52:34:51.04	19.6	F	I3	0.062	0.36
ABELL 3158 †	3201	03:42:54.675	-53:37:40.36	24.8	VF	I3	0.059	3.04
ABELL 3158 †	3712	03:42:54.530	-53:37:40.60	30.9	VF	I3	0.059	3.04
ABELL 3164	6955	03:46:16.839	-57:02:11.38	13.5	VF	I3	0.057	0.19
ABELL 3376	3202	06:02:05.122	-39:57:42.82	44.3	VF	I3	0.046	0.76
ABELL 3376	3450	06:02:05.248	-39:57:42.90	19.8	VF	I3	0.046	0.76
ABELL 3391 †	4943	06:26:21.511	-53:41:44.81	18.4	VF	I3	0.056	1.45
ABELL 3921	4973	22:49:57.829	-64:25:42.17	29.4	VF	I3	0.093	3.40
AC 114	1562	22:58:48.196	-34:47:56.89	72.5	F	S3	0.312	11.00
CL 0024+17	929	00:26:35.996	+17:09:45.37	39.8	F	S3	0.394	2.91
CL 1221+4918	1662	12:21:26.709	+49:18:21.60	79.1	VF	I3	0.700	8.75
CL J0030+2618	5762	00:30:33.571	+26:18:09.45	17.9	VF	I3	0.500	3.46
CL J0152-1357	913	01:52:42.141	-13:57:59.71	36.5	F	I3	0.831	13.47
CL J0542.8-4100	914	05:42:49.994	-40:59:58.50	50.4	F	I3	0.630	6.27
CL J0848+4456	1708	08:48:48.235	+44:56:17.30	61.4	VF	I1	0.574	0.64
CL J0848+4456	927	08:48:47.233	+44:56:17.13	125.1	VF	I1	0.574	0.64
CL J1113.1-2615	915	11:13:05.167	-26:15:40.43	104.6	F	I3	0.730	2.27
CL J1213+0253	4934	12:13:34.948	+02:53:45.45	18.9	VF	I3	0.409	1.35
CL J1226.9+3332	3180	12:26:58.058	+33:32:46.87	31.7	VF	I3	0.890	31.00
CL J1226.9+3332	5014	12:26:58.372	+33:32:47.67	32.7	VF	I3	0.890	31.00
CL J1641+4001	3575	16:41:53.704	+04:01:44.40	46.5	VF	I3	0.464	1.21
CL J2302.8+0844	918	23:02:48.156	+08:43:52.74	108.6	F	I3	0.730	3.00
DLS J0514-4904	4980	05:14:40.037	-49:03:15.07	19.9	VF	I3	0.091	0.68
EXO 0422-086 †	4183	04:25:51.271	-08:33:36.42	10.0	VF	I3	0.040	0.66
HERCULES A †	1625	16:51:08.161	+04:59:32.44	14.8	VF	S3	0.154	3.31
IRAS 09104+4109	509	09:13:45.481	+40:56:27.49	9.1	F	S3	0.442	20.31
LYNX E	17081	08:48:58.841	+44:51:51.63	61.4	VF	I2	1.260	0.44
LYNX E	9271	08:48:58.858	+44:51:51.46	125.1	VF	I2	1.260	0.44
MACS J0011.7-1523	6105	00:11:42.957	-15:23:20.46	37.3	VF	I3	0.360	10.98
MACS J0025.4-1222	3251	00:25:29.368	-12:22:38.05	19.3	VF	I3	0.584	13.15
MACS J0025.4-1222	5010	00:25:29.332	-12:22:37.61	24.8	VF	I3	0.584	13.15
MACS J0159.8-0849	3265	01:59:49.320	-08:50:00.41	17.9	VF	I3	0.405	26.51
MACS J0159.8-0849	6106	01:59:49.422	-08:50:00.42	35.3	VF	I3	0.405	26.51
MACS J0242.5-2132	3266	02:42:35.906	-21:32:26.30	11.9	VF	I3	0.314	12.89
MACS J0257.1-2325	1654	02:57:09.130	-23:26:05.85	19.8	F	I3	0.505	21.90
MACS J0257.1-2325	3581	02:57:09.188	-23:26:06.70	18.5	VF	I3	0.505	21.90
MACS J0257.6-2209	3267	02:57:41.024	-22:09:11.12	20.5	VF	I3	0.322	10.85
MACS J0308.9+2645	3268	03:08:55.927	+26:45:38.34	24.4	VF	I3	0.324	20.56
MACS J0329.6-0211	3257	03:29:41.616	-02:11:49.15	9.9	VF	I3	0.450	12.98
MACS J0329.6-0211	3582	03:29:41.622	-02:11:49.82	19.9	VF	I3	0.450	12.98
MACS J0329.6-0211	6108	03:29:41.681	-02:11:49.57	39.6	VF	I3	0.450	12.98
MACS J0404.6+1109	3269	04:04:32.491	+11:08:02.10	21.8	VF	I3	0.355	3.95
MACS J0417.5-1154	3270	04:17:34.686	-11:54:32.71	12.0	VF	I3	0.440	38.24
MACS J0429.6-0253	3271	04:29:36.088	-02:53:09.02	23.2	VF	I3	0.399	11.72
MACS J0451.9-0006	5815	04:51:54.291	+00:06:20.20	10.2	VF	I3	0.430	8.29
MACS J0547.0-3904	3273	05:47:01.582	-39:04:28.24	21.7	VF	I3	0.210	1.62
MACS J0717.5+3745	1655	07:17:32.443	+37:45:29.83	19.9	F	I3	0.548	46.89
MACS J0717.5+3745	4200	07:17:32.651	+37:45:29.95	59.2	VF	I3	0.548	46.89
MACS J0744.8+3927	3197	07:44:52.801	+39:27:25.40	20.2	VF	I3	0.686	24.93
MACS J0744.8+3927	3585	07:44:52.779	+39:27:24.90	19.9	VF	I3	0.686	24.93
MACS J0744.8+3927	6111	07:44:52.842	+39:27:26.28	49.5	VF	I3	0.686	24.93
MACS J0911.2+1746	3587	09:11:11.291	+17:46:31.75	17.9	VF	I3	0.541	11.67
MACS J0949+1708	3274	09:49:51.824	+17:07:05.62	14.3	VF	I3	0.382	19.34
MACS J1115.8+0129	3275	11:15:52.048	+01:29:56.56	15.9	VF	I3	0.120	1.49
MACS J1131.8-1955	3276	11:31:56.011	-19:55:55.85	13.9	VF	I3	0.307	17.59
MACS J1149.5+2223	1656	11:49:35.466	+22:23:55.06	18.5	VF	I3	0.176	2.53
MACS J1149.5+2223	3589	11:49:35.848	+22:23:55.04	20.0	VF	I3	0.176	2.53
MACS J1206.2-0847	3277	12:06:12.276	-08:48:02.40	23.5	VF	I3	0.440	37.29
MACS J1226.8+2153	3590	12:26:51.207	+21:49:55.22	19.0	VF	I3	0.370	2.67
MACS J1311.0-0310	3258	13:11:01.665	-03:10:39.50	14.9	VF	I3	0.494	10.15
MACS J1311.0-0310	6110	13:11:01.647	-03:10:39.78	63.2	VF	I3	0.494	10.15
MACS J1319+7003	3278	13:20:08.370	+70:04:33.81	21.6	VF	I3	0.328	7.08
MACS J1427.6-2521	3279	14:27:39.389	-25:21:04.66	16.9	VF	I3	0.220	1.57

TABLE 1 — *Continued*

Cluster (1)	Obs.ID (2)	R.A. hr:min:sec (3)	Dec. ° : ' : " (4)	ExpT ksec (5)	Mode (6)	ACIS (7)	z (8)	L _{bol.} 10 ⁴⁴ h ₇₀ ⁻² ergs s ⁻¹ (9)
MACS J1621.3+3810	3254	16:21:24.759	+38:10:07.18	9.8	VF	I3	0.461	11.61
MACS J1621.3+3810	3594	16:21:24.933	+38:10:06.57	19.7	VF	I3	0.461	11.61
MACS J1621.3+3810	6109	16:21:24.742	+38:10:08.92	37.5	VF	I3	0.461	11.61
MACS J1621.3+3810	6172	16:21:24.849	+38:10:08.72	29.8	VF	I3	0.461	11.61
MACS J1824.3+4309	3255	18:24:18.444	+43:09:43.39	14.9	VF	I3	0.487	2.51
MACS J1931.8-2634	3282	19:31:49.656	-26:34:33.99	13.6	VF	I3	0.352	23.38
MACS J2211.7-0349	3284	22:11:45.856	-03:49:37.24	17.7	VF	I3	0.270	22.24
MACS J2214.9-1359	3259	22:14:57.467	-14:00:09.35	19.5	VF	I3	0.503	24.23
MACS J2214.9-1359	5011	22:14:57.515	-14:00:10.68	18.5	VF	I3	0.503	24.23
MACS J2228+2036	3285	22:28:33.241	+20:37:11.42	19.9	VF	I3	0.412	18.08
MACS J2229.7-2755	3286	22:29:45.358	-27:55:38.41	16.4	VF	I3	0.324	9.60
MACS J2243.3-0935	3260	22:43:21.537	-09:35:44.30	20.5	VF	I3	0.101	0.79
MACS J2245.0+2637	3287	22:45:04.547	+26:38:07.88	16.9	VF	I3	0.304	9.46
MACS J2311+0338	3288	23:11:33.213	+03:38:06.51	13.6	VF	I3	0.300	11.08
MKW3S	900	15:21:51.930	+07:42:31.97	57.3	VF	I3	0.045	1.16
MS 0016.9+1609	520	00:18:33.503	+16:26:12.99	67.4	VF	I3	0.541	33.24
MS 0302.7+1658	525	03:05:31.614	+17:10:02.06	10.0	VF	I3	0.424	2.46
MS 0440.5+2024 †	4196	04:43:09.952	+02:10:18.70	59.4	VF	S3	0.190	2.19
MS 0451.6-0305	902	04:54:11.004	-03:00:52.19	44.2	F	S3	0.539	33.63
MS 0735.6+7421	4197	07:41:44.245	+74:14:38.23	45.5	VF	S3	0.216	7.65
MS 0839.8+2938	2224	08:42:55.969	+29:27:26.97	29.8	F	S3	0.194	3.13
MS 0906.5+1110	924	09:09:12.753	+10:58:32.00	29.7	VF	I3	0.163	4.69
MS 1006.0+1202	925	10:08:47.194	+11:47:55.99	29.4	VF	I3	0.221	4.81
MS 1008.1-1224	926	10:10:32.312	-12:39:56.80	44.2	VF	I3	0.301	8.53
MS 1054.5-0321	512	10:56:58.499	-03:37:32.76	89.1	F	S3	0.830	27.50
MS 1455.0+2232	4192	14:57:15.088	+22:20:32.49	91.9	VF	I3	0.259	10.38
MS 1621.5+2640	546	16:23:35.522	+26:34:25.67	30.1	F	I3	0.426	6.56
MS 2053.7-0449	1667	20:56:21.295	-04:37:46.61	44.5	VF	I3	0.583	3.03
MS 2053.7-0449	551	20:56:21.264	-04:37:46.80	44.3	F	I3	0.583	3.03
MS 2137.3-2353	4974	21:40:15.178	-23:39:40.71	57.4	VF	S3	0.313	11.40
MS J1157.3+5531 †	4964	11:59:52.295	+55:32:05.61	75.1	VF	S3	0.081	0.12
NGC 6338 †	4194	17:15:23.036	+57:24:40.29	47.3	VF	I3	0.028	0.14
PKS 0745-191	6103	07:47:31.295	-19:17:40.50	10.3	VF	I3	0.103	18.56
RBS 0797	2202	09:47:12.971	+76:23:13.90	11.7	VF	I3	0.354	26.29
RDCS 1252-29	4198	12:52:54.221	-29:27:21.01	163.4	VF	I3	1.237	2.34
RX J0232.2-4420	4993	02:32:18.771	-44:20:46.68	23.4	VF	I3	0.284	18.32
RX J0340-4542	6954	03:40:44.765	-45:41:18.41	17.9	VF	I3	0.082	0.33
RX J0439+0520	527	04:39:02.218	+05:20:43.11	9.6	VF	I3	0.208	3.61
RX J0439.0+0715	1449	04:39:00.710	+07:16:08.15	6.3	F	I3	0.230	9.56
RX J0439.0+0715	3583	04:39:00.710	+07:16:07.82	19.2	VF	I3	0.230	9.56
RX J0528.9-3927	4994	05:28:53.039	-39:28:15.53	22.5	VF	I3	0.263	13.09
RX J0647.7+7015	3196	06:47:50.029	+70:14:54.15	19.3	VF	I3	0.584	26.68
RX J0647.7+7015	3584	06:47:50.919	+70:14:54.91	20.0	VF	I3	0.584	26.68
RX J0819.6+6336 †	2199	08:19:26.007	+63:37:26.53	14.9	F	S3	0.119	1.00
RX J0910+5422	2452	09:10:44.478	+54:22:04.26	65.3	VF	I3	1.100	1.36
RX J1053+5735	4936	10:53:39.844	+57:35:18.42	92.2	F	S3	1.140	1.61
RX J1347.5-1145	3592	13:47:30.593	-11:45:10.05	57.7	VF	I3	0.451	100.89
RX J1347.5-1145	507	13:47:30.632	-11:45:09.78	10.0	F	S3	0.451	100.89
RX J1350+6007	2229	13:50:48.038	+60:07:08.39	58.3	VF	I3	0.804	2.23
RX J1423.8+2404	1657	14:23:47.759	+24:04:42.95	18.5	VF	I3	0.545	16.02
RX J1423.8+2404	4195	14:23:47.942	+24:04:43.09	115.6	VF	S3	0.545	16.02
RX J1504.1-0248	5793	15:04:07.415	-02:48:15.70	39.2	VF	I3	0.215	34.92
RX J1525+0958	1664	15:24:39.729	+09:57:44.42	50.9	VF	I3	0.516	3.33
RX J1532.9+3021	1649	15:32:53.781	+30:20:58.72	9.4	VF	S3	0.345	20.98
RX J1532.9+3021	1665	15:32:53.817	+30:20:58.34	10.0	VF	I3	0.345	20.98
RX J1716.9+6708	548	17:16:49.015	+67:08:25.80	51.7	F	I3	0.810	8.16
RX J1720.1+2638	4361	17:20:09.941	+26:37:29.11	25.7	VF	I3	0.164	11.50
RX J1720.2+3536	3280	17:20:16.792	+35:36:26.08	20.8	VF	I3	0.391	13.15
RX J1720.2+3536	6107	17:20:16.908	+35:36:26.43	33.9	VF	I3	0.391	13.15
RX J1720.2+3536	7225	17:20:16.947	+35:36:26.78	2.0	VF	I3	0.391	13.15
RX J2011.3-5725	4995	20:11:26.889	-57:25:09.08	24.0	VF	I3	0.279	2.81
RX J2129.6+0005	552	21:29:39.944	+00:05:18.83	10.0	VF	I3	0.235	12.70
S0463	6956	04:29:47.040	-53:49:43.02	29.3	VF	I3	0.099	0.49
S0463	7250	04:28:47.724	-53:49:43.00	29.1	VF	I3	0.099	0.49
TRIANG AUSTR †	1281	16:38:22.712	-64:21:19.70	11.4	F	I3	0.051	9.47
V 1121.0+2327	1660	11:20:57.195	+23:26:27.60	71.3	VF	I3	0.560	3.35
ZWCL 1215	4184	12:17:40.787	+03:39:39.42	12.1	VF	I3	0.075	3.52
ZWCL 1358+6245	516	13:59:50.526	+62:31:04.57	54.1	F	S3	0.328	12.49
ZWCL 1953	1659	08:50:06.677	+36:04:16.16	24.9	F	I3	0.380	17.28
ZWCL 3146	909	10:23:39.735	+04:11:08.05	46.0	F	I3	0.290	29.85
ZWCL 5247	539	12:34:21.928	+09:47:02.83	9.3	VF	I3	0.229	4.93
ZWCL 7160	543	14:57:15.158	+22:20:33.85	9.9	F	I3	0.258	10.27
ZWICKY 2701	3195	09:52:49.183	+51:53:05.27	26.9	VF	S3	0.210	5.24
ZwCL 1332.8+5043	5772	13:34:20.698	+50:31:04.64	19.5	VF	I3	0.620	4.54

TABLE 1 — *Continued*

Cluster (1)	Obs.ID (2)	R.A. hr:min:sec (3)	Dec. $^{\circ} : ' : ''$ (4)	ExpT ksec (5)	Mode (6)	ACIS (7)	z (8)	$L_{bol.}$ $10^{44} h_{70}^{-2}$ ergs s $^{-1}$ (9)
ZwCl 0848.5+3341	4205	08:51:38.873	+33:31:08.00	11.4	VF	S3	0.371	4.62

NOTE. — (1) Cluster name, (2) CDA observation identification number, (3) centroid R.A., (4) centroid Dec., (5) nominal exposure time, (6) observing mode, (7) CCD location of centroid, (8) redshift, (9) NRAO absorbing Galactic neutral hydrogen column density, (10) fiducial temperature, (11) fiducial abundance, (12) bolometric luminosity. † indicates clusters analyzed within R_{5000} only.

TABLE 2
WEIGHTED AVERAGES FOR VARIOUS APERTURES

Aperture	[0.7-7.0] keV	[2.0 _{rest} -7.0] keV	T _{HFR}	[0.7-7.0] keV	[2.0 _{rest} -7.0] keV	T _{HFR}
Without Core				With Core		
R ₂₅₀₀	4.78±0.03	6.12±0.07	1.16±0.01	4.27±0.02	5.32±0.05	1.13±0.01
R ₅₀₀₀	4.82±0.02	6.07±0.09	1.14±0.01	4.31±0.02	5.26±0.05	1.14±0.01
Simulated	3.85±0.004	4.45±0.009	1.13±0.002

NOTE. — Simulated sample has been culled to include only T₂=0.75 keV.

TABLE 3
CLUSTERS WITH T_{HFR} > 1.1 AT THE 1 σ LEVEL.

Name	T _{HFR}	Merger	Core	T _{dec}	X-ray Morphology	Ref.
RX J1525+0958	1.83 ^{+0.80} _{-0.48}	Unknown	CC	0.43 ^{+0.14} _{-0.08}	Arrowhead shape w/ no visible core	none
MS 1008.1-1224 ...	1.59 ^{+0.27} _{-0.27}	Y	NCC	0.93 ^{+0.18} _{-0.14}	Wide gas tail extending ~550 kpc north	[1]
ABELL 2034	1.40 ^{+0.14}	Y	NCC	1.07 ^{+0.11} _{-0.09}	Prominent cold front, gas tail extending south	[2]
ABELL 401	1.37 ^{+0.15} _{-0.10}	Y	NCC	1.13 ^{+0.12} _{-0.09}	Highly spherical w/ possible cold front to north	[3]
RX J0439.0+0715 ..	1.42 ^{+0.24} _{-0.18}	Unknown	NCC	0.98 ^{+0.11} _{-0.09}	Bright core w/ possibly cold front to north	none
ABELL 3376	1.33 ^{+0.18} _{-0.10}	Y	NCC	0.97 ^{+0.07} _{-0.07}	Highly disturbed w/ broad gas tail to west	[4],[5]
ABELL 1689	1.40 ^{+0.21} _{-0.17}	Y	NCC	0.95 ^{+0.09} _{-0.07}	Exceptionally spherical w/ bright central core	[6],[7]
ABELL 2255	1.32 ^{+0.12} _{-0.10}	Y	NCC	1.48 ^{+0.32} _{-0.23}	Spherical w/ compressed isophotes west of core	[8],[9]
ABELL 2218	1.36 ^{+0.19} _{-0.15}	Y	NCC	1.39 ^{+0.23} _{-0.19}	Spherical, core of cluster elongated NW-SE	[10]
ABELL 1763	1.48 ^{+0.39} _{-0.26}	Y	NCC	0.83 ^{+0.17} _{-0.13}	Elongated ENE-SSW w/ cold front to west of core	[11],[12]
MACS J2243.3-0935	1.76 ^{+0.81} _{-0.55}	Unknown	NCC	1.73 ^{+0.44} _{-0.32}	No core, highly flattened along WNW-ESE axis	none
ABELL 2069	1.32 ^{+0.17} _{-0.14}	Y	NCC	1.00 ^{+0.18} _{-0.14}	No core, highly elongated NNW-SSE	[13]
ABELL 2384	1.31 ^{+0.16} _{-0.14}	Unknown	CC	0.59 ^{+0.03} _{-0.03}	Gas tail extending 1.1 Mpc from core	none
ABELL 168	1.31 ^{+0.16} _{-0.14}	Y	NCC	1.16 ^{+0.14} _{-0.10}	Highly disrupted and irregular	[14],[15]
ABELL 209	1.38 ^{+0.22} _{-0.22}	Y	NCC	1.08 ^{+0.19} _{-0.17}	Asymmetric core structure w/ possible cold front	[16]
ABELL 665	1.29 ^{+0.15} _{-0.13}	Y	NCC	1.14 ^{+0.15} _{-0.10}	Wide, broad gas tail extending north w/ prominent cold front	[17]
1E0657-56	1.21 ^{+0.06} _{-0.05}	Y	NCC	1.04 ^{+0.10} _{-0.08}	The famous “Bullet Cluster”	[18]
MACS J0547.0-3904	1.51 ^{+0.50} _{-0.36}	Unknown	NCC	0.79 ^{+0.11} _{-0.09}	Bright core w/ gas spur extending NW	none
ZWCL 1215	1.31 ^{+0.21} _{-0.18}	Unknown	NCC	0.95 ^{+0.15} _{-0.12}	No core, flattened along NE-SW axis	none
ABELL 1204	1.26 ^{+0.44} _{-0.34}	Unknown	NCC	0.96 ^{+0.05} _{-0.05}	Highly spherical w/ bright centralized core	none
MKW3S	1.17 ^{+0.04} _{-0.05}	Y	CC	0.87 ^{+0.03} _{-0.02}	High mass group, egg shaped w/ bright core	[19]
MACS J2311+0338 .	1.54 ^{+0.68} _{-0.42}	Unknown	NCC	0.69 ^{+0.20} _{-0.15}	Elongated N-S w/ disc-like core elongated toward gas clump	none
ABELL 267	1.33 ^{+0.27} _{-0.21}	Unknown	NCC	1.09 ^{+0.20} _{-0.16}	Elongated NNE-SSW w/ cold front to north	none
RX J1720.1+2638 ..	1.22 ^{+0.12} _{-0.11}	Y	CC	0.73 ^{+0.04} _{-0.04}	Highly spherical w/ bright peaky core and cold front	[20]
ABELL 907	1.20 ^{+0.09} _{-0.08}	Unknown	CC	0.77 ^{+0.03} _{-0.03}	NW-SW elongation and western cold front	none
ABELL 514	1.26 ^{+0.19} _{-0.15}	Y	NCC	1.56 ^{+1.07} _{-0.40}	Very diffuse and disrupted	[21]
ABELL 1651	1.24 ^{+0.16} _{-0.13}	Y	NCC	1.07 ^{+0.10} _{-0.08}	Spherical w/ compressed isophotes to SW	[22]
3C 28.0	1.23 ^{+0.14} _{-0.12}	Y	CC	0.54 ^{+0.03} _{-0.03}	Obvious merger w/ ~1 Mpc gas tail	[23]
MACS J1427.6-2521	1.80 ^{+1.13} _{-0.69}	Unknown	NCC	0.85 ^{+0.19} _{-0.14}	Highly spherical w/ bright peaky core	none

NOTE. — Clusters ordered by lower limit of T_{HFR}. [1] Ettori & Lombardi (2003), [2] Kempner et al. (2003), [3] Yuan et al. (2005), [4] Markevitch et al. (1998), [5] Bagchi et al. (2006), [6] Teague et al. (1990), [7] Andersson & Madejski (2004), [8] Burns et al. (1995), [9] Feretti et al. (1997), [10] Girardi et al. (1997), [11] Dahle et al. (2002), [12] Smith et al. (2005), [13] Gioia et al. (1982), [14] Hallman & Markevitch (2004), [15] Yang et al. (2004), [16] Mercurio et al. (2003), [17] Gómez et al. (2000), [18] Tucker et al. (1998), [19] Krempeck-Krygier & Krygier (1999), [20] Mazzotta et al. (2001), [21] Govoni et al. (2001), [22] Bliton et al. (1998), [23] Gutierrez & Krawczynski (2005)

TABLE 4
 SUMMARY OF EXCISED R₂₅₀₀ SPECTRAL FITS

Cluster	R _{CORE} kpc (2)	R ₂₅₀₀ kpc (3)	N _H 10 ²⁰ cm ⁻² (4)	T ₇₇ keV (5)	T ₂₇ keV (6)	T _{HFR} (7)	Z ₇₇ Z _⊙ (8)	χ _{red,77} (9)	χ _{red,27} (10)	% Source (11)
1E0657 56 †	69	687	6.53	11.99 ^{+0.27} _{-0.26}	14.54 ^{+0.67} _{-0.53}	1.21 ^{+0.06} _{-0.05}	0.29 ^{+0.03} _{-0.02}	1.24	1.11	92
1RXS J2129.4-0741 †	68	504	4.36	8.22 ^{+0.18} _{-0.25}	8.10 ^{+1.47} _{-0.10}	0.99 ^{+0.05} _{-0.18}	0.43 ^{+0.08} _{-0.06}	1.07	1.05	80
2PIGG J0011.5-2850	70	547	2.18	5.15 ^{+0.25} _{-0.24}	6.20 ^{+0.19} _{-0.65}	1.20 ^{+0.08} _{-0.14}	0.26 ^{+0.06} _{-0.08}	1.09	1.00	70
2PIGG J2227.0-3041	70	378	1.11	2.80 ^{+0.15} _{-0.14}	2.97 ^{+0.34} _{-0.34}	1.06 ^{+0.13} _{-0.11}	0.35 ^{+0.08} _{-0.08}	1.16	1.15	69
3C 220.1	70	437	1.91	6.51 ^{+0.73} _{-0.72}	7.18 ^{+1.75} _{-1.77}	1.10 ^{+0.23} _{-0.08}	0.00 ^{+0.00} _{-0.00}	1.15	1.39	61
3C 28.0	70	420	5.71	5.53 ^{+0.29} _{-0.27}	6.81 ^{+0.71} _{-0.60}	1.23 ^{+0.12} _{-0.14}	0.30 ^{+0.08} _{-0.07}	0.98	0.88	87
3C 295	69	466	1.35	5.16 ^{+0.32} _{-0.38}	5.93 ^{+0.84} _{-0.69}	1.15 ^{+0.16} _{-0.16}	0.38 ^{+0.12} _{-0.11}	0.91	0.93	79
3C 388	70	419	6.11	3.23 ^{+0.23} _{-0.23}	3.26 ^{+0.49} _{-0.37}	1.01 ^{+0.17} _{-0.16}	0.51 ^{+0.16} _{-0.14}	0.95	0.95	68
4C 55.16	70	425	4.00	4.98 ^{+0.17} _{-0.17}	5.54 ^{+0.70} _{-0.67}	1.11 ^{+0.08} _{-0.08}	0.49 ^{+0.07} _{-0.07}	0.89	0.80	58
ABELL 0068	69	652	4.60	9.01 ^{+1.53} _{-1.16}	9.13 ^{+2.80} _{-2.23}	1.01 ^{+0.24} _{-0.23}	0.46 ^{+0.24} _{-0.22}	1.15	1.13	79
ABELL 0168 †	69	382	3.27	2.65 ^{+0.16} _{-0.09}	3.67 ^{+0.47} _{-0.37}	1.38 ^{+0.18} _{-0.15}	0.31 ^{+0.05} _{-0.05}	1.09	1.03	44
ABELL 0209 †	70	609	1.68	7.30 ^{+0.39} _{-0.51}	10.07 ^{+1.91} _{-1.41}	1.38 ^{+0.28} _{-0.22}	0.23 ^{+0.10} _{-0.09}	1.12	1.11	82
ABELL 0267 †	69	545	2.74	6.70 ^{+0.36} _{-0.47}	8.88 ^{+1.68} _{-1.27}	1.33 ^{+0.27} _{-0.21}	0.32 ^{+0.11} _{-0.11}	1.18	1.15	82
ABELL 0370	71	517	3.37	7.35 ^{+0.84} _{-0.84}	10.35 ^{+1.89} _{-2.27}	1.41 ^{+0.29} _{-0.35}	0.45 ^{+0.06} _{-0.23}	1.08	1.04	39
ABELL 0383	69	424	4.07	4.91 ^{+0.29} _{-0.27}	5.42 ^{+0.74} _{-0.59}	1.10 ^{+0.16} _{-0.13}	0.44 ^{+0.11} _{-0.11}	0.97	0.90	64
ABELL 0399	70	546	7.57 ^{+0.71} _{-0.71}	7.95 ^{+0.35} _{-0.35}	8.87 ^{+0.55} _{-0.50}	1.12 ^{+0.08} _{-0.08}	0.30 ^{+0.05} _{-0.05}	1.12	0.99	82
ABELL 0401	70	643	12.48	6.37 ^{+0.19} _{-0.19}	8.71 ^{+0.82} _{-0.68}	1.37 ^{+0.28} _{-0.28}	0.26 ^{+0.06} _{-0.06}	1.44	1.05	78
ABELL 0478	70	597	30.90	7.30 ^{+0.26} _{-0.24}	8.62 ^{+0.88} _{-0.54}	1.18 ^{+0.09} _{-0.08}	0.45 ^{+0.06} _{-0.05}	1.05	0.95	91
ABELL 0514	70	495	3.14	3.60 ^{+0.18} _{-0.18}	4.55 ^{+0.63} _{-0.50}	1.26 ^{+0.19} _{-0.15}	0.30 ^{+0.09} _{-0.08}	1.08	0.97	56
ABELL 0520	69	576	1.06 ^{+1.06} _{-1.05}	9.29 ^{+0.67} _{-0.60}	9.88 ^{+0.85} _{-0.73}	1.06 ^{+0.12} _{-0.10}	0.37 ^{+0.07} _{-0.07}	1.11	1.04	87
ABELL 0521	69	535	6.17	7.03 ^{+0.59} _{-0.53}	8.39 ^{+1.62} _{-1.22}	1.19 ^{+0.25} _{-0.20}	0.39 ^{+0.13} _{-0.12}	1.10	1.15	49
ABELL 0586	70	635	4.71	6.47 ^{+0.35} _{-0.47}	8.06 ^{+1.46} _{-1.46}	1.25 ^{+0.25} _{-0.19}	0.56 ^{+0.17} _{-0.16}	0.91	0.81	82
ABELL 0611	69	524	4.99	7.06 ^{+0.35} _{-0.38}	7.97 ^{+1.09} _{-1.01}	1.13 ^{+0.18} _{-0.10}	0.35 ^{+0.11} _{-0.10}	0.97	0.98	54
ABELL 0665	69	618	4.24	7.45 ^{+0.34} _{-0.37}	9.61 ^{+1.02} _{-0.95}	1.29 ^{+0.13} _{-0.13}	0.31 ^{+0.06} _{-0.06}	1.02	0.93	87
ABELL 0697	70	611	3.34	9.52 ^{+0.36} _{-0.36}	12.24 ^{+2.05} _{-1.63}	1.29 ^{+0.25} _{-0.20}	0.37 ^{+0.12} _{-0.11}	1.08	1.02	89
ABELL 0773	69	614	1.46	7.83 ^{+0.66} _{-0.57}	9.75 ^{+1.65} _{-1.27}	1.25 ^{+0.24} _{-0.19}	0.44 ^{+0.12} _{-0.12}	1.06	1.09	84
ABELL 0781	69	661	1.90	5.81 ^{+1.01} _{-0.79}	7.50 ^{+3.57} _{-1.81}	1.29 ^{+0.65} _{-0.36}	0.31 ^{+0.24} _{-0.20}	1.38	1.61	74
ABELL 0907	70	488	5.69	5.59 ^{+0.18} _{-0.18}	6.69 ^{+0.47} _{-0.42}	1.20 ^{+0.09} _{-0.08}	0.42 ^{+0.06} _{-0.05}	1.13	0.99	88
ABELL 0963	70	543	1.39	6.73 ^{+0.32} _{-0.32}	6.98 ^{+0.66} _{-0.57}	1.04 ^{+0.11} _{-0.10}	0.29 ^{+0.07} _{-0.07}	1.06	1.02	64
ABELL 1063S	70	650	1.77	11.96 ^{+0.88} _{-0.79}	13.70 ^{+1.68} _{-1.68}	1.15 ^{+0.14} _{-0.14}	0.38 ^{+0.09} _{-0.09}	1.02	0.98	90
ABELL 1204	70	419	1.44	3.63 ^{+0.18} _{-0.19}	4.58 ^{+0.57} _{-0.45}	1.26 ^{+0.17} _{-0.14}	0.31 ^{+0.09} _{-0.09}	1.06	0.90	88
ABELL 1423	70	614	1.60	6.01 ^{+0.35} _{-0.64}	7.53 ^{+2.35} _{-1.55}	1.25 ^{+0.24} _{-0.24}	0.30 ^{+0.18} _{-0.17}	0.87	0.65	78
ABELL 1651	70	595	2.02	6.26 ^{+0.30} _{-0.27}	7.78 ^{+0.76} _{-0.76}	1.24 ^{+0.16} _{-0.13}	0.42 ^{+0.09} _{-0.09}	1.19	1.20	86
ABELL 1682	70	624	1.10	7.06 ^{+1.76} _{-1.26}	10.30 ^{+8.85} _{-3.42}	1.46 ^{+1.31} _{-0.55}	0.60 ^{+0.40} _{-0.33}	1.19	1.33	64
ABELL 1689	70	681	1.87	9.46 ^{+0.34} _{-0.48}	13.23 ^{+1.87} _{-1.87}	1.40 ^{+0.21} _{-0.17}	0.38 ^{+0.07} _{-0.07}	1.31	1.16	91
ABELL 1758	70	573	1.09	12.14 ^{+1.51} _{-0.92}	11.16 ^{+3.08} _{-2.84}	0.92 ^{+0.27} _{-0.19}	0.56 ^{+0.13} _{-0.13}	1.21	1.09	58
ABELL 1763	69	562	0.82	7.78 ^{+0.60} _{-0.60}	11.49 ^{+2.84} _{-2.34}	1.48 ^{+0.19} _{-0.19}	0.25 ^{+0.11} _{-0.10}	1.12	0.92	84
ABELL 1835	69	571	2.36	9.77 ^{+0.57} _{-0.52}	11.00 ^{+1.03} _{-1.03}	1.13 ^{+0.14} _{-0.12}	0.31 ^{+0.08} _{-0.07}	0.98	1.02	86
ABELL 1914	70	698	0.97	9.62 ^{+0.35} _{-0.49}	11.42 ^{+1.26} _{-1.06}	1.19 ^{+0.15} _{-0.13}	0.30 ^{+0.08} _{-0.07}	1.07	1.03	92
ABELL 1942	70	474	2.75	4.77 ^{+0.38} _{-0.35}	5.49 ^{+0.98} _{-0.74}	1.15 ^{+0.22} _{-0.18}	0.33 ^{+0.12} _{-0.11}	1.06	1.04	70
ABELL 1995	70	366	1.44	8.37 ^{+0.70} _{-0.61}	9.23 ^{+1.44} _{-1.13}	1.10 ^{+0.20} _{-0.15}	0.39 ^{+0.12} _{-0.11}	1.02	0.96	74
ABELL 2034	69	594	1.58	7.15 ^{+0.23} _{-0.22}	10.02 ^{+0.92} _{-0.75}	1.40 ^{+0.15} _{-0.14}	0.32 ^{+0.05} _{-0.05}	1.22	1.00	84
ABELL 2069	69	623	1.97	6.50 ^{+0.33} _{-0.33}	8.61 ^{+1.03} _{-0.84}	1.32 ^{+0.17} _{-0.14}	0.26 ^{+0.08} _{-0.07}	1.04	0.96	71
ABELL 2111	69	592	2.20	7.13 ^{+0.25} _{-0.25}	11.10 ^{+1.67} _{-1.67}	1.56 ^{+0.26} _{-0.26}	0.13 ^{+0.10} _{-0.09}	1.06	0.88	76
ABELL 2125	69	370	2.75	2.88 ^{+0.30} _{-0.27}	3.76 ^{+0.98} _{-0.65}	1.31 ^{+0.27} _{-0.26}	0.31 ^{+0.13} _{-0.16}	1.26	1.30	61
ABELL 2163	69	751	12.04	19.20 ^{+0.87} _{-0.80}	21.30 ^{+1.77} _{-1.47}	1.11 ^{+0.11} _{-0.09}	0.10 ^{+0.06} _{-0.06}	1.37	1.26	90
ABELL 2204	70	574	5.84	8.65 ^{+0.58} _{-0.58}	10.57 ^{+1.48} _{-1.23}	1.22 ^{+0.19} _{-0.18}	0.37 ^{+0.10} _{-0.09}	0.95	1.00	90
ABELL 2218	70	557	3.12	7.35 ^{+0.39} _{-0.35}	10.03 ^{+1.26} _{-0.98}	1.36 ^{+0.26} _{-0.15}	0.22 ^{+0.07} _{-0.06}	1.01	0.90	87
ABELL 2255	70	571	2.53	6.12 ^{+0.20} _{-0.19}	8.10 ^{+0.66} _{-0.58}	1.32 ^{+0.16} _{-0.10}	0.30 ^{+0.06} _{-0.06}	1.13	0.95	76
ABELL 2259	70	481	3.70	5.18 ^{+0.46} _{-0.46}	6.40 ^{+1.33} _{-0.97}	1.24 ^{+0.28} _{-0.28}	0.41 ^{+0.14} _{-0.14}	1.05	1.01	85
ABELL 2261	70	577	3.31	7.63 ^{+0.37} _{-0.43}	9.30 ^{+1.91} _{-0.91}	1.22 ^{+0.18} _{-0.14}	0.36 ^{+0.08} _{-0.08}	0.99	0.95	90
ABELL 2294	69	572	6.10	9.98 ^{+1.33} _{-1.23}	11.07 ^{+3.19} _{-2.11}	1.11 ^{+0.36} _{-0.25}	0.53 ^{+0.21} _{-0.21}	1.07	0.95	82
ABELL 2384	69	436	2.99	4.75 ^{+0.22} _{-0.20}	6.22 ^{+0.71} _{-0.60}	1.31 ^{+0.16} _{-0.16}	0.23 ^{+0.07} _{-0.07}	1.06	0.92	81
ABELL 2409	69	512	6.72	5.94 ^{+0.43} _{-0.38}	6.77 ^{+0.99} _{-0.82}	1.14 ^{+0.19} _{-0.16}	0.37 ^{+0.13} _{-0.11}	1.13	0.96	88
ABELL 2537	68	497	4.26	8.40 ^{+0.76} _{-0.68}	7.81 ^{+1.15} _{-0.93}	0.93 ^{+0.16} _{-0.13}	0.40 ^{+0.13} _{-0.13}	0.91	0.84	46
ABELL 2550	69	349	2.03	2.06 ^{+0.12} _{-0.11}	2.17 ^{+0.46} _{-0.46}	1.05 ^{+0.23} _{-0.17}	0.33 ^{+0.09} _{-0.08}	1.26	1.11	34
ABELL 2631	70	631	3.74	7.06 ^{+1.06} _{-0.84}	7.83 ^{+2.18} _{-1.45}	1.11 ^{+0.35} _{-0.24}	0.34 ^{+0.19} _{-0.18}	0.97	0.88	83
ABELL 2667	69	524	1.64	6.75 ^{+0.48} _{-0.34}	7.45 ^{+1.45} _{-0.88}	1.10 ^{+0.18} _{-0.15}	0.36 ^{+0.11} _{-0.11}	1.17	1.08	76
ABELL 2670	69	451	2.88	3.95 ^{+0.39} _{-0.34}	4.65 ^{+0.88} _{-0.48}	1.18 ^{+0.17} _{-0.10}	0.42 ^{+0.08} _{-0.08}	1.13	1.07	70
ABELL 2717	69	298	1.12	2.63 ^{+0.17} _{-0.16}	3.17 ^{+0.48} _{-0.43}	1.21 ^{+0.23} _{-0.18}	0.48 ^{+0.13} _{-0.13}	0.88	0.87	55
ABELL 2744	68	620	1.82	9.18 ^{+0.68} _{-0.60}	10.20 ^{+1.38} _{-1.10}	1.11 ^{+0.17} ₋				

TABLE 4 — *Continued*

Cluster	R _{CORE} kpc (2)	R ₂₅₀₀ kpc (3)	N _H 10 ²⁰ cm ⁻² (4)	T ₇₇ keV (5)	T ₂₇ keV (6)	T _{HFR} (7)	Z ₇₇ Z _⊙ (8)	χ _{red,77} (9)	χ _{red,27} (10)	% Source (11)
ABELL 3921	70	535	3.07	5.70 ^{+0.24} _{-0.23}	6.65 ^{+0.65} _{-0.54}	1.17 ^{+0.12} _{-0.11}	0.31 ^{+0.08} _{-0.07}	1.02	0.96	77
AC 114	69	528	1.44	7.53 ^{+0.49} _{-0.44}	8.30 ^{+1.03} _{-0.95}	1.10 ^{+0.15} _{-0.13}	0.26 ^{+0.08} _{-0.09}	1.07	1.06	55
CL 0024+17	70	417	4.36	6.03 ^{+1.66} _{-1.40}	7.18 ^{+3.16} _{-1.74}	1.19 ^{+0.35} _{-0.32}	0.60 ^{+0.37} _{-0.30}	1.00	1.44	37
CL 1221+4918	68	427	1.44	6.62 ^{+0.99} _{-1.32}	7.11 ^{+1.31} _{-1.29}	1.07 ^{+0.23} _{-0.25}	0.34 ^{+0.18} _{-0.18}	0.94	0.93	62
CL J0030+2618	69	753	4.10	4.63 ^{+0.72} _{-1.02}	5.18 ^{+0.83} _{-1.96}	1.12 ^{+0.91} _{-0.53}	0.26 ^{+0.26} _{-0.26}	1.00	1.23	37
CL J0152-1357	69	375	1.45	7.33 ^{+2.78} _{-1.32}	7.31 ^{+3.43} _{-2.77}	1.00 ^{+0.60} _{-0.37}	0.00 ^{+0.24} _{-0.00}	0.89	1.00	36
CL J0542.8-4100	68	427	3.59	6.07 ^{+1.47} _{-1.05}	6.29 ^{+2.14} _{-1.41}	1.04 ^{+0.43} _{-0.29}	0.16 ^{+0.23} _{-0.16}	1.04	0.91	66
CL J0848+4456 †	68	306	2.53	4.53 ^{+1.57} _{-1.13}	5.52 ^{+3.28} _{-1.74}	1.22 ^{+0.84} _{-0.49}	0.00 ^{+0.45} _{-0.00}	0.92	0.93	58
CL J1113.1-2615	69	417	5.51	4.19 ^{+1.61} _{-1.02}	4.10 ^{+2.47} _{-1.44}	0.98 ^{+0.70} _{-0.42}	0.46 ^{+0.63} _{-0.44}	1.01	1.08	23
CL J1213+0253	69	362	1.78	4.83 ^{+3.25} _{-1.32}	5.05 ^{+5.43} _{-3.43}	1.05 ^{+1.33} _{-0.53}	0.06 ^{+0.95} _{-0.06}	0.48	0.62	56
CL J1226.9+3332 †	70	450	1.37	11.81 ^{+2.55} _{-1.70}	11.29 ^{+2.45} _{-1.77}	0.96 ^{+0.98} _{-0.98}	0.21 ^{+0.20} _{-0.21}	0.81	0.86	86
CL J1641+4001	69	234	1.09	3.29 ^{+0.93} _{-0.74}	5.75 ^{+3.80} _{-2.01}	1.75 ^{+1.26} _{-0.67}	0.77 ^{+0.92} _{-0.59}	1.63	1.77	74
CL J2302.8+0844	69	493	5.05	4.25 ^{+1.77} _{-1.32}	4.67 ^{+2.00} _{-1.80}	1.10 ^{+0.56} _{-0.48}	0.13 ^{+0.33} _{-0.13}	0.89	0.97	50
DLS J0514-4904	69	486	2.52	4.62 ^{+0.53} _{-0.47}	6.14 ^{+2.08} _{-1.34}	1.33 ^{+0.48} _{-0.32}	0.37 ^{+0.24} _{-0.20}	1.04	1.12	54
MACS J0011.7-1523	69	452	2.08	6.64 ^{+0.62} _{-0.53}	6.90 ^{+1.05} _{-0.82}	1.04 ^{+0.19} _{-0.15}	0.32 ^{+0.12} _{-0.12}	0.90	0.87	81
MACS J0025.4-1222 †	69	454	2.72	6.33 ^{+0.85} _{-0.70}	6.01 ^{+1.05} _{-0.85}	0.95 ^{+0.21} _{-0.15}	0.37 ^{+0.16} _{-0.08}	0.90	0.92	80
MACS J0159.8-0849 †	69	587	2.01	9.16 ^{+0.63} _{-0.63}	9.83 ^{+0.96} _{-0.83}	1.07 ^{+0.23} _{-0.23}	0.30 ^{+0.09} _{-0.09}	1.08	1.09	90
MACS J0242.5-2132	69	497	2.71	5.58 ^{+0.63} _{-0.52}	6.26 ^{+1.38} _{-0.99}	1.12 ^{+0.28} _{-0.21}	0.34 ^{+0.16} _{-0.13}	1.03	0.83	87
MACS J0257.1-2323 †	70	579	2.09	9.25 ^{+1.28} _{-1.01}	10.16 ^{+1.95} _{-1.54}	1.10 ^{+0.26} _{-0.26}	0.14 ^{+0.15} _{-0.12}	0.99	1.08	84
MACS J0257.6-2209	68	540	2.02	8.02 ^{+1.12} _{-0.88}	8.17 ^{+1.92} _{-1.30}	1.02 ^{+0.28} _{-0.20}	0.30 ^{+0.16} _{-0.13}	1.12	1.26	84
MACS J0308.9+2645	69	539	11.88	10.54 ^{+1.28} _{-1.07}	11.38 ^{+2.16} _{-1.66}	1.08 ^{+0.24} _{-0.19}	0.28 ^{+0.13} _{-0.14}	0.97	1.01	87
MACS J0329.6-0211 †	71	419	6.21	6.30 ^{+0.47} _{-0.41}	7.50 ^{+0.83} _{-0.69}	1.19 ^{+0.16} _{-0.13}	0.41 ^{+0.10} _{-0.09}	1.10	1.17	86
MACS J0404.6+1109	71	473	14.96	5.77 ^{+1.14} _{-0.88}	6.15 ^{+2.00} _{-1.44}	1.07 ^{+0.41} _{-0.30}	0.24 ^{+0.22} _{-0.22}	0.85	0.78	73
MACS J0417.5-1154	70	430	4.00	11.07 ^{+1.98} _{-1.69}	14.90 ^{+3.03} _{-2.24}	1.35 ^{+0.58} _{-0.34}	0.33 ^{+0.19} _{-0.18}	1.07	0.97	94
MACS J0429.6-0253	68	495	5.70	5.66 ^{+0.64} _{-0.54}	6.71 ^{+1.26} _{-0.98}	1.19 ^{+0.21} _{-0.15}	0.35 ^{+0.14} _{-0.13}	1.21	1.12	82
MACS J0451.9+0006	69	440	7.65	5.80 ^{+0.46} _{-0.38}	7.02 ^{+3.80} _{-1.80}	1.21 ^{+0.38} _{-0.38}	0.51 ^{+0.33} _{-0.29}	1.25	1.35	83
MACS J0547.0-3904	69	363	4.08	3.58 ^{+0.44} _{-0.37}	5.41 ^{+1.67} _{-1.18}	1.51 ^{+0.50} _{-0.36}	0.09 ^{+0.15} _{-0.09}	1.16	1.42	75
MACS J0717.5+3745 †	70	565	6.75	12.77 ^{+1.16} _{-1.00}	13.21 ^{+1.58} _{-1.29}	1.03 ^{+0.16} _{-0.13}	0.30 ^{+0.10} _{-0.11}	0.93	0.90	88
MACS J0744.8+3927 †	71	539	4.66	8.09 ^{+0.77} _{-0.66}	8.77 ^{+1.04} _{-0.87}	1.08 ^{+0.16} _{-0.14}	0.32 ^{+0.10} _{-0.10}	1.14	1.18	82
MACS J0911.2+1746	69	518	3.55	8.30 ^{+2.64} _{-1.72}	8.66 ^{+4.42} _{-2.97}	1.04 ^{+0.63} _{-0.63}	0.21 ^{+0.28} _{-0.18}	0.69	0.76	78
MACS J0949+1708	69	556	3.17	9.16 ^{+1.53} _{-1.18}	9.11 ^{+2.39} _{-1.55}	0.99 ^{+0.30} _{-0.21}	0.37 ^{+0.20} _{-0.20}	0.89	0.84	89
MACS J1115.8-0129	69	448	4.36	6.78 ^{+0.91} _{-0.91}	8.27 ^{+1.16} _{-1.16}	1.22 ^{+0.36} _{-0.36}	0.07 ^{+0.21} _{-0.07}	1.00	0.97	65
MACS J1131.8-1955	70	576	4.49	8.64 ^{+1.23} _{-0.97}	11.01 ^{+3.61} _{-2.10}	1.27 ^{+0.46} _{-0.28}	0.42 ^{+0.17} _{-0.17}	1.00	1.00	87
MACS J1149.5+2223 †	69	505	2.32	7.65 ^{+0.89} _{-0.89}	8.13 ^{+1.36} _{-1.04}	1.06 ^{+0.22} _{-0.17}	0.20 ^{+0.12} _{-0.11}	1.00	1.09	87
MACS J1206.2-0847	70	519	4.15	10.21 ^{+1.19} _{-0.97}	12.51 ^{+2.44} _{-1.87}	1.23 ^{+0.28} _{-0.22}	0.33 ^{+0.13} _{-0.13}	0.96	1.05	93
MACS J1226.8-2153	70	469	1.82	4.21 ^{+1.07} _{-0.80}	5.02 ^{+3.29} _{-1.84}	1.19 ^{+0.84} _{-0.43}	0.23 ^{+0.38} _{-0.23}	1.02	0.81	67
MACS J1311.0-0310 †	69	425	2.18	5.76 ^{+0.38} _{-0.32}	5.91 ^{+0.73} _{-0.62}	1.03 ^{+0.13} _{-0.13}	0.39 ^{+0.13} _{-0.13}	0.96	0.98	72
MACS J1319+7003	69	476	1.53	7.99 ^{+2.08} _{-1.52}	10.62 ^{+3.55} _{-2.52}	1.33 ^{+0.98} _{-0.98}	0.30 ^{+0.29} _{-0.29}	1.25	1.24	74
MACS J1427.6-2521	70	409	6.11	4.66 ^{+0.33} _{-0.22}	8.37 ^{+5.00} _{-2.72}	1.80 ^{+1.13} _{-0.69}	0.18 ^{+0.28} _{-0.28}	1.19	1.39	68
MACS J1621.3+3810 †	69	505	1.07	7.12 ^{+0.66} _{-0.55}	7.09 ^{+0.95} _{-1.46}	1.00 ^{+0.16} _{-0.13}	0.34 ^{+0.11} _{-0.11}	0.93	0.86	73
MACS J1931.8-2634	70	535	9.13	6.97 ^{+0.72} _{-0.61}	7.72 ^{+1.31} _{-0.99}	1.11 ^{+0.22} _{-0.17}	0.27 ^{+0.11} _{-0.11}	0.95	0.86	90
MACS J2211.7-0349	70	663	5.86	11.30 ^{+1.46} _{-1.17}	13.82 ^{+3.54} _{-2.41}	1.22 ^{+0.35} _{-0.25}	0.15 ^{+0.13} _{-0.14}	1.24	1.26	88
MACS J2214.9-1359 †	70	531	3.32	9.78 ^{+1.38} _{-1.09}	10.45 ^{+2.19} _{-1.56}	1.07 ^{+0.27} _{-0.27}	0.23 ^{+0.14} _{-0.14}	0.99	1.06	87
MACS J2228+2036	70	546	4.52	7.86 ^{+0.85} _{-0.75}	9.17 ^{+2.05} _{-1.46}	1.17 ^{+0.31} _{-0.22}	0.39 ^{+0.16} _{-0.16}	0.99	1.00	88
MACS J2229.7-2755	69	466	1.34	5.01 ^{+0.43} _{-0.31}	5.79 ^{+1.11} _{-0.86}	1.16 ^{+0.25} _{-0.25}	0.55 ^{+0.19} _{-0.18}	1.05	1.08	85
MACS J2243.3-0935	70	550	4.31	4.09 ^{+0.45} _{-0.45}	7.20 ^{+1.12} _{-0.77}	1.76 ^{+0.80} _{-0.80}	0.03 ^{+0.29} _{-0.03}	1.17	0.92	51
MACS J2245.0+2637	70	452	5.50	6.06 ^{+0.63} _{-0.54}	6.76 ^{+1.24} _{-0.93}	1.12 ^{+0.24} _{-0.18}	0.60 ^{+0.20} _{-0.20}	0.94	1.09	88
MACS J2311.0+0338	69	348	5.23	8.14 ^{+1.45} _{-1.16}	12.53 ^{+5.10} _{-2.93}	1.54 ^{+0.68} _{-0.42}	0.46 ^{+0.38} _{-0.20}	1.07	1.15	88
MKW3S	69	338	3.05	3.91 ^{+0.66} _{-0.66}	4.58 ^{+0.18} _{-0.18}	1.17 ^{+0.05} _{-0.05}	0.34 ^{+0.03} _{-0.04}	1.38	0.97	86
MS 0016.9+1609	69	549	4.06	8.94 ^{+0.71} _{-0.62}	9.78 ^{+1.09} _{-0.90}	1.09 ^{+0.15} _{-0.13}	0.29 ^{+0.09} _{-0.08}	0.91	0.88	83
MS 0302.7+1658	68	354	10.95	3.27 ^{+0.05} _{-0.04}	2.60 ^{+0.23} _{-0.23}	0.80 ^{+0.45} _{-0.45}	0.81 ^{+0.56} _{-0.56}	1.14	1.12	70
MS 0451.6-0305	69	514	5.68	8.90 ^{+0.85} _{-0.85}	10.43 ^{+3.59} _{-2.59}	1.17 ^{+0.27} _{-0.27}	0.37 ^{+0.11} _{-0.11}	1.00	0.93	60
MS 0735.6+7421	69	491	3.40	5.55 ^{+0.24} _{-0.22}	6.34 ^{+0.56} _{-0.50}	1.14 ^{+0.17} _{-0.17}	0.35 ^{+0.07} _{-0.06}	1.05	1.05	62
MS 0839.8+2938	70	415	3.92	4.68 ^{+0.32} _{-0.29}	5.05 ^{+0.82} _{-0.65}	1.08 ^{+0.19} _{-0.15}	0.46 ^{+0.13} _{-0.12}	0.90	0.87	60
MS 0906.5+1110	70	616	3.60	5.38 ^{+0.33} _{-0.29}	6.76 ^{+1.77} _{-1.77}	1.26 ^{+0.19} _{-0.16}	0.27 ^{+0.09} _{-0.09}	1.21	1.08	75
MS 1006.0+1202	69	557	3.63	5.61 ^{+0.51} _{-0.51}	7.48 ^{+1.66} _{-1.22}	1.33 ^{+0.32} _{-0.24}	0.24 ^{+0.11} _{-0.11}	1.30	1.34	75
MS 1008.1-1224	69	549	6.71	5.65 ^{+0.49} _{-0.43}	9.01 ^{+1.95} _{-1.38}	1.59 ^{+0.37} _{-0.27}	0.26 ^{+0.11} _{-0.19}	1.21	0.98	78
MS 1054.5-0321	69	535	3.69	9.38 ^{+1.72} _{-1.72}	9.91 ^{+2.69} _{-2.77}	1.06 ^{+0.34} _{-0.34}	0.13 ^{+0.19} _{-0.13}	1.02	1.03	41
MS 1455.0+2232	70	436	3.35	4.77 ^{+0.13} _{-0.13}	5.37 ^{+0.26} _{-0.22}	1.13 ^{+0.06} _{-0.06}	0.44 ^{+0.05} _{-0.05}	1.29	1.10	90
MS 1621.5+2640										

TABLE 4 — *Continued*

Cluster (1)	R _{CORE} kpc (2)	R ₂₅₀₀ kpc (3)	N _{HI} 10 ²⁰ cm ⁻² (4)	T ₇₇ keV (5)	T ₂₇ keV (6)	T _{HFR} (7)	Z ₇₇ Z _⊙ (8)	χ _{red,77} (9)	χ _{red,27} (10)	% Source (11)
RDCS 1252-29	68	264	6.06	4.25 ^{+1.82} _{-1.14}	4.47 ^{+2.16} _{-1.29}	1.05 ^{+0.68} _{-0.41}	0.79 ^{+1.01} _{-0.62}	1.07	1.17	50
RX J0232.2-4420	69	569	2.53	7.83 ^{+0.77} _{-0.68}	9.92 ^{+2.11} _{-0.34}	1.27 ^{+0.30} _{-0.21}	0.36 ^{+0.12} _{-0.13}	1.13	1.09	85
RX J0340-4542	69	395	1.63	3.16 ^{+0.38} _{-0.25}	2.80 ^{+0.34} _{-0.57}	0.89 ^{+0.32} _{-0.22}	0.62 ^{+0.31} _{-0.26}	1.27	1.22	43
RX J0439+0520	69	454	10.02	4.60 ^{+0.48} _{-0.59}	4.95 ^{+1.57} _{-0.88}	1.08 ^{+0.24} _{-0.24}	0.44 ^{+0.24} _{-0.24}	1.03	1.14	77
RX J0439.0+0715 †	69	533	11.16	5.63 ^{+0.36} _{-0.32}	8.02 ^{+1.33} _{-0.93}	1.42 ^{+0.24} _{-0.18}	0.32 ^{+0.10} _{-0.08}	1.28	1.16	82
RX J0528.9-3927	69	641	2.36	7.89 ^{+0.36} _{-0.76}	8.91 ^{+2.30} _{-1.42}	1.13 ^{+0.32} _{-0.21}	0.27 ^{+0.14} _{-0.14}	0.92	0.93	83
RX J0647.7+7015 †	69	513	5.18	11.28 ^{+1.85} _{-1.45}	11.01 ^{+2.17} _{-1.63}	0.98 ^{+0.25} _{-0.19}	0.20 ^{+0.14} _{-0.17}	1.02	1.00	80
RX J0910+5422 †	70	235	2.07	4.53 ^{+1.70} _{-0.34}	5.98 ^{+5.02} _{-2.49}	1.32 ^{+1.46} _{-0.74}	0.00 ^{+0.73} _{-0.00}	0.90	0.71	31
RX J1053+5735	71	241	0.59	7.03 ^{+17.25} _{-3.47}	5.06 ^{+12.74} _{-2.48}	0.72 ^{+2.53} _{-2.50}	0.55 ^{+2.26} _{-0.55}	1.48	1.27	16
RX J1347.5-1145 †	68	607	4.89	14.62 ^{+0.87} _{-0.79}	16.62 ^{+1.54} _{-1.54}	1.14 ^{+0.13} _{-0.13}	0.32 ^{+0.08} _{-0.08}	1.12	1.12	93
RX J1350+6007	68	320	1.77	4.48 ^{+0.32} _{-1.49}	5.31 ^{+3.04} _{-2.07}	1.19 ^{+0.91} _{-0.91}	0.13 ^{+0.13} _{-0.13}	0.82	0.72	57
RX J1423.8+2404 †	70	423	2.65	6.64 ^{+0.38} _{-0.34}	7.01 ^{+0.59} _{-0.51}	1.06 ^{+0.61} _{-0.59}	0.37 ^{+0.07} _{-0.07}	1.02	0.98	86
RX J1504.1-0248	69	628	6.27	8.00 ^{+0.27} _{-0.24}	8.92 ^{+0.53} _{-0.54}	1.11 ^{+0.08} _{-0.07}	0.40 ^{+0.04} _{-0.05}	1.29	1.25	91
RX J1525+0958	71	399	2.96	3.67 ^{+0.24} _{-0.44}	6.70 ^{+2.72} _{-1.57}	1.83 ^{+0.80} _{-0.48}	0.68 ^{+0.36} _{-0.29}	1.27	0.93	78
RX J1532.9+3021 †	69	458	2.21	6.03 ^{+0.38} _{-0.38}	6.95 ^{+0.88} _{-0.72}	1.15 ^{+0.17} _{-0.14}	0.42 ^{+0.11} _{-0.10}	0.94	1.05	73
RX J1716.9+6708	68	466	3.71	5.71 ^{+1.47} _{-1.06}	5.77 ^{+1.88} _{-1.28}	1.01 ^{+0.42} _{-0.29}	0.68 ^{+0.42} _{-0.35}	0.79	0.74	55
RX J1720.1+2638	70	510	4.02	6.37 ^{+0.28} _{-0.28}	7.78 ^{+0.69} _{-0.61}	1.22 ^{+0.12} _{-0.12}	0.35 ^{+0.07} _{-0.07}	1.10	1.02	90
RX J1720.2+3536 †	70	453	3.35	7.21 ^{+0.35} _{-0.35}	6.97 ^{+0.66} _{-0.59}	0.97 ^{+0.13} _{-0.10}	0.41 ^{+0.08} _{-0.10}	1.12	1.09	85
RX J2011.3-5725	70	399	4.76	3.94 ^{+0.45} _{-0.45}	4.40 ^{+1.20} _{-0.81}	1.12 ^{+0.33} _{-0.23}	0.34 ^{+0.21} _{-0.18}	0.94	1.09	76
RX J2129.6+0005	70	690	4.30	5.91 ^{+0.34} _{-0.47}	7.02 ^{+1.30} _{-0.99}	1.19 ^{+0.25} _{-0.19}	0.45 ^{+0.15} _{-0.15}	1.21	1.07	80
S0463 †	69	415	1.06	2.96 ^{+0.20} _{-0.17}	3.13 ^{+0.49} _{-0.40}	1.06 ^{+0.18} _{-0.15}	0.23 ^{+0.10} _{-0.07}	1.15	1.14	50
V 1121.0+2327	71	426	1.30	3.60 ^{+0.62} _{-0.39}	4.08 ^{+1.09} _{-0.80}	1.13 ^{+0.36} _{-0.27}	0.36 ^{+0.29} _{-0.24}	1.21	1.19	66
ZWCL 1215	69	392	1.76	6.62 ^{+0.36} _{-0.36}	8.67 ^{+1.06} _{-1.06}	1.31 ^{+0.21} _{-0.18}	0.29 ^{+0.09} _{-0.09}	1.17	1.04	88
ZWCL 1358+6245	69	530	1.94	10.66 ^{+1.48} _{-1.00}	10.19 ^{+4.83} _{-3.24}	0.96 ^{+0.47} _{-0.47}	0.47 ^{+0.19} _{-0.19}	1.08	1.04	55
ZWCL 1953	69	732	3.10	7.37 ^{+1.00} _{-0.78}	10.44 ^{+2.20} _{-2.20}	1.42 ^{+0.33} _{-0.33}	0.19 ^{+0.13} _{-0.13}	0.84	0.78	74
ZWCL 3146	70	722	2.70	7.48 ^{+0.32} _{-0.30}	8.61 ^{+0.66} _{-0.61}	1.15 ^{+0.10} _{-0.10}	0.31 ^{+0.03} _{-0.06}	1.03	0.98	86
ZWCL 5247	69	609	1.70	5.06 ^{+0.85} _{-0.64}	5.91 ^{+2.09} _{-1.30}	1.17 ^{+0.46} _{-0.39}	0.22 ^{+0.21} _{-0.19}	0.83	0.72	74
ZWCL 7160	70	637	3.10	4.53 ^{+0.40} _{-0.35}	5.16 ^{+1.01} _{-0.77}	1.14 ^{+0.24} _{-0.19}	0.40 ^{+0.15} _{-0.14}	0.94	0.92	80
ZWICKY 2701	69	445	0.83	5.21 ^{+0.34} _{-0.30}	5.68 ^{+0.85} _{-0.85}	1.09 ^{+0.18} _{-0.14}	0.43 ^{+0.13} _{-0.11}	0.89	0.94	57
ZwCL 1332.8+5043	71	616	1.10	3.62 ^{+3.36} _{-1.20}	3.84 ^{+5.93} _{-1.48}	1.06 ^{+1.93} _{-0.54}	0.76 ^{+12.45} _{-0.76}	0.24	0.29	48
ZwCl 0848.5+3341	70	497	1.12	6.83 ^{+2.18} _{-1.33}	7.24 ^{+5.11} _{-2.26}	1.06 ^{+0.82} _{-0.39}	0.56 ^{+0.54} _{-0.45}	0.82	0.93	37

NOTE. — Note: '77' refers to 0.7-7.0 keV band, '27' refers to 2.0_{rest}-7.0 keV band. (1) Cluster name, (2) absorbing, Galactic neutral hydrogen column density, (3,4) best-fit MeKaL temperatures, (5) best-fit 77 MeKaL abundance, (6) T_{0.7-7.0}/T_{2.0-7.0} also called T_{HFR}, (7,8) reduced χ² statistics, (9) percent of emission attributable to source. † indicates cluster with multiple independent, simultaneously fit spectra.

TABLE 5
 SUMMARY OF EXCISED R₅₀₀₀ SPECTRAL FITS

Cluster	R _{CORE} kpc (2)	R ₅₀₀₀ kpc (3)	N _H 10 ²⁰ cm ⁻² (4)	T ₇₇ keV (5)	T ₂₇ keV (6)	T _{HFR} (7)	Z ₇₇ Z _⊙ (8)	χ _{red,77} ² (9)	χ _{red,27} ² (10)	% Source (11)
1E0657 56 †	69	486	6.53	11.81 ^{+0.29} _{-0.27}	14.13 ^{+0.58} _{-0.53}	1.20 ^{+0.06} _{-0.05}	0.29 ^{+0.03} _{-0.03}	1.22	1.10	95
1RXS J2129.4-0741 †	68	358	4.36	8.47 ^{+1.34} _{-0.94}	8.57 ^{+1.73} _{-0.83}	1.01 ^{+0.19} _{-0.17}	0.51 ^{+0.04} _{-0.19}	1.16	1.27	87
2PIGG J0011.5-2850	70	387	2.18	5.25 ^{+0.29} _{-0.27}	6.21 ^{+0.83} _{-0.91}	1.18 ^{+0.14} _{-0.14}	0.23 ^{+0.09} _{-0.13}	1.08	1.01	78
2PIGG J0311.8-2655	69	320	1.46	3.35 ^{+0.25} _{-0.22}	3.67 ^{+0.91} _{-0.54}	1.10 ^{+0.23} _{-0.18}	0.33 ^{+0.13} _{-0.16}	1.03	1.10	51
2PIGG J2227.0-3041	70	267	1.11	2.81 ^{+0.16} _{-0.15}	2.99 ^{+0.36} _{-0.36}	1.06 ^{+0.14} _{-0.11}	0.35 ^{+0.11} _{-0.08}	1.14	1.10	77
3C 220.1	70	308	1.91	6.75 ^{+3.80} _{-2.59}	2.52 ^{+0.40} _{-1.37}	0.37 ^{+0.00} _{-0.25}	0.00 ^{+0.62} _{-0.00}	0.79	0.76	64
3C 28.0	70	297	5.71	5.18 ^{+0.28} _{-0.27}	7.11 ^{+1.15} _{-0.90}	1.37 ^{+0.23} _{-0.19}	0.30 ^{+0.09} _{-0.07}	0.96	0.77	90
3C 295	69	329	1.35	5.35 ^{+0.48} _{-0.41}	8.06 ^{+2.35} _{-0.52}	1.51 ^{+0.46} _{-0.31}	0.29 ^{+0.12} _{-0.10}	1.01	1.07	86
3C 388	70	297	6.11	3.27 ^{+0.24} _{-0.24}	3.44 ^{+0.53} _{-0.51}	1.05 ^{+0.34} _{-0.34}	0.43 ^{+0.16} _{-0.16}	1.09	1.04	76
4C 55.16	70	300	4.00	4.88 ^{+0.16} _{-0.16}	5.11 ^{+0.39} _{-0.34}	1.05 ^{+0.10} _{-0.09}	0.52 ^{+0.07} _{-0.07}	0.93	0.85	71
ABELL 0013	70	404	2.03	6.84 ^{+0.36} _{-0.36}	9.29 ^{+1.37} _{-1.08}	1.36 ^{+0.21} _{-0.17}	0.55 ^{+0.10} _{-0.12}	1.14	1.10	56
ABELL 0068	69	460	4.60	9.72 ^{+1.82} _{-1.36}	10.89 ^{+5.21} _{-2.85}	1.12 ^{+0.58} _{-0.33}	0.41 ^{+0.24} _{-0.23}	1.08	1.03	87
ABELL 0119	69	399	3.30	5.86 ^{+0.28} _{-0.27}	6.20 ^{+0.74} _{-0.59}	1.06 ^{+0.14} _{-0.11}	0.44 ^{+0.10} _{-0.09}	0.98	0.89	75
ABELL 0168 †	69	270	3.27	2.60 ^{+0.12} _{-0.11}	3.55 ^{+0.56} _{-0.42}	1.37 ^{+0.22} _{-0.17}	0.33 ^{+0.07} _{-0.06}	1.06	0.99	48
ABELL 0209 †	70	430	1.68	7.32 ^{+0.26} _{-0.26}	10.05 ^{+2.33} _{-1.28}	1.37 ^{+0.34} _{-0.24}	0.21 ^{+0.11} _{-0.19}	1.07	1.15	88
ABELL 0267 †	69	385	2.74	6.46 ^{+0.31} _{-0.35}	7.46 ^{+1.22} _{-0.91}	1.15 ^{+0.21} _{-0.18}	0.37 ^{+0.12} _{-0.14}	1.18	1.29	88
ABELL 0370	71	365	3.37	8.74 ^{+0.38} _{-0.38}	10.15 ^{+1.17} _{-1.52}	1.16 ^{+0.16} _{-0.16}	0.37 ^{+0.13} _{-0.14}	1.05	1.02	50
ABELL 0383	69	299	4.07	4.95 ^{+0.30} _{-0.28}	5.92 ^{+1.05} _{-0.85}	1.20 ^{+0.22} _{-0.21}	0.43 ^{+0.13} _{-0.11}	1.12	1.10	75
ABELL 0399	70	386	8.33 ^{+0.82} _{-0.80}	7.93 ^{+0.38} _{-0.35}	8.86 ^{+0.67} _{-0.59}	1.12 ^{+0.18} _{-0.16}	0.32 ^{+0.06} _{-0.05}	1.06	0.96	87
ABELL 0401	70	454	12.48	6.54 ^{+0.22} _{-0.20}	9.37 ^{+0.91} _{-0.74}	1.43 ^{+0.15} _{-0.12}	0.29 ^{+0.07} _{-0.06}	1.53	1.10	85
ABELL 0478	70	422	30.90	7.27 ^{+0.26} _{-0.25}	8.19 ^{+0.56} _{-0.50}	1.13 ^{+0.09} _{-0.09}	0.47 ^{+0.06} _{-0.06}	1.02	0.93	95
ABELL 0514	70	350	3.14	3.85 ^{+0.27} _{-0.27}	4.92 ^{+0.75} _{-0.75}	1.28 ^{+0.28} _{-0.28}	0.29 ^{+0.12} _{-0.12}	1.00	1.01	58
ABELL 0520	69	408	1.14 ^{+1.16} _{-1.14}	9.15 ^{+0.73} _{-0.63}	10.43 ^{+1.06} _{-1.01}	1.14 ^{+0.18} _{-0.14}	0.36 ^{+0.07} _{-0.07}	1.12	1.01	91
ABELL 0521	69	378	6.17	7.31 ^{+0.79} _{-0.64}	9.01 ^{+3.73} _{-1.81}	1.23 ^{+0.53} _{-0.28}	0.48 ^{+0.17} _{-0.16}	1.11	0.95	55
ABELL 0586	70	449	4.71	6.43 ^{+0.55} _{-0.49}	8.06 ^{+1.81} _{-1.14}	1.25 ^{+0.28} _{-0.20}	0.50 ^{+0.16} _{-0.15}	0.88	0.81	87
ABELL 0611	69	369	4.99	6.79 ^{+0.51} _{-0.46}	6.88 ^{+1.23} _{-0.95}	1.01 ^{+0.20} _{-0.16}	0.32 ^{+0.10} _{-0.10}	1.04	1.07	67
ABELL 0644	69	411	6.31	7.81 ^{+0.19} _{-0.19}	8.08 ^{+0.44} _{-0.39}	1.03 ^{+0.06} _{-0.06}	0.42 ^{+0.05} _{-0.04}	1.15	1.05	92
ABELL 0665	69	437	4.24	7.35 ^{+0.40} _{-0.37}	10.43 ^{+1.76} _{-1.31}	1.42 ^{+0.25} _{-0.19}	0.29 ^{+0.07} _{-0.07}	1.07	0.94	91
ABELL 0697	70	433	3.34	9.78 ^{+0.39} _{-0.35}	14.71 ^{+1.37} _{-2.20}	1.50 ^{+0.48} _{-0.32}	0.48 ^{+0.13} _{-0.13}	1.06	0.95	93
ABELL 0773	69	434	1.46	8.08 ^{+0.65} _{-0.65}	11.24 ^{+2.34} _{-1.94}	1.39 ^{+0.32} _{-0.26}	0.37 ^{+0.13} _{-0.12}	1.03	0.96	89
ABELL 0907	70	345	5.69	5.60 ^{+0.19} _{-0.18}	6.26 ^{+0.49} _{-0.44}	1.12 ^{+0.10} _{-0.09}	0.46 ^{+0.06} _{-0.06}	1.17	1.02	92
ABELL 0963	70	385	1.39	6.97 ^{+0.35} _{-0.32}	7.65 ^{+1.00} _{-0.82}	1.10 ^{+0.15} _{-0.15}	0.29 ^{+0.08} _{-0.07}	1.13	1.12	74
ABELL 1063S	70	458	1.77	11.94 ^{+0.91} _{-0.80}	14.04 ^{+1.83} _{-1.47}	1.18 ^{+0.18} _{-0.15}	0.38 ^{+0.10} _{-0.09}	1.01	0.98	94
ABELL 1068	70	304	0.71	4.67 ^{+0.18} _{-0.18}	5.49 ^{+0.71} _{-0.58}	1.18 ^{+0.16} _{-0.13}	0.37 ^{+0.06} _{-0.07}	0.92	0.91	77
ABELL 1201	69	401	1.85	5.74 ^{+0.40} _{-0.39}	5.99 ^{+1.39} _{-0.95}	1.04 ^{+0.26} _{-0.18}	0.35 ^{+0.13} _{-0.11}	1.06	1.10	50
ABELL 1204	70	295	1.44	3.67 ^{+0.18} _{-0.18}	4.72 ^{+0.75} _{-0.57}	1.29 ^{+0.21} _{-0.15}	0.32 ^{+0.09} _{-0.09}	1.11	0.92	92
ABELL 1361	70	316	2.18	5.14 ^{+1.06} _{-0.74}	7.24 ^{+2.78} _{-2.39}	1.41 ^{+0.52} _{-0.58}	0.29 ^{+0.17} _{-0.27}	1.10	0.82	61
ABELL 1423	70	435	1.60	6.04 ^{+0.82} _{-0.68}	7.93 ^{+4.09} _{-2.20}	1.31 ^{+0.70} _{-0.39}	0.33 ^{+0.20} _{-0.17}	0.95	0.91	84
ABELL 1651	70	421	2.02	6.30 ^{+0.28} _{-0.28}	7.46 ^{+0.99} _{-0.91}	1.18 ^{+0.17} _{-0.14}	0.44 ^{+0.09} _{-0.09}	1.13	1.17	91
ABELL 1664	70	291	8.47	4.26 ^{+0.30} _{-0.26}	4.91 ^{+1.05} _{-0.80}	1.15 ^{+0.26} _{-0.20}	0.31 ^{+0.12} _{-0.11}	1.07	1.08	70
ABELL 1689	70	480	1.87	9.53 ^{+0.55} _{-0.51}	13.73 ^{+2.51} _{-1.95}	1.44 ^{+0.28} _{-0.22}	0.36 ^{+0.08} _{-0.07}	1.30	1.16	94
ABELL 1758	70	406	1.09	9.66 ^{+0.75} _{-0.64}	9.90 ^{+1.22} _{-1.89}	1.02 ^{+0.15} _{-0.14}	0.48 ^{+0.11} _{-0.11}	1.03	0.96	68
ABELL 1763	69	396	0.82	7.74 ^{+0.73} _{-0.73}	12.56 ^{+6.70} _{-12.12}	1.62 ^{+0.88} _{-0.82}	0.22 ^{+0.13} _{-0.12}	1.16	1.02	89
ABELL 1795	69	449	1.22	6.05 ^{+0.15} _{-0.15}	6.85 ^{+0.42} _{-0.38}	1.13 ^{+0.07} _{-0.07}	0.33 ^{+0.05} _{-0.05}	1.19	1.03	93
ABELL 1835	69	404	2.36	9.55 ^{+0.55} _{-0.51}	11.99 ^{+1.44} _{-1.44}	1.26 ^{+0.22} _{-0.17}	0.35 ^{+0.07} _{-0.08}	0.91	0.88	91
ABELL 1914	70	494	0.97	9.73 ^{+0.58} _{-0.51}	11.97 ^{+1.90} _{-1.40}	1.23 ^{+0.21} _{-0.21}	0.32 ^{+0.08} _{-0.07}	1.11	1.03	95
ABELL 1942	70	334	2.75	4.96 ^{+0.45} _{-0.39}	5.94 ^{+2.24} _{-0.99}	1.20 ^{+0.46} _{-0.22}	0.37 ^{+0.15} _{-0.14}	1.04	0.87	77
ABELL 1995	70	260	1.44	8.50 ^{+0.83} _{-0.71}	9.41 ^{+1.87} _{-1.87}	1.11 ^{+0.25} _{-0.17}	0.33 ^{+0.12} _{-0.12}	1.05	1.02	81
ABELL 2029	69	434	3.26	8.20 ^{+0.32} _{-0.29}	9.90 ^{+0.90} _{-0.73}	1.21 ^{+0.12} _{-0.10}	0.40 ^{+0.06} _{-0.06}	1.07	1.03	94
ABELL 2034	69	420	1.58	7.35 ^{+0.26} _{-0.26}	9.96 ^{+1.08} _{-0.98}	1.36 ^{+0.16} _{-0.12}	0.34 ^{+0.05} _{-0.05}	1.17	1.02	90
ABELL 2065	70	370	2.96	5.75 ^{+0.17} _{-0.17}	6.39 ^{+0.36} _{-0.31}	1.11 ^{+0.09} _{-0.08}	0.28 ^{+0.05} _{-0.05}	1.11	1.01	89
ABELL 2069	69	441	1.97	6.33 ^{+0.36} _{-0.32}	8.29 ^{+0.92} _{-1.02}	1.31 ^{+0.23} _{-0.17}	0.24 ^{+0.08} _{-0.08}	1.14	1.15	78
ABELL 2111	69	418	2.20	5.74 ^{+1.43} _{-0.97}	7.18 ^{+1.93} _{-2.52}	1.25 ^{+1.21} _{-0.49}	0.16 ^{+0.30} _{-0.16}	1.06	0.97	74
ABELL 2125	69	262	2.75	3.09 ^{+0.37} _{-0.31}	3.69 ^{+1.99} _{-0.81}	1.19 ^{+0.66} _{-0.29}	0.36 ^{+0.25} _{-0.20}	1.25	1.22	68
ABELL 2163	69	531	12.04	18.78 ^{+0.89} _{-0.83}	19.49 ^{+2.03} _{-1.86}	1.04 ^{+0.12} _{-0.11}	0.09 ^{+0.06} _{-0.05}	1.33	1.25	93
ABELL 2204 †	70	406	5.84	9.35 ^{+0.43} _{-0.41}	10.18 ^{+0.95} _{-0.77}	1.09 ^{+0.11} _{-0.10}	0.37 ^{+0.07} _{-0.07}	0.95	0.97	86
ABELL 2218	70	394	3.12	7.37 ^{+0.40} _{-0.37}	9.36 ^{+1.42} _{-1.07}	1.27 ^{+0.20} _{-0.18}	0.22 ^{+0.07} _{-0.06}	1.00	0.91	91
ABELL 2219	70	463	1.76	12.60 ^{+0.65} _{-0.61}	12.54 ^{+1.21} _{-1.21}	1.00 ^{+0.13} _{-0.13}	0.31 ^{+0.07} _{-0.06}	1.02	0.98	81
ABELL 2255	70	404	2.53	6.37 ^{+0.24} _{-0.23}	7.70 ^{+0.79} _{-0.69}	1.21 ^{+0.13} _{-0.13}	0.34 ^{+0.06} _{-0.06}	0.93	0.84	81
ABELL 2256	69	423	4.05	5.66 ^{+0.17} _{-0.17}	7.30 ^{+0.89} _{-0.63}	1.29 ^{+0.13} _{-0.12}	0.31 ^{+0.07} _{-0.07}	1.61	1.44	79
ABELL 2259	70	339	3.70	5.07 ^{+0.46} _{-0.40}	5.4					

TABLE 5 — *Continued*

Cluster	R _{CORE} kpc (2)	R ₅₀₀₀ kpc (3)	N _H 10 ²⁰ cm ⁻² (4)	T ₇₇ keV (5)	T ₂₇ keV (6)	T _{HFR} (7)	Z ₇₇ Z _⊙ (8)	χ _{red,77} (9)	χ _{red,27} (10)	% Source (11)
ABELL 2384	69	309	2.99	4.53 ^{+0.22} _{-0.21}	6.78 ^{+1.13} _{-0.89}	1.50 ^{+0.26} _{-0.21}	0.15 ^{+0.07} _{-0.06}	0.99	0.88	86
ABELL 2390	69	447	6.71	10.85 ^{+0.34} _{-0.31}	10.53 ^{+0.62} _{-0.53}	0.97 ^{+0.06} _{-0.06}	0.35 ^{+0.05} _{-0.04}	1.15	1.03	81
ABELL 2409	69	362	6.72	5.93 ^{+0.35} _{-0.39}	5.87 ^{+0.95} _{-0.76}	0.99 ^{+0.18} _{-0.14}	0.35 ^{+0.13} _{-0.14}	1.05	0.76	92
ABELL 2537	68	351	4.26	8.83 ^{+0.74} _{-0.78}	7.83 ^{+1.14} _{-0.74}	0.89 ^{+0.14} _{-0.15}	0.39 ^{+0.14} _{-0.14}	0.93	0.83	59
ABELL 2550	69	247	2.03	2.12 ^{+0.11} _{-0.11}	2.56 ^{+0.69} _{-0.49}	1.21 ^{+0.33} _{-0.34}	0.36 ^{+0.08} _{-0.08}	1.34	1.14	47
ABELL 2554	70	398	2.04	5.35 ^{+0.45} _{-0.40}	6.46 ^{+1.93} _{-1.24}	1.21 ^{+0.37} _{-0.34}	0.35 ^{+0.13} _{-0.13}	0.93	0.79	40
ABELL 2556	70	323	2.02	3.57 ^{+0.16} _{-0.15}	4.07 ^{+0.56} _{-0.46}	1.14 ^{+0.16} _{-0.14}	0.36 ^{+0.07} _{-0.07}	0.99	0.95	58
ABELL 2631	70	446	3.74	7.18 ^{+1.18} _{-0.94}	9.18 ^{+3.19} _{-1.96}	1.28 ^{+0.49} _{-0.32}	0.34 ^{+0.20} _{-0.19}	1.03	0.99	89
ABELL 2667	69	371	1.64	6.68 ^{+0.48} _{-0.43}	7.35 ^{+1.27} _{-0.55}	1.10 ^{+0.21} _{-0.17}	0.41 ^{+0.12} _{-0.12}	1.05	0.95	84
ABELL 2670	69	319	2.88	3.96 ^{+0.13} _{-0.13}	4.75 ^{+0.50} _{-0.50}	1.20 ^{+0.13} _{-0.13}	0.45 ^{+0.08} _{-0.08}	1.16	1.09	80
ABELL 2717	69	210	1.12	2.59 ^{+0.17} _{-0.16}	3.18 ^{+0.39} _{-0.44}	1.23 ^{+0.24} _{-0.19}	0.53 ^{+0.14} _{-0.12}	0.90	0.95	67
ABELL 2744	68	439	1.82	9.82 ^{+0.89} _{-0.77}	11.21 ^{+2.76} _{-1.81}	1.14 ^{+0.30} _{-0.29}	0.30 ^{+0.12} _{-0.12}	0.88	0.73	74
ABELL 3128	69	305	1.59	3.04 ^{+0.23} _{-0.21}	3.48 ^{+0.73} _{-0.54}	1.14 ^{+0.26} _{-0.19}	0.33 ^{+0.13} _{-0.10}	1.05	1.13	64
ABELL 3158 †	70	381	1.60	5.08 ^{+0.08} _{-0.08}	6.26 ^{+0.26} _{-0.24}	1.23 ^{+0.05} _{-0.05}	0.40 ^{+0.03} _{-0.03}	1.15	0.97	89
ABELL 3164	69	306	2.55	2.40 ^{+0.65} _{-0.48}	3.19 ^{+5.68} _{-1.41}	1.33 ^{+2.39} _{-0.64}	0.23 ^{+0.32} _{-0.19}	1.29	1.59	30
ABELL 3376 †	69	327	5.21	4.44 ^{+0.14} _{-0.13}	5.94 ^{+0.55} _{-0.47}	1.34 ^{+0.13} _{-0.11}	0.36 ^{+0.06} _{-0.06}	1.18	1.13	65
ABELL 3391	69	397	5.46	5.72 ^{+0.31} _{-0.28}	6.44 ^{+0.80} _{-0.91}	1.13 ^{+0.15} _{-0.15}	0.11 ^{+0.08} _{-0.08}	1.00	0.97	67
ABELL 3921	70	378	3.07	5.69 ^{+0.28} _{-0.24}	6.74 ^{+0.58} _{-0.58}	1.18 ^{+0.14} _{-0.11}	0.34 ^{+0.08} _{-0.07}	0.93	0.85	84
AC 114	69	373	1.44	7.75 ^{+0.56} _{-0.50}	9.76 ^{+2.58} _{-1.55}	1.26 ^{+0.31} _{-0.24}	0.36 ^{+0.11} _{-0.10}	1.01	0.95	63
CL 0024+17	70	296	4.36	4.75 ^{+1.07} _{-0.76}	7.14 ^{+5.42} _{-2.83}	1.50 ^{+1.19} _{-0.64}	0.58 ^{+0.35} _{-0.30}	1.07	0.97	44
CL 1221+4918	68	300	1.44	6.73 ^{+1.29} _{-1.02}	7.60 ^{+4.33} _{-3.01}	1.13 ^{+0.68} _{-0.68}	0.32 ^{+0.20} _{-0.19}	0.92	0.69	73
CL J0030+2618	69	532	4.10	4.48 ^{+2.43} _{-1.14}	3.77 ^{+9.73} _{-9.73}	0.84 ^{+0.22} _{-0.22}	0.00 ^{+0.37} _{-0.37}	1.01	0.85	51
CL J0152-1357	69	266	1.45	7.20 ^{+1.38} _{-1.34}	6.07 ^{+6.16} _{-5.16}	0.84 ^{+1.20} _{-1.20}	0.00 ^{+0.63} _{-0.63}	2.97	3.26	49
CL J0542.8-4100	68	300	3.59	5.65 ^{+1.21} _{-1.20}	5.93 ^{+3.32} _{-1.68}	1.05 ^{+0.66} _{-0.55}	0.25 ^{+0.22} _{-0.22}	0.67	0.58	72
CL J0848+4456 †	68	215	2.53	3.73 ^{+1.47} _{-0.85}	4.96 ^{+1.81} _{-1.52}	1.33 ^{+0.57} _{-0.57}	0.17 ^{+0.17} _{-0.17}	0.87	0.82	64
CL J1113.1-2615	69	295	5.51	4.74 ^{+0.82} _{-0.98}	4.79 ^{+1.15} _{-1.26}	1.01 ^{+0.30} _{-0.34}	0.53 ^{+0.52} _{-0.37}	1.02	1.01	32
CL J1226.9+3332 †	70	316	1.37	13.02 ^{+2.69} _{-2.00}	12.33 ^{+2.78} _{-2.13}	0.95 ^{+0.29} _{-0.22}	0.18 ^{+0.23} _{-0.18}	0.75	0.80	91
CL J2302.8+0844	69	347	5.05	5.94 ^{+1.73} _{-1.86}	6.58 ^{+8.08} _{-2.67}	1.11 ^{+1.40} _{-0.57}	0.10 ^{+0.29} _{-0.10}	0.94	1.01	56
DLS J0514-4904	69	344	2.52	4.94 ^{+0.61} _{-0.55}	6.26 ^{+2.33} _{-1.30}	1.27 ^{+0.50} _{-0.39}	0.35 ^{+0.27} _{-0.23}	0.86	1.03	63
EXO 0422-086	70	294	6.22	3.41 ^{+0.14} _{-0.12}	3.44 ^{+0.37} _{-0.36}	1.01 ^{+0.12} _{-0.12}	0.37 ^{+0.08} _{-0.08}	0.96	0.93	80
HERCULES A	69	313	1.49 ^{+2.01} _{-1.49}	5.28 ^{+0.60} _{-0.50}	4.50 ^{+0.88} _{-0.85}	0.85 ^{+0.15} _{-0.15}	0.42 ^{+0.15} _{-0.14}	0.98	0.98	70
LYNX E †	68	215	2.53	4.74 ^{+1.72} _{-1.76}	5.10 ^{+8.00} _{-2.41}	1.08 ^{+1.91} _{-0.65}	0.00 ^{+0.14} _{-0.14}	0.54	0.70	65
MACS J0011.7-1523	69	320	2.08	6.81 ^{+0.68} _{-0.57}	7.30 ^{+1.80} _{-1.24}	1.07 ^{+0.29} _{-0.29}	0.28 ^{+0.12} _{-0.11}	0.94	0.85	88
MACS J0025.4-1222 †	69	321	2.72	6.65 ^{+1.07} _{-0.85}	6.31 ^{+1.38} _{-1.02}	0.95 ^{+0.26} _{-0.20}	0.39 ^{+0.22} _{-0.19}	0.66	0.75	86
MACS J0159.8-0849 †	69	414	2.01	9.36 ^{+0.77} _{-0.67}	10.37 ^{+1.29} _{-1.04}	1.11 ^{+0.17} _{-0.14}	0.29 ^{+0.09} _{-0.09}	1.05	1.01	94
MACS J0242.5-2132	69	351	2.71	5.48 ^{+0.62} _{-0.51}	5.99 ^{+2.04} _{-1.19}	1.09 ^{+0.39} _{-0.39}	0.32 ^{+0.16} _{-0.16}	1.08	1.06	92
MACS J0257.1-2325 †	70	409	2.09	9.42 ^{+1.37} _{-1.37}	10.76 ^{+2.05} _{-1.69}	1.14 ^{+0.27} _{-0.22}	0.14 ^{+0.13} _{-0.13}	1.03	1.13	90
MACS J0257.6-2209	68	382	2.02	8.09 ^{+1.08} _{-0.88}	7.90 ^{+1.64} _{-1.20}	0.98 ^{+0.24} _{-0.24}	0.41 ^{+0.18} _{-0.18}	1.13	1.24	90
MACS J0308.9+2645	69	381	11.88	10.64 ^{+1.38} _{-1.14}	11.12 ^{+2.23} _{-1.68}	1.05 ^{+0.19} _{-0.19}	0.37 ^{+0.15} _{-0.15}	0.96	0.97	92
MACS J0329.6-0211 †	71	296	6.21	6.44 ^{+0.45} _{-0.45}	7.55 ^{+0.88} _{-0.73}	1.17 ^{+0.16} _{-0.14}	0.40 ^{+0.10} _{-0.09}	1.12	1.16	91
MACS J0404.6+1109	71	334	14.96	6.90 ^{+2.01} _{-1.29}	7.40 ^{+3.63} _{-1.93}	1.07 ^{+0.61} _{-0.34}	0.22 ^{+0.27} _{-0.22}	0.96	0.92	80
MACS J0417.5-1154	70	303	4.00	10.44 ^{+2.08} _{-1.56}	14.46 ^{+5.92} _{-3.41}	1.39 ^{+0.63} _{-0.39}	0.41 ^{+0.23} _{-0.21}	1.10	1.17	96
MACS J0429.6-0253	68	349	5.70	5.96 ^{+0.72} _{-0.60}	7.48 ^{+2.65} _{-1.64}	1.26 ^{+0.47} _{-0.30}	0.34 ^{+0.15} _{-0.14}	1.02	0.78	89
MACS J0451.9-0006	69	312	7.65	5.76 ^{+1.77} _{-1.77}	6.68 ^{+4.50} _{-4.50}	1.16 ^{+0.86} _{-0.86}	0.47 ^{+0.46} _{-0.39}	1.03	1.33	89
MACS J0547.0-3904	69	256	4.08	3.70 ^{+0.37} _{-0.37}	5.82 ^{+2.94} _{-1.66}	1.57 ^{+0.82} _{-0.82}	0.24 ^{+0.27} _{-0.27}	1.14	1.21	83
MACS J0717.5+3745 †	70	400	6.75	13.30 ^{+1.74} _{-1.21}	12.82 ^{+1.39} _{-1.39}	0.96 ^{+0.48} _{-0.48}	0.32 ^{+0.13} _{-0.13}	0.91	0.87	91
MACS J0744.8+3927 †	71	379	4.66	8.58 ^{+0.85} _{-0.73}	9.32 ^{+1.20} _{-0.96}	1.09 ^{+0.18} _{-0.15}	0.30 ^{+0.11} _{-0.11}	1.14	1.19	89
MACS J0911.2+1746	69	367	3.55	8.85 ^{+3.55} _{-2.11}	10.23 ^{+5.89} _{-3.13}	1.16 ^{+0.81} _{-0.45}	0.20 ^{+0.36} _{-0.20}	0.61	0.74	84
MACS J0949+1708	69	395	3.17	8.94 ^{+1.57} _{-1.20}	10.29 ^{+5.60} _{-5.60}	1.15 ^{+0.66} _{-0.66}	0.48 ^{+0.23} _{-0.23}	0.74	0.58	93
MACS J1115.8+0129	69	317	4.36	6.82 ^{+1.15} _{-0.88}	9.39 ^{+4.77} _{-2.84}	1.38 ^{+0.74} _{-0.74}	0.07 ^{+0.19} _{-0.19}	0.94	0.85	77
MACS J1131.8-1955	70	408	4.49	8.64 ^{+1.32} _{-0.93}	9.45 ^{+2.52} _{-1.68}	1.09 ^{+0.34} _{-0.34}	0.49 ^{+0.19} _{-0.19}	1.07	1.02	91
MACS J1149.5+2223 †	69	359	2.32	7.72 ^{+0.79} _{-0.79}	8.36 ^{+1.31} _{-1.14}	1.08 ^{+0.24} _{-0.24}	0.25 ^{+0.13} _{-0.13}	0.87	0.94	75
MACS J1206.2-0847	70	368	4.15	9.98 ^{+0.27} _{-0.27}	11.93 ^{+2.56} _{-1.88}	1.20 ^{+0.38} _{-0.38}	0.32 ^{+0.13} _{-0.13}	1.02	1.15	95
MACS J1226.8+2153	70	333	1.82	4.86 ^{+1.58} _{-1.08}	5.84 ^{+3.45} _{-2.14}	1.20 ^{+0.81} _{-0.51}	0.00 ^{+0.28} _{-0.00}	1.32	1.36	78
MACS J1311.0-0310 †	69	300	2.18	5.73 ^{+0.46} _{-0.40}	5.92 ^{+0.70} _{-0.60}	1.03 ^{+0.15} _{-0.13}	0.44 ^{+0.12} _{-0.12}	0.93	1.00	83
MACS J1319.7+7003	69	337	1.53	8.08 ^{+0.14} _{-0.16}	10.12 ^{+5.50} _{-2.78}	1.25 ^{+0.76} _{-0.42}	0.10 ^{+0.25} _{-0.10}	1.00	1.07	82
MACS J1427.6-2521	70	289	6.11	4.43 ^{+0.86} _{-0.64}	5.54 ^{+3.81} _{-1.77}	1.25 ^{+0.89} _{-0.44}	0.21 ^{+0.26} _{-0.21}	1.08	1.15	79
MACS J1621.3+3810 †	69	357	1.07	7.49 ^{+0.73} _{-0.83}	7.75 ^{+1.12} _{-0.89}	1.03 ^{+0.18} _{-0.15}	0.35 ^{+0.13} _{-0.13}	0.98	0.92	82
MACS J1824.3+4309	68	246	4.52	4.13 ^{+1.81} _{-1.81}	4.76 ^{+0.39} _{-1.86}	1.15 ^{+0.57} _{-0.53}	0.76 ^{+0.14} _{-0.14}	0.52	0.13	78
MACS J1931.8-2634	70	377	9.13	6.85 ^{+0.73} _{-0.61}	6.86 ^{+1.68} _{-1.15}	1.00<sup				

TABLE 5 — *Continued*

Cluster (1)	R _{CORE} kpc (2)	R ₅₀₀₀ kpc (3)	N _H 10 ²⁰ cm ⁻² (4)	T ₇₇ keV (5)	T ₂₇ keV (6)	T _{HFR} (7)	Z ₇₇ Z _⊙ (8)	χ ² _{red,77} (9)	χ ² _{red,27} (10)	% Source (11)
MACS J2243.3-0935	70	389	4.31	5.15 ^{+0.65} _{-0.54}	8.81 ^{+4.31} _{-2.67}	1.71 ^{+0.86} _{-0.55}	0.05 ^{+0.17} _{-0.05}	1.38	1.27	66
MACS J2245.0+2637	70	320	5.50	6.05 ^{+0.66} _{-0.56}	7.05 ^{+1.31} _{-1.00}	1.17 ^{+0.25} _{-0.11}	0.64 ^{+0.21} _{-0.20}	0.78	0.95	92
MACS J2311+0338	69	247	5.23	7.60 ^{+0.49} _{-0.36}	11.76 ^{+8.05} _{-3.81}	1.55 ^{+0.71} _{-0.56}	0.44 ^{+0.24} _{-0.22}	1.21	0.96	92
MKW3S	69	239	3.05	3.93 ^{+0.06} _{-0.06}	4.58 ^{+0.81} _{-0.17}	1.17 ^{+0.05} _{-0.05}	0.35 ^{+0.02} _{-0.03}	1.28	0.93	88
MS 0016.9+1609	69	388	4.06	9.11 ^{+0.79} _{-0.68}	11.73 ^{+2.98} _{-1.84}	1.29 ^{+0.35} _{-0.22}	0.32 ^{+0.10} _{-0.09}	0.91	0.92	88
MS 0440.5+0204	70	477	9.10	5.99 ^{+0.91} _{-0.73}	4.45 ^{+1.61} _{-1.37}	0.74 ^{+0.29} _{-0.22}	0.66 ^{+0.32} _{-0.29}	0.89	0.74	28
MS 0451.6-0305	69	363	5.68	9.25 ^{+0.89} _{-0.77}	11.55 ^{+2.88} _{-1.91}	1.25 ^{+0.33} _{-0.23}	0.42 ^{+0.12} _{-0.11}	0.95	0.94	71
MS 0735.6+7421	69	347	3.40	5.54 ^{+0.24} _{-0.23}	6.47 ^{+0.75} _{-1.00}	1.17 ^{+0.14} _{-0.13}	0.35 ^{+0.07} _{-0.07}	1.09	1.08	74
MS 0839.8+2938	70	293	3.92	4.63 ^{+0.30} _{-0.28}	4.64 ^{+0.94} _{-0.71}	1.00 ^{+0.21} _{-0.16}	0.49 ^{+0.13} _{-0.13}	0.97	0.91	69
MS 0906.5+1110	70	436	3.60	5.56 ^{+0.34} _{-0.34}	6.94 ^{+0.71} _{-0.71}	1.25 ^{+0.23} _{-0.23}	0.34 ^{+0.10} _{-0.10}	1.20	0.97	82
MS 1006.0+1202	69	393	3.63	5.79 ^{+0.34} _{-0.46}	7.76 ^{+2.55} _{-1.56}	1.34 ^{+0.41} _{-0.29}	0.28 ^{+0.12} _{-0.12}	1.22	1.24	82
MS 1008.1-1224	69	388	6.71	5.76 ^{+0.36} _{-0.47}	9.88 ^{+2.54} _{-1.70}	1.72 ^{+0.47} _{-0.33}	0.24 ^{+0.11} _{-0.11}	1.29	1.08	83
MS 1054.5-0321	69	378	3.69	9.75 ^{+1.69} _{-1.28}	14.17 ^{+12.06} _{-4.93}	1.45 ^{+0.26} _{-0.54}	0.16 ^{+0.16} _{-0.16}	1.05	0.85	51
MS 1455.0+2232	70	308	3.35	4.81 ^{+0.13} _{-0.13}	5.81 ^{+0.42} _{-0.36}	1.21 ^{+0.09} _{-0.08}	0.46 ^{+0.05} _{-0.05}	1.34	1.12	94
MS 1621.5+2640	69	363	3.59	5.72 ^{+0.90} _{-0.72}	5.10 ^{+2.04} _{-1.27}	0.89 ^{+0.38} _{-0.25}	0.37 ^{+0.23} _{-0.21}	1.00	0.98	74
MS 2053.7-0449 †	69	381	5.16	4.68 ^{+1.04} _{-0.75}	5.37 ^{+1.73} _{-1.19}	1.15 ^{+0.45} _{-0.31}	0.26 ^{+0.26} _{-0.24}	0.99	0.94	65
MS 2137.3-2353	69	355	3.40	6.00 ^{+0.35} _{-0.37}	7.56 ^{+2.79} _{-1.62}	1.26 ^{+0.48} _{-0.39}	0.35 ^{+0.13} _{-0.13}	1.08	1.28	69
MS J1157.3+5531	70	272	1.22	3.28 ^{+0.36} _{-0.32}	10.57 ^{+6.36} _{-3.33}	3.22 ^{+1.89} _{-1.06}	0.76 ^{+0.30} _{-0.19}	1.22	1.15	37
NGC 6338	70	254	2.60	2.34 ^{+0.08} _{-0.07}	3.03 ^{+0.30} _{-0.30}	1.29 ^{+0.14} _{-0.12}	0.24 ^{+0.04} _{-0.03}	1.06	1.00	54
PKS 0745-191	69	460	40.80	8.30 ^{+0.39} _{-0.36}	9.69 ^{+0.84} _{-0.73}	1.17 ^{+0.12} _{-0.10}	0.42 ^{+0.06} _{-0.07}	1.01	0.97	93
RBS 0797	70	350	2.22	7.63 ^{+0.94} _{-0.75}	8.62 ^{+2.60} _{-1.69}	1.13 ^{+0.37} _{-0.25}	0.25 ^{+0.13} _{-0.13}	1.06	0.83	93
RDCS 1252-29	68	188	6.06	4.63 ^{+2.39} _{-1.41}	4.94 ^{+9.84} _{-2.82}	1.07 ^{+2.20} _{-0.69}	1.14 ^{+2.11} _{-0.83}	1.36	0.28	60
RX J0232.2-4420	69	402	2.53	7.92 ^{+0.85} _{-0.74}	10.54 ^{+2.53} _{-2.53}	1.33 ^{+0.35} _{-0.35}	0.38 ^{+0.13} _{-0.13}	1.05	0.98	91
RX J0340-4542	69	279	1.63	3.10 ^{+0.45} _{-0.38}	2.75 ^{+1.15} _{-0.87}	0.89 ^{+0.39} _{-0.39}	0.63 ^{+0.39} _{-0.39}	1.22	1.30	48
RX J0439+0520	69	322	10.02	4.67 ^{+0.47} _{-0.47}	5.37 ^{+2.03} _{-1.24}	1.15 ^{+0.46} _{-0.29}	0.36 ^{+0.28} _{-0.29}	0.91	0.81	85
RX J0439.0+0715 †	69	376	11.16	5.65 ^{+0.38} _{-0.34}	8.21 ^{+1.39} _{-0.96}	1.45 ^{+0.25} _{-0.19}	0.34 ^{+0.09} _{-0.09}	1.32	1.14	87
RX J0528.9-3927	69	452	2.36	7.96 ^{+0.71} _{-0.81}	9.84 ^{+2.92} _{-1.81}	1.24 ^{+0.40} _{-0.26}	0.26 ^{+0.14} _{-0.15}	0.96	1.04	88
RX J0647.7+7015 †	69	362	5.18	11.46 ^{+2.05} _{-1.58}	11.18 ^{+2.46} _{-1.77}	0.98 ^{+0.28} _{-0.20}	0.24 ^{+0.18} _{-0.20}	1.00	0.92	88
RX J0819.6+6336	70	308	4.11	3.92 ^{+0.46} _{-0.40}	3.24 ^{+1.26} _{-0.66}	0.83 ^{+0.34} _{-0.19}	0.16 ^{+0.17} _{-0.14}	1.00	1.00	50
RX J0910+5422 †	70	165	2.07	4.08 ^{+3.11} _{-0.75}	5.00 ^{+5.09} _{-2.03}	1.23 ^{+1.56} _{-0.64}	0.43 ^{+1.89} _{-0.43}	0.64	0.56	42
RX J1347.5-1145 †	68	431	4.89	15.12 ^{+1.03} _{-0.86}	17.32 ^{+1.77} _{-1.73}	1.15 ^{+0.44} _{-0.37}	0.33 ^{+0.07} _{-0.07}	1.12	1.11	96
RX J1350+6007	68	227	1.77	4.22 ^{+2.05} _{-1.53}	3.29 ^{+16.32} _{-1.93}	0.78 ^{+0.54} _{-0.54}	0.63 ^{+0.85} _{-0.63}	1.00	0.14	66
RX J1423.8+2404 †	70	301	2.65	6.90 ^{+0.39} _{-0.37}	7.19 ^{+0.59} _{-0.52}	1.04 ^{+0.10} _{-0.09}	0.38 ^{+0.08} _{-0.08}	0.94	0.90	90
RX J1504.1-0248	69	445	6.27	8.02 ^{+0.26} _{-0.25}	8.52 ^{+3.58} _{-2.58}	1.06 ^{+0.08} _{-0.08}	0.39 ^{+0.04} _{-0.05}	1.25	1.17	95
RX J1532.9+3021 †	69	323	2.21	6.06 ^{+0.43} _{-0.39}	7.20 ^{+0.94} _{-0.77}	1.19 ^{+0.18} _{-0.15}	0.46 ^{+0.10} _{-0.11}	0.92	1.02	83
RX J1716.9+6708	68	328	3.71	6.51 ^{+1.79} _{-1.24}	6.21 ^{+4.03} _{-3.11}	0.95 ^{+0.67} _{-0.57}	0.56 ^{+0.39} _{-0.32}	0.84	0.92	63
RX J1720.1+2638	70	361	4.02	6.33 ^{+0.29} _{-0.25}	7.71 ^{+0.84} _{-0.72}	1.22 ^{+0.14} _{-0.12}	0.37 ^{+0.07} _{-0.07}	1.04	0.96	94
RX J1720.2+3536 †	70	320	3.35	7.34 ^{+0.35} _{-0.31}	7.40 ^{+0.86} _{-0.81}	1.01 ^{+0.14} _{-0.12}	0.43 ^{+0.11} _{-0.11}	1.03	0.94	91
RX J2011.3-5725	70	283	4.76	4.10 ^{+0.50} _{-0.39}	3.93 ^{+0.98} _{-0.70}	0.96 ^{+0.26} _{-0.19}	0.41 ^{+0.20} _{-0.20}	0.95	1.08	84
RX J2129.6+0005	70	488	4.30	6.01 ^{+0.35} _{-0.35}	7.19 ^{+1.68} _{-1.70}	1.20 ^{+0.30} _{-0.22}	0.51 ^{+0.16} _{-0.16}	1.29	1.34	87
S0463 †	69	294	1.06	3.27 ^{+0.28} _{-0.25}	3.79 ^{+0.88} _{-0.62}	1.16 ^{+0.29} _{-0.21}	0.22 ^{+0.15} _{-0.11}	1.16	1.20	57
TRIANG AUSTR	70	516	13.27	9.37 ^{+0.32} _{-0.30}	14.68 ^{+1.18} _{-1.08}	1.57 ^{+0.14} _{-0.13}	0.09 ^{+0.04} _{-0.04}	0.01	1.89	88
V 1121.0+2327	71	302	1.30	4.17 ^{+0.78} _{-0.60}	4.70 ^{+3.00} _{-1.17}	1.13 ^{+0.75} _{-0.22}	0.46 ^{+0.36} _{-0.28}	1.09	0.87	74
ZWCL 1215	69	277	1.76	6.63 ^{+0.45} _{-0.40}	7.64 ^{+1.34} _{-1.21}	1.15 ^{+0.22} _{-0.17}	0.37 ^{+0.11} _{-0.11}	1.10	1.04	91
ZWCL 1358+6245	69	375	1.94	9.70 ^{+0.94} _{-0.94}	9.04 ^{+2.08} _{-1.06}	0.93 ^{+0.24} _{-0.24}	0.57 ^{+0.16} _{-0.16}	1.03	0.90	65
ZWCL 1953	69	517	3.10	8.28 ^{+1.25} _{-0.89}	15.12 ^{+11.45} _{-5.45}	1.83 ^{+0.11} _{-0.69}	0.20 ^{+0.14} _{-0.15}	0.87	0.74	82
ZWCL 3146	70	512	2.70	7.46 ^{+0.30} _{-0.30}	8.99 ^{+0.94} _{-0.78}	1.21 ^{+0.14} _{-0.12}	0.31 ^{+0.06} _{-0.05}	1.06	0.97	91
ZWCL 5247	69	430	1.70	4.89 ^{+0.86} _{-0.65}	4.39 ^{+2.30} _{-1.34}	0.90 ^{+0.50} _{-0.27}	0.37 ^{+0.30} _{-0.25}	1.09	0.93	78
ZWCL 7160	70	451	3.10	4.64 ^{+0.41} _{-0.37}	6.82 ^{+2.26} _{-1.44}	1.47 ^{+0.50} _{-0.33}	0.36 ^{+0.14} _{-0.14}	0.94	0.76	87
ZWICKY 2701	69	315	0.83	5.08 ^{+0.32} _{-0.30}	4.96 ^{+0.87} _{-0.69}	0.98 ^{+0.18} _{-0.15}	0.45 ^{+0.13} _{-0.11}	0.95	0.76	70
ZwCL 1332.8+5043	71	434	1.10	3.82 ^{+3.34} _{-2.12}	2.86 ^{+3.96} _{-1.71}	0.75 ^{+1.23} _{-0.42}	0.16 ^{+0.75} _{-0.16}	0.71	0.95	60
ZwCl 0848.5+3341	70	350	1.12	6.54 ^{+2.04} _{-1.27}	6.41 ^{+3.79} _{-1.88}	0.98 ^{+0.66} _{-0.34}	0.59 ^{+0.59} _{-0.48}	0.89	1.01	47

NOTE. — Note: '77' refers to 0.7-7.0 keV band, '27' refers to 2.0_{rest}-7.0 keV band. (1) Cluster name, (2) absorbing, Galactic neutral hydrogen column density, (3,4) best-fit MeKaL temperatures, (5) best-fit 77 MeKaL abundance, (6) T_{0.7-7.0}/T_{2.0-7.0} also called T_{HFR}, (7,8) reduced χ² statistics, (9) percent of emission attributable to source. † indicates cluster with multiple independent, simultaneously fit spectra.